ELECTRICAL SWITCHING AND MEMORY EFFECTS IN ELECTROACTIVE POLYMERS CONTAINING ELECTRON-DONOR AND -ACCEPTOR MOIETIES

LIU YILIANG

NATIONAL UNIVERSITY OF SINGAPORE

2011

ELECTRICAL SWITCHING AND MEMORY EFFECTS IN ELECTROACTIVE POLYMERS CONTAINING ELECTRON-DONOR AND -ACCEPTOR MOIETIES

LIU YILIANG

(M.Eng, XJTU)

A THESIS SUBMITTED

FOR THE DEGREE OF DOCTOR OF PHILOSOPHY

DEPARTMENT OF CHEMICAL & BIOMOLECULAR

ENGINEERING

NATIONAL UNIVERSITY OF SINGAPORE

2011

ACKNOWLEDGEMENT

TABLE OF CONTENTS

SUMMARY

Electroactive polymers have been widely investigated as the active materials in electronic memory devices. In comparison to the traditional silicon-based memories, polymer electronic memories exhibit advantages of low-cost potential, simplicity in structure, good scalability, 3D stacking capability, and device flexibility. In this work, a series of electroactive polymers that can provide the required electronic properties within a single macromolecule and yet still possess good chemical, mechanical and morphological characteristics, have been designed. These polymers include functional polyimides, polyfluorene copolymers, azobenzene-containing polymers and graphene oxide (GO)-polymer complexes. Electrical switching and memory effects of these polymers have been studied in terms of their current density-voltage ($J\text{-}V$) characteristics under electrical sweeps. The effects of different functional groups (electron-donor or -acceptor moieties) on the resultant switching effects have been studied with the aid of molecular simulation and experimental characterizations.

First of all, a series of functional polyimides were designed and studied for their electrical switching and memory effects. All the functional polyimides contain the same electron-acceptor moiety (phthalimide) but different electron-donor moieties (e.g., oxadiazole, triphenylamine-substituted oxadiazole, triphenylamine-substituted triazole, etc). Memory devices based on the polyimides were found to exhibit different memory effects, including write-once read-many times (WORM), static

random access memory (SRAM) and dynamic random access memory (DRAM) effects. The variation in memory effects arises from the difference in molecular conformation, molecular polarity, and stability of the charge transfer (CT) state, associated with the different donor moieties. Electric field-induced CT between the electron-donor and -acceptor moieties accounts for the observed electrical switching and memory effects.

Two polyfluorene copolymers, TPATz-F8 and TPATz-F8BT, containing the fluorene, triphenylamine and triazole moieties, with TPATz-F8BT containing also the benzothiadiazole moiety, were developed for memory application. Similar non-volatile and rewritable memory effects were observed for these two polyfluorenes, except for the different ON state current magnitudes. Electric field-induced CT between the donor (fluorene and triphenylamine) and acceptor (triazole, or triazole and benzothiadiazole) moieties gives rise to a conductive CT state, resulting in the electrical switching effects. Incorporation of the electron-deficient benzothiadiazole group in the TPATz-F8BT backbone blocks the charge migration and thus lowers the ON state current by about one order of magnitude.

Subsequently, two azo polymers, with the pendant azobenzene moiety attached by no terminal group (AzoNEt) or cyano terminal group (AzoNEtCN), were studied for their electrical switching and memory effects. Both polymers exhibited uni-directional electrical switching from the initial OFF state to the ON state during the negative

electrical sweep. The volatility of the ON state was found to be dependant on the terminal group in the pendant azobenzene moiety. Non-volatile ON state was observed when the azobenzene moiety is attached by an electron-acceptor terminal group (cyano group in AzoNEtCN), while volatile ON state was observed when the azobenzene moiety has no terminal group (AzoNEt). The strong cyano acceptor terminal group in AzoNEtCN can induce a large dipole moment and a strong intramolecular CT, which help to stabilize the ON state.

Lastly, two graphene oxide (GO)-polymer complexes, GO-PFTPA and GO-PFCzTPA, were designed and characterized for their electrical switching and memory effects. In these two functionalized GOs, the GO moiety is attached by different polymer segments, which contains fluorene (GO-PFTPA) or fluorene and carbazole (GO-PFCzTPA) in the backbone and triphenylamine in the side chain. Memory devices based on the two GO-polymer complexes exhibited similar non-volatile and rewritable electrical bistability. Electrical field-induced CT between the polymer donor and GO acceptor is responsible for the observed electrical switching effects. Incorporation of the carbazole group in GO-PFCzTPA can stabilize the CT state and interrupt the backbone conjugation, leading to a larger switch-off threshold voltage and a higher ON/OFF current ratio in the GO-PFCzTPA device.

NOMENCLATURE

2NT	2-Naphthalenethiol
6FDA	4,4'-Hexafluoroisopropylidenediphthalic anhydride
8HQ	8-Hydroxyquinline
AFM	Atomic Force Microscope
AIBN	2,2'-Azobisisobutyronitrile
AZTA	*N*-(4-(3,5-Bis(4-aminophenyl)-4H-1,2,4-triazol-4-yl)phenyl)-N-phenylbenzenamine
AZTAE	*N*-(4-(3,5-Bis(4-(4-aminophenoxy)phenyl)-4H-1,2,4-triazol-4-yl)phenyl)-N-phenylbenzenamine
B3LYP	Becke's Three-Parameter Functional with the Lee, Yang and Parr Correlation Functional Method
BAOXD	2,5-Bis(p-aminophenoxy-phenyl)-1,3,4-oxadiazole
BFOXD	2,5-Bis(4-fluorophenyl)-1,3,4-oxadiazole
BPPO	2,5-Bis(4-phenoxyphenyl)-1,3,4-oxadiazole
BU	Basic Unit
CIS	Configuration Interaction Involving Single Electron Excitations
CNTs	Carbon Nanotubes
CPDB	2-Cyanoprop-2-yl Dithiobenzoate
CT	Charge Transfer
CyV	Cyclic voltammetry
DBC	1,4-Dibenzyl C_{60}
DFT	Density Function Theory
DMA	9,10-Dimethylanthracene
DMAc	*N,N*-Dimethylacetamide
DMF	*N,N*-Dimethylformamide

DMPU	1,3-Dimethyl-3,4,5,6-tetrahydro-2(1H)-pyrimidinone
DMSO	Dimethyl Sulfoxide
DRAM	Dynamic Random Access Memory
DSC	Differential scanning calorimetric analysis
EA	Electron Affinity
ESP	Electrostatic Potential
Et$_3$N	Triethylamine
EUV	Extreme Ultraviolet
FeRAM	Ferroelectric Random Access Memory
FPYE	*N*-Methyl-2-((3',4'-dibenzyloxy)phenyl) Fulleropyrrolidine
GO	Graphene Oxide
GPC	Gel Permeation Chromatography
HOMO	Highest Occupied Molecular Orbital
HVSR	High-Voltage Switching Regime
IP	Ionization Potential
ITO	Indium-Tin Oxide
LUMO	Lowest Unoccupied Molecular Orbital
LVSR	Low-Voltage Switching Regime
MACP	2-Methyl-acrylic-acid-2-{[4-(4-cyano-phenylazo)-3-methyl-phenyl]-ethyl-amino}-ethyl ester
MAEA	2-Methyl-acrylic-acid-2-[ethyl-(4-phenylazo-3-methyl-phenyl)-amino]-ethyl ester
MEH-PPV	Poly(2-methoxy-5-(2'-ehtylhexyloxy)-1,4-phenylenevinylene)
MOSFET	Metal-Oxide-Semiconductor Field-Effect Transistor
MRAM	Magnetoresistive Random Access Memory
MS	Mass Spectra

NBS	*N*-Bromosuccinimide
NDR	Negative Differential Resistance
NMP	*N*-Methyl-2-pyrrolidinone
NP	Nanoparticle
OFF	Low-Conductivity
ON	High-Conductivity
OXTA	5-(5-(4-(Diphenylamino)phenyl)-1,3,4-oxadiazol-2-yl)benzene-1,3-diamine
OXZ-TPA	Oxadiazole-Triphenylamine
P2VP	Poly(2-vinyl pyridine)
P3HT	Poly(3-hexylthiophene)
P4VP	Poly(4-vinyl pyridine)
PBD	2-(4-Biphenylyl)-5-(4-*tert*-butylphenyl)-1,3,4-oxadiazole
PCM	Phase Change Memory
PCNT	Poly(4,4''-dipentoxy-4'-(2,2'-dicyano)ethenyl-2,2':5',2''-terthiophene)
PCz	Poly(2-(9*H*-carbazol-9-yl)ethyl methacrylate)
Pd/C	Palladium on Activated Carbon
PDI	Polydispersity Index
PEN	Poly(ethylene naphthalate)
PEDOT	Poly(ethylenedioxythiophene)
PF6	Poly(9,9'-dihexylfluorene)
PHTP	Poly(2,3-dihexylthieno (3,4-b)pyrazine)
PL	Photoluminescence
PLED	Polymer Light-Emitting Diode
PMMA	Poly(methyl methacrylate)

PPV   Poly(phenylene vinylene)

PPV-DR1   Poly(phenylene vinylene)-disperse Red 1

PSS   Poly(styrenesulfonic acid)

PSX-Cz   Poly(siloxane carbazole)

PVBCz   Poly(9-(2-((4-vinylbenzyl)oxy)ethyl)-9H-carbazole)

PVK   Poly(N-vinylcarbazole)

PVP   Poly(vinyl phenol)

SRAM   Static Random Access Memory

STM   Scanning Tunneling Microscopy

TAZ-TPA   Triazole-Triphenylamine

TCI   Tokyo Chemical Industry

TCNQ   Tetracyanoquinodimethane

TGA   Thermogravimetric Analysis

THF   Tetrahydrofuran

TMS   Tetramethylsilane

TPATz   4-(3,5-Diphenyl-4H-1,2,4-triazol-4-yl)-N,N-diphenylaniline

TTF   Tetrathiofulvalene

WORM   Write-Once Read-Many Times

ZnPc   Zinc Phthalocyanine

LIST OF FIGURES

LIST OF TABLES

CHAPTER 1

INTRODUCTION

Digital memories refer to computer components and recording media that can retain digital data and retrieve the stored data conveniently for computing. Current memory technology is based to a large extent on advances in the fabrication of silicon-based integrated circuits, such as resistors, transistors and capacitors. By developing new technologies to shrink the size of the components, and thus fit more components into a single piece of silicon, engineers have driven the speed and capability of computation at a predictable fast pace. Progress in computational power is often related to "Moore's Law", which indicates that the performance of semiconductor devices doubles roughly every 18 ~ 24 months (Service, 2003; Compano, 2001). However, along with the reduction in component size and thus increase in speed, the structures of electronic devices are becoming more and more complicated and the fabrication processes are becoming more and more difficult and expensive (Gordon et al., 1997). The development of alternative technologies for data storage is thus indispensable.

So far, efforts have been devoted to new technologies and concepts, including ferroelectric random access memory (FeRAM) (Setter et al., 2006), magnetoresistive random access memory (MRAM) (Boeck et al., 2002), phase change memory (PCM) (Hudgens and Johnson, 2004), and organic/polymer memories (Möller et al., 2003). Instead of information storage and retrieval by encoding "0" and "1" as the amount of stored charges in the current silicon-based memory devices, the new technologies are based on electrical bistability of materials arising from changes in certain intrinsic properties, such as magnetism, polarity, phase, conformation and conductivity, in

response to the applied electric field.

Organic and polymer materials are promising alternatives or supplements to traiditonal inorganic semiconductor materials for future memory applications. One attractive feature of organic and polymer materials is the possibility for continuous tuning of the electronic properties via molecular design and synthesis (Raymo, 2002). Advantages of organic and polymer memories also include simplicity in device structure, good scalability, low-cost potential, multiple state property and 3D stacking capability (Yang et al., 2006; Li et al., 2004; Service, 2001). In particular, polymer materials possess unique properties, such as good mechanical strength, flexibility, and most important of all, ease of processing. As alternatives to the more elaborated processes of vacuum deposition, solution processes, including spin-coating, spray-coating, dip-coating, roller-coating and ink-jet printing, promise much less expensive fabrication of electronic devices. These techniques also allow for fabricating electronic devices on a variety of flexible substrates, such as plastics, textiles and metal foils (Stikeman, 2002).

In recent works on polymer memory devices, polymers were employed as polyelectrolytes (Möller et al., 2003; Bandyopadhyay and Pal, 2003) and as matrices for metal nanoparticles (Tseng et al., 2005), fullerene (Chu et al., 2005), and carbon nanotubes (Pradhan et al., 2006). However, in these doped or composite systems, phase separation and ion aggregation that arise from non-uniformly dispersed or

non-compatible components are normally unfavorable to the performance of a device (Zhong et al., 2002). To avoid these drawbacks, a series of electroactive polymers that can provide the required electronic properties within a single macromolecule and yet still possess good chemical, mechanical and morphological characteristics, were designed in this work. In these polymers, electron-donor and -acceptor moieties were covalently incorporated in a single macromolecule to act as the electroactive components. Soluble groups, e.g., long alphatic substituent, were also introduced to improve the solubility and processability in common organic solvents.

In addition, it is predicted that the electrical switching and memory effects of a polymer are dependant on its molecular structure. To elucidate this relationship, different donor or acceptor moieties were introduced into the polymer molecules and the resultant memory effects were studied. Based on different electron-donating or -withdrawing ability, conformational feature and flexibility of the component moieties, different memory effects, e.g., different switching threshold voltage, ON state volatility and ON/OFF state current magnitudes, are expected. Experimental characterizations and molecular simulation were carried out to investigate the mechanisms underlying the electrical switching phenomena as well as explore the effect of different functional group on the resultant memory effects.

Chapter 2 gives an overview of the related literatures. This chapter starts with a brief introduction of the polymer electronic memories. Subsequently, classification of the

electronic memories is introduced, along with the features and applications of each type of the electronic memories. Lastly, the major mechanisms proposed for memory effects of organic and polymer electronic memories are elaborated in detail.

In Chapter 3, a series of functional polyimides were designed and studied for their electrical switching and memory effects. In these polyimides, the same phthalimide group acts as the electron-acceptor moiety, while different groups, e.g., oxadiazole, triphenylamine-substituted oxadiazole, triphenylamine-substituted triazole, etc, were introduced as the electron-donor moiety. Hexafluoroisopropyl group was also introduced into the imide moiety to improve the solubility and processability. Under an electric field, charge transfer (CT) occurs between the donor and acceptor moieties, resulting in a conductive CT state (ON state). Due to the different electron-donating ability, conformation and flexibility of the donor moieties, the required energy for triggering CT and stability of the CT state are varied. As a result, different electrical switching and memory effects are expected for these polyimides. Experimental characterizations and molecular simulation were carried out to investigate the underlying mechanisms.

In Chapter 4, two polyfluorene copolymers, TPATz-F8 and TPATz-F8BT, were designed and characterized for their memory effects. Due to their good electron-donating abilities, tripheylamine and fluorine groups were incorporated into the backbone to act as the donor moieties. Triazole group with moderate

electron-withdrawing ability was introduced into the side chain and employed as the acceptor moiety. Electric field-induced CT from the donor moiety to the acceptpr moiety results in a conductive CT state and switches the memory device to the ON state. In comparison to TPATz-F8, TPATz-F8BT has an additional benzothiadiazole group in the backbone. Due to its electron-deficient feature, the benzothiadiazole group can affect charge migratipon along the conjuaged backbone and thus the ON state current magnitude.

In Chapter 5, two azo polymers, AzoNEt and AzoNEtCN, with azobenzene chromophore in the pendant moiety, were developed for memory applications. Different terminal groups were introduced to the pendant azobenzene moiety to adjust the polarity of the molecules. In AzoNEtCN, the pendant moiety is attached by a cyano terminal group which has strong electron-withdrawing ability, while in AzoNEt, there is no terminal group. Due to this difference in molecular structure, the two polymers exhibit different polarities and CT degrees, which can determine stability of the conducting channel and thus volatility of the ON state.

In Chapter 6, two graphene oxide (GO)-polymer complexes, GO-PFTPA and GO-PFCzTPA, were designed and studied for their memory effects. As graphene possesses a giant π-conjugated plane, it exhibits excellent electron conductivity within the graphene plane. However, this good conductivity limits its application in memory device, as it never turns off to be encoded binarily. Thus, oxygen-containing groups,

e.g., carbonyls and carboxyls, were introduced into graphene to reduce its initial electron conducitity. Subsequently, polymer segments were grafted onto the oxygen-containing groups to act as the donor moieties and improve the solubility and processability of GO in organic solvents. Electrical filed-induced CT between the polymer donor and GO acceptor moieties generates a conductive CT state and switches the memory device to the ON state. Due to the different polymer segments, different memory effects are expected in the two GO-polymer complexes. Molecular simulation was carried out to elucidate the underlying mechanisms.

CHAPTER 2

LITERATURE REVIEW

2.1 Introduction of Polymer Electronic Memories

An electronic memory usually refers to a medium or device which can store digital information via binary patterns and has a convenient way to retrieve the stored data. In the conventional silicon-based electronic memory, data are stored based on the amount of charges stored in the memory cells. Polymer electronic memory stores data in an entirely different way, for instance, based on the different electrical conductivity states (ON and OFF states) in response to the applied electric field (Stikeman, 2002).

The polymer electronic memory usually has a simple structure with the polymer thin film sandwiched between two electrodes on a supporting substrate (glass, silicon wafer, plastics or metal foil). The configuration of the top and bottom electrodes can be either symmetric or asymmetric, with Al, Au, Cu and ITO as the most widely used electrode materials. Figure 2.1 shows the schematic diagram of a typical polymer electronic memory.
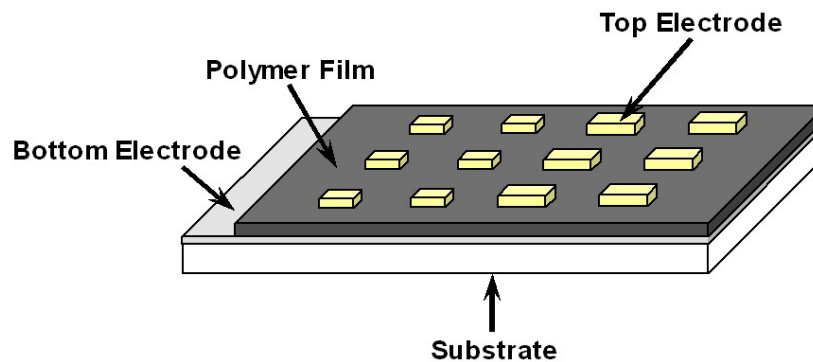
Figure 2.1 Schematic diagram of a typical polymer memory device structure

2.2 Classification of Polymer Electronic Memories

According to the volatility, polymer electronic memories can be divided into two primary categories: volatile and non-volatile memories. A volatile memory eventually loses the stored information unless it is provided with a constant power supply or refreshed periodically with a pulse. A non-volatile memory, however, is able to retain the stored data even after the power supply has been turned off. Write-once read-many times (WORM) memory (Song et al., 2006), hybrid non-volatile and rewritable (flash) memory (Ling et al., 2006), dynamic random access memory (DRAM) (Ling et al., 2006), and static random access memory (SRAM) (Liu et al., 2009) are the most widely reported polymer memories, with the former two belonging to non-volatile memories and the latter two being volatile memories.

A WORM memory allows the information to be written to the storage medium only once physically, but can be read from repeatedly. Because of this feature, WORM memory device can be used for archival purposes of organizations such as government agencies or large enterprises where the data need to be preserved for a long time. In these cases, WORM memory functions as the conventional CD-R or DVD±R device.

Another non-volatile memory is the flash memory. Different from the WORM memory, the flash memory can be electrically erased and reprogrammed. Thus, it has the ability to write, read, erase and sustain the stored data and possesses both the

non-volatile and rewritable features. Flash memory is primarily used as memory cards and USB flash drives for general data storage and transfer of data between computers and other digital products, such as digital cameras, digital audio players and mobile phones.

DRAM is a type of random access memory that stores each bit of data in a separate capacitor within an integrated circuit. Since real capacitors leak charge, the stored data eventually fade unless the device is refreshed periodically. Because of this feature, it is a volatile and dynamic memory. DRAM is used as the main memory in personal computers. A polymer memory, which exhibits a volatile high-conductivity (ON) state and has the ability to write, read, erase and refresh the electrical states, shares the common features with a DRAM device.

SRAM is another type of volatile memory. The word "static" indicates that, unlike "dynamic" RAM (DRAM), it does not need to be periodically refreshed. SRAM exhibits data remanence after the power has been turned off. The memory, however, is still volatile and the stored data are eventually lost when the memory remains in the power-off state. As SRAM is faster but more expensive than DRAM, it is used where either bandwidth or low power, or both, are principal considerations, such as cache memory in microprocessors. A polymer memory with a remanent yet volatile ON state and the ability to write, read and refresh the electrical state, shares the common features with a SRAM device.

2.3 Mechanisms Underlying Polymer Electronic Memories

Various mechanisms have been proposed to explain the electrical conductance switching in response to the applied electric field in organic/polymer memory devices. Among them, the most widely reported mechanisms include filament conduction, charge trapping-detrapping process, conformational changes, and charge transfer process. In the following sections, these major mechanisms will be elucidated in detail based on the previous publications.

2.3.1 Filamentary Conduction

Generally, when the ON state current of a memory device is highly localized to a small fraction of the device area, the phenomenon is termed as "filamentary" conduction (Dearnaley et al., 1970; Jakobsson et al., 2007). According to the filamentary theory (Segui et al., 1976; Henisch and Smith, 1974), (i) the ON state current will exhibit metallic current-voltage characteristics and will increase as the temperature is decreased, (ii) the injected current will be insensitive to the device area or show a random dependence, because the dimension of the filaments is much smaller in comparison to the device area. It is believed that filament conduction is normally associated with physical damages in the device, and thus results in artifact memory effects which are difficult to control and reproduce. However, some controllable filamentary conductions have been demonstrated in polymers for non-volatile memory applications (Joo et al., 2006; Sivaramakrishnan et al., 2007).

2.3.1.1 Filamentary Conduction Mechanisms

Electrical switching phenomena with filamentary mechanism have been widely reported in the glow discharge polymerized materials, such as polystyrene, polyacetylene, and polyaniline (Pender and Fleming, 1975). In these materials, two distinct types of electrical switching phenomena have been observed. One type is called high-voltage switching regime (HVSR) which is characterized by a high switching threshold voltage (> 20 V), and the other type is called low-voltage switching regime (LVSR) which is characterized by a low switching threshold voltage (1 ~ 5 V). Due to the remarkable difference in the electrical characteristics, different filamentary mechanisms have been put forward to explain these two types of electrical switching. In the HVSR modal, the filaments are metallic and arise from localized fusing of the top and bottom electrodes due to complete vaporization of the intervening polymer film, while in the LVSR modal, the filaments are associated with the carbon formed from localized pyrolysis of the polymer film (Pender and Fleming, 1975). In an insulator under sufficiently high electric field, Joule heating may exceed heat losses. Thermal runaway will then occur at the "weakest" points of the sample. In vacuum or an oxygen-free atmosphere, the localized high temperature (at the thermal runaway points) leads to pyrolysis of the polymer and the subsequent formation of a carbon-rich area surrounding the breakdown region. Afterwards, further breakdown produces narrow highly conductive carbon filaments linking the top and bottom electrodes, making the device switch to the ON state. This is the filaments forming process in the LVSR modal. Alternatively, in an atmosphere containing oxygen, the

polymer will oxidize, leaving little or no residue. Afterwards, the electrostatic attraction between the electrodes leads to the formation of a metallic contact. This is the filaments forming process in the HVSR modal.

Rupture of the filaments can remove the ON state, as supported by the fact that traces of the filaments have been observed after the device is returned to the OFF state (Sliva et al., 1970). For the HVSR modal, new breakdown regions are formed in each switching cycle, suggesting that the preformed metallic filament is completely destroyed in the switching process from the ON state to the OFF state, and the formation of another metallic filament is necessary for switching the device back to the ON state. Switching cycles continues until the sample is completely destroyed, usually within 10 cycles. For the LVSR modal, no new breakdown regions are observed after each switching cycle, indicating that this modal is probably associated with only one breakdown region (pseudo-breakdown). It is suggested that only a small section within a filament is ruptured, and the switching threshold voltage is thus dependent on the length of this section rather than the polymer film thickness. A large number of switching cycles ($>10^3$) can usually be obtained with no obvious change in the sample after each cycle (Pender and Fleming, 1975). The reverse switching from the ON state to the OFF state is performed by applying a pulse to vaporize carbon and thus rupture the carbon filament (Tyczkowski, 1991). In order to rupture a formed carbon filament, it would be necessary to supply enough heat to rupture at least a portion of the filament and cool it quickly enough so that the ruptured section does not

reform. Thus, the current pulse must have sufficient magnitude and duration to rupture the filament, but also be short enough so that the produced heat does not become too dispersed. Based on the above description, electrical switching in these polymer memory devices is a consequence of the formation, rupture and reformation of the filaments, as demonstrated in Figure 2.2.
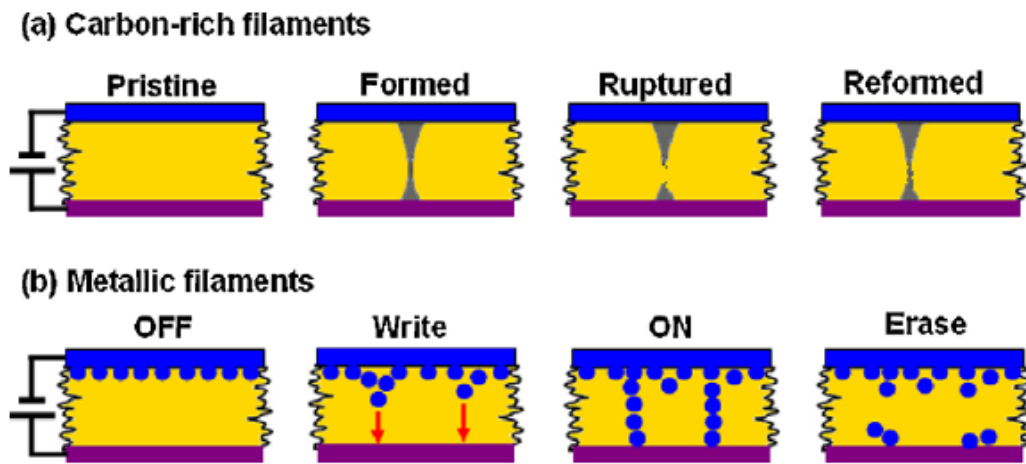
Figure 2.2 Schematic illustrations of the formation of (a) carbon-rich filaments and (b) metallic filaments, and their respective rupturing process.

2.3.1.2 Filaments Forming Conditions

In recent years, a series of polymers with different structures and physical properties have been screened and studied to figure out the forming conditions of the filaments (Joo et al., 2006). It has been found that, (i) polymers without the π-conjugation and strongly coordinating heteroatom (such as S or N), such as polystyrene and poly(methyl methacrylate) (PMMA), did not show any memory behaviors, (ii) non-conjugated polymers that can strongly coordinate to the metal ions, such as

poly(2-vinyl pyridine) (P2VP), poly(4-vinyl pyridine) (P4VP) and poly(vinyl pyrrolidone), also did not yield metal filament, (iii) conjugated polymers without strong metal binding moiety, such as polyfluorene and poly(2-methoxy-5-(2'-ehtylhexyloxy)-1,4-phenylenevinylene) (MEH-PPV), also gave no noticeable memory effect, (iv) conjugated polymers containing strongly coordinating heteroatom, such as polypyrrole, polyaniline, poly(3-hexylthiophene) (P3HT), and poly(phenylene vinylene)-disperse red 1 (PPV-DR1), showed reproducible memory behaviors. Based on the above screening results, it can be concluded that both the π-conjugation and coordinating heteroatom that can bind to metal ions, regardless of the position of binding sites (side chain or main chain), are essential for the production of metal filament. In addition, non-conjugated polymers containing the coordinating atom and possessing good charge conductivity, such as poly(siloxane carbazole) (PSX-Cz) with charge transport functionality lying in the side chain, were also able to produce memory effect, implying that the conjugated system is not necessary as long as the polymer is conductive.

2.3.2 Charge Trapping-Detrapping Process

2.3.2.1 Trapping-Detrapping in Poly(N-vinylcarbazole)

Electrical switching between two conductivity states without any structural changes has been observed in a Ag/poly(N-vinylcarbazole) (PVK)/Ag memory device (Sadaoka and Sakai, 1976). Initially, the device was in the OFF state. When an electric

field larger than the switching threshold was applied, the current increased abruptly after a delay time, forming the ON state. Afterwards, this ON state can be quenched by short circuiting the memory device (Sadaoka and Sakai, 1976; Sakai et al., 1983). The memory switching delay time is due to the transit time of the injected hole carriers through the PVK film. Since the delay time for switching and the fastest transit time of the photoinjected hole carriers show the same dependence on the applied electric field (Mort, 1972), the transition from the OFF state to the ON state may be related to the occupancy level of the traps. As more holes are injected with increasing voltage, the number of trapped holes increases and, finally, when all the traps are filled with holes, the holes newly injected would not be affected by this trap level and cause a steep rise in current. In this sense, the delay time is the time necessary to achieve the trap-filled state. Essentially, the electrical switching characteristics were not observed in the pristine PVK film (Ling et al., 2005; Teo et al., 2006). It is reported that the absorbed oxygen molecules in PVK films act as the hole trapping centers. After the initial reports, switching phenomena in PVK have gained attention for potential application in non-volatile memories (Lai et al., 2005; Lai et al., 2006).

2.3.2.2 Trapping-Detrapping in Polyfluorene Derivatives

For the 9,9-dialkylfluorene homopolymer, it does not show any memory switching. After incorporation of electron acceptor moieties, such as pyridyl, oxadiazole or rare

earth complexes, the functional polyfluorene can exhibit various types of memory switching. These effects are a strong indication that electron acceptors can play an important role (trapping centers) in the electrical bistability phenomena.

For conjugated copolymers of 9,9-dialkylfluorene and europium complex-chelated benzoate, WORM type memory effects have been observed (Ling et al., 2006; Song et al., 2006). The devices were initially in the OFF state, and switched to the ON state after applying the switching threshold voltage. The ON state cannot be erased by a reverse bias or turning off the power, and is thus irreversible and non-volatile. In the copolymer, the fluorene moiety acts as the electron donor, while the europium complex acts as the electron acceptor. Under a low electric field, hole mobility in the copolymer is blocked by the europium complex. When the electric field increases to the switching threshold voltage, electrons are injected into the LUMO of the europium complexes and holes are injected into the HOMO of the fluorene moieties. The charged LUMO (radical anion) of the europium complex and the charged HOMO (radical cation) of the fluorene moiety form a channel for charge carriers, switching the device to the ON state. Due to the high electron affinity of the europium complex, the radical anions can coexist with the surrounding radical cations, resulting in the stable ON state. In addition, a flexible memory device based on a copolymer containing fluorene group and europium complex has been fabricated with a conductive polypyrrole film as the bottom electrode and gold as the top electrode, and exhibited WORM type memory effect (Li et al., 2007).

When the electron acceptor changes from the europium complex to the 1,3,4-oxadiazole and 2,2'-bipyridine moieties in PFOxPy, a DRAM memory effect was observed (Ling et al., 2006). Different from the above WORM type memory device, the DRAM type memory device exhibits a volatile and rewritable ON state, which can be electrically sustained by a refreshing voltage pulse in every few seconds. Essentially, PFOxPy is a *p*-type material and holes dominate the conduction process. The molecular electrostatic surface (ESP) of PFOxPy shows continuous positive ESP region along the conjugated backbone, allowing the charge carrier to migrate through this open channel. However, there are also some negative ESP regions, lateral to the conjugated backbone, arising from the 1,3,4-oxadiazole and 2,2'-bipyridine moieties. These negative ESP regions can serve as traps to block the mobility of charge carriers. At the switching threshold, the charge traps are filled by the injected holes and electron injection also becomes feasible. As a result, conducting channels are formed for both holes and electrons, and the current increases rapidly to switch the device to the ON state. In the presence of the incorporated 2,2'-bipyridine groups, the depth of the traps is reduced from 0.6 eV to 0.3 eV. Thus, the traps are shallow, and the filled traps are easily detrapped, resulting in the unstable ON state which can be erased by either a reversed voltage or turning off the power for a few minutes.

2.3.2.3 Trapping-Detrapping in Polythiophene Derivatives

Memory effect based on charge trapping-detrapping process has also been observed in

the electronic device based on a composite film of polyethylenedioxythiophene (PEDOT):polystyrene sulphonic acid (PSS) sandwiched between the Al and heavily doped silicon electrodes (Liu et al., 2005). The charges trapped in the polymer are believed to be responsible for the memory effect. With a positive bias voltage, charges are injected into the region near the Al/PEDOT:PSS interface. The charges are then trapped at the interface and will resist the subsequent charge injection, resulting in the low conductivity state. Negative bias can remove the trapped charges and returning the device back to the high conductivity state.

The phenomenon of charge trapping has also been investigated in polythiophene derivatives bearing the donor-acceptor structure or in donor-acceptor blends. Some examples of this kind of polythiophene system include poly (4,4''-dipentoxy-4'-(2,2'-dicyano)ethenyl-2,2':5',2''-terthiophene) (PCNT) and poly(2,3-dihexylthieno (3,4-b)pyrazine) (PHTP), as well as a composite of P3HT:FPYE (FPYE = N-methyl-2-((3',4'-dibenzyloxy)phenyl) fulleropyrrolidine) (Casalbore-Miceli et al., 2007). Although the systems are very different, the charge trapping phenomena can be attributed to two similar mechanisms that differ only in the steps in which the negative charges are electrochemically injected into the acceptor moiety and become delocalized in the material. For PCNT and PHTP, an intramolecular delocalization occurs through their conjugative electronic system, while for the P3HT:FPYE blend, the delocalization follows an intermolecular path. A more stable structure can be attained for the above systems after the reduction process.

The enhanced stability of the charged state provides basis for the potential memory applications.

2.3.2.4 Trapping-Detrapping in Poly(*p*-phenylene vinylene) Derivatives

Electrical bistability of Poly(*p*-phenylene vinylene) (PPV) has been realized in an electronic device with the ITO/PPV/Al sandwich structure (Majee et al., 2006). For this PPV device, it can show rewritable electrical switching and can be continuously switched between the ON and OFF states. In addition, when either state (ON or OFF state) is induced, the device can retain in the state for several hours, allowing for the potential application in data storage. The assumed conduction mechanism is that the injected holes can charge up the residual sulfur impurities (contamination from the PPV precursor) within the system and the charged sulfur impurities in the PPV matrix may create filamentary conditions in the device. The impurities can act in a similar manner as nanoparticles in the polymer matrix (Ouyang et al., 2004; Tseng et al., 2005), such that electric field-induced charge transfer between the sulfur moieties and their conjugated capping may occur in the device at a certain electric field. This phenomenon shows that the increase in conductivity is due to trap-filling/charging of the segregated sulfur nanoparticles under bias, leading to an increased current through the device.

2.3.2.5 Trapping-Detrapping in Polymer-Nanoparticle Composite Materials

Electrical switching effects have also been observed in many polymer films embedded with granular metal particles or semiconducting islands to serve as the trapping sites (Bozano et al., 2004; Bozano et al., 2005; Lin et al., 2007). My, Ag, Al, Cr, Au, CdSe, ZnS and CuPc particles have been used as the nano-traps, and some cross-linkable polymers as the semiconducting hosts (Simon et al., 2006; Li et al., 2007). Three architectures have been fabricated for the memory devices: (i) spun-cast polymer-nanopartilce (NP) blends where the NPs are randomly distributed throughout the entire host matrix, (ii) spun-cast bilayer polymer-NP blends, (iii) evaporated structures where the NPs are located in the middle of the organic layer.

The current-voltage characteristics of the polymer-NP memory devices have the following features: the current switches between the OFF and ON states at the switching threshold voltage, reaches a maximum, and then goes through a negative differential resistance (NDR) region to a minimum, after which it increases again almost exponentially. A single-layer device without NPs has also been studied as the reference. It is observed that in absence of the metal NPs, the device exhibit no bistable conductivity states, indicating that the discrete NPs embedded in the semiconducting polymer host is necessary for the switching behavior.

The thicker the metal NP layer, the greater are both the ON and OFF currents of the device. However, the ON/OFF current ratio decreases for thicknesses greater than 10

nm. The most reliable and reproducible devices have been obtained for the device with Al NP thicknesses of 5 and 10nm (Bozano et al., 2005). It is expected that smaller particles, with higher charging energies, contribute primarily to the conduction process, while larger particles, which have longer retention times, are more effective as traps. Both the OFF and ON currents are found to scale proportionally with area, indicating that switching is, most likely, not related to filament formation within the organic film. Charge transport through these devices can occur either through the semiconducting medium itself or by tunneling among the NPs. In both cases, the charge transport falls into the category of "hopping", and the electronic states are highly localized.

The current-voltage characteristics have been interpreted primarily within the context of the SV modal (Simmons and Verderber, 1967). According to this modal, the electroforming process moves metal atoms from the electrode into the semiconducting polymer layer where they form an impurity band of charge transport levels, as well as deeper charge-trapping levels. The pristine state of the formed device is in the ON state in which the transport levels and the traps are uncharged. At low voltages, charge is injected primarily from one of the electrodes and moves through the transport states. At voltages in the NDR region, charge tunnels into the trapping sites and a space-charge field builds up, which inhibits further charge injection from the electrode, and leads to the current decrease.

2.3.3 Conformational Changes

2.3.3.1 Conformational Change in Biphenyl/Bipyridine Molecules

Electrical bistability arising from electric field-induced conformational changes has been reported in molecular switches (Donhauser et al., 2001). Substituted biphenyl or bipyridine molecules have been widely investigated in this area (Cacelli et al., 2006; Cacelli et al., 2007). The molecule is inserted as the active material between a pair of metallic electrodes, to control the longitudinal conduction in response to the applied electric field. The mechanism of operation is based on the action of an electric field perpendicular to the ring-ring bond on the torsional angle and, as a consequence, the inter-ring conjugation. With the inclusion of suitable substituents on the aromatic rings, the transverse electric field can increase the dihedral angle, and thus change the conformation from one in which electrons can flow freely from side to side, to one in which this flow is hindered. As a result, the conductance of the molecule is varied, providing a way for potential data storage.

2.3.3.2 Conformational Change in Azobenzene Derivatives

Azobenzene derivatives are another family of materials which can undergo conformational change (*trans-cis* isomerization) under the excitation of applied electric field. By tunneling electrons with a specific bias in the scanning tunneling microscopy (STM), an azobenzene molecule has been observed to exhibit reversible *trans-cis* conformational change and conductance switching between a low- and

high-conductivity state (Choi et al., 2006). This reversible isomerization is believed to arise from either electron impact resonant excitation or vibrational excitation. The *trans-cis* isomerization of the azobenzene molecule (such as 3,3',5,5'-tetra-*tert*-butylazobenzene) can also be induced by an electric field without tunneling of electrons (Alemani et al., 2006). The underlying mechanism has not been observed experimentally so far, but has been predicted by calculations. In the presence of an electric field, the potential energy surface related to the isomerization can be deformed, leading to an effective lowering of the isomerization barrier and thus facilitating the isomerization process. In addition to the small molecules, electrical conduction transitions associated with conformational changes have also been observed in azobenzene-containing polymers (Attianese et al., 2008). Memory device based on the azo polymer was initially in the low-conductivity state and switched to the high-conductivity state during the negative electrical sweep. The initial low-conductivity state cannot be recovered anymore, and a reversible switching between the high-conductivity state and a middle-conductivity state was observed. The electrical switching from the initial low-conductivity state to the high-conductivity state originates from the antiparallel arrangement of the conjugate segments, while the reversible switching between the high- and middle-conductivity states is due to the electric field-induced conformational changes, which reduce the mean distance between the polymeric chains and increase the conductance of the sample.

2.3.3.3 Conformational Change in Rose Bengal Molecules

Conduction switching phenomena associated with conformational changes have also been observed in devices with Rose Bengal molecules embedded in the supramolecular matrices (Bandyopadhyay and Pal, 2004). In these devices, conductance switching between at least three levels can be achieved when swept to the high voltage range (Mukherjee and Pal, 2005). Two mechanisms, namely, electro-reduction and conformational change of the molecules, which can lead to the conjugation modification, have been proposed. In the low voltage region, electro-reduction of the Rose Bengal molecules facilitates the restoration of conjugation in the backbone and, thus, switches the molecule to the ON state. In the high voltage regime, conformational change of the molecule to orient both planes of the molecule along the field results in another ON state. The devices can be switched between either of the two pairs of conductivity states, following the respective mechanism.

2.3.3.4 Conformational Change in Carbazole Polymers

Electrical bistability effects have also been observed in non-conjugated polymers containing carbazole pendant groups, such as poly(2-(9*H*-carbazol-9-yl)ethyl methacrylate) (PCz) and poly(9-(2-((4-vinylbenzyl)oxy)ethyl)-9*H*-carbazole) (PVBCz). WORM and SRAM type memory effects have been reported for memory device based on PCz and PVBCz, respectively (Teo et al., 2006; Lim et al., 2007).

The switching effect arises from the electric field-induced changes in conformation of the polymer via rotations of the randomly oriented carbazole groups to a more regioregular arrangement for facilitated carrier delocalization and transport. The differences in memory behavior between PCz and PVBCz can be attributed to their inherent differences in the degree of regioregularity and the ease of conformational relaxation. In comparison to PCz, the bulkier spacer between the pendant carbazole group and the backbone in PVBCz allows a larger free volume and a greater conformational freedom for relaxation through, for example, rotation of the carbazole and phenyl rings about the C-O bond, causing the ON state to be unstable. Once the applied electric field is removed, the carbazole groups in PVBCz return to the original random conformation, and switching the PVBCz device back to the OFF state.

2.3.3.5 Conformational Change in Acene Polymers

Acene molecules are among the earliest organic materials that can exhibit memory effect (Szymanski et al., 1969). In recent years, some acenyl moieties, such as anthracenyl and naphthalenyl, have been incorporated into polymers, for ease of preparation and processing, diversity in the backbone, and improved thermal stability (Arias et al., 1997; Ma et al., 2000; Mello et al., 2002). In 2000, a copolymer of methylmethacrylate and anthracene (MDCPAC) has been found to exhibit volatile memory effect (Ma et al., 2000). The Au/MDCPAC/Al device can be switched from the OFF state to the ON state when the applied electric field reaches the switching

threshold voltage (V_{th}). If the voltage is progressively reduced, the device remains in the ON state until the holding voltage (V_{hold}) is reached. Thus, the device is able to exhibit electrical bistability in the voltage range between V_{hold} and V_{th}. In MDCPAC, the charge transport is expected to involve mainly holes, and the anthracenyl moiety plays the role of a trapping center. The abrupt change in resistance of the MDCPAC device above V_{th} is not simply due to trap filling, as commonly observed in conjugated polymers. The high-density of charges after trap filling can induce changes in the molecular conformation of the anthracenyl moiety, with the associated changes in the energy levels. As a result, bulk charge recombination is improved. The process is analogous to the neutralization effect of charged traps in chalcogenide glasses (Alder et al., 1980). The ON state remains and a high charge density is present in the MDCPAC layer. This situation can be maintained as long as the voltage is above the holding voltage. The phenomenon is supported by picosecond time-resolved excited state absorption spectroscopy experiments, which suggest that the photochromic behavior in anthracene-based molecular systems is associated with conformational changes driven by energy relaxation (Anders et al., 1993). Thus, the anthracene derivatives can also be used as materials for photoswitching applications.

In addition to volatile memory effect, non-volatile memory effect has also been observed in the acene polymers, such as poly(ethylene naphthalate) (PEN) (Jiang et al., 2005). It is proposed that the difference in conductance between the high- and low-impedance states is associated with the field-induced intramolecular structural

change in the conjugated system. When electrons are injected into the PEN film, they can induce structural distortions of the surrounding molecular chains. A composite particle, polaron, which is an electron surrounded by the distorted molecular chains, will be formed (Heeger et al., 1988). Since the energy level of the polaron is below the LUMO, the electron can enter this level easily. For organic molecules, the separation between the polaron level and the Fermi level is 0.1 ~ 0.5 eV. Electrons or holes can be injected easily into such materials with narrow bandgaps. Since the interactions between organic molecule chains are very weak, molecular arrangement can be readily varied by an applied electric field, resulting in the electrical switching from one state to another.

2.3.4 Charge Transfer Process

A charge transfer (CT) complex is defined as an electron donor-acceptor complex, characterized by electronic transition to an excited state in which a partial transfer of charge occurs from the donor moiety to the acceptor moiety. For a stable CT complex, a relationship between ionic binding and conductivity exists (Torrance, 1979; Dei et al., 2004). For instance, in the equimolecular complex of Tetracyanoquinodimethane (TCNQ) and a donor material, (i) if the donor is characterized by small size and low ionization potential, a strongly ionic salt forms and a complete transfer of charge (or with the CT degree value, $\delta > 0.7$) occurs from the donor to TCNQ, making the ionic salt insulating (due to Coulomb interactions), (ii) if the donor are very large and have

a high ionization potential, a neutral molecular solid ($\delta < 0.4$) forms, which is also insulating, (iii) if the donor has intermediate size and ionization potential, it tends to form a weakly ionic salt with TCNQ, which possesses incomplete CT ($0.4 < \delta < 0.7$) and thus is potentially conductive.

2.3.4.1 Organometallic CT complex

The bistable electrical switching and memory effects of CT complexes have been firstly reported in electronic device based on Cu-TCNQ (Potember et al., 1979). In a device with a film of microcrystalline Cu-TCNQ sandwiched between Cu and Al electrodes, the current-voltage characteristics reveal an abrupt decrease in impedance from 2 MΩ to less than 200 Ω at a field strength of 4×10^3 V cm^{-1}. It was possible to drive the device back to the high-impedance state either by applying a short current pulse of either polarity, or by allowing the cell to remain for extended periods of time without an applied electric field. Similar electrical switching effects have also been observed in memory devices based on Li-TCNQ (Gong and Osada, 1992) and Ag-TCNQ (Shang et al., 2006). This switching effect is generally understood in terms of a reversible phase transition resulting in the formation of neutral moieties and a residual CT complex (Sun et al., 1997).

2.3.4.2 Fullerene Based CT Complex

It is reported that fullerene derivatives possess high electron-withdrawing ability and

are able to capture up to six electrons. Thus, they have been widely used as electron acceptors to form CT complexes with some organic electron donors, such as thiophene, fluorene, carbazole and aniline derivatives.

Recently, an electronic device based on the spin-coated film of a soluble methanofullerene (PCBM), tetrathiofulvalene (TTF) and polystyrene has been reported to exhibit bistable electrical switching (Chu et al., 2005). In this composite film, TTF and PCBM act as electron donor and acceptor, respectively, while polystyrene serves as the matrix. The electrical switching is attributed to the electric field-induced CT between the TTF donor and PCBM acceptor moieties. In the ground state, no electronic transfer occurs between TTF and PCBM, while only a low concentration of charge carriers due to impurities exist in the film. Thus, the as-fabricated device exhibits a low conductivity. A high electric field, however, may facilitate electron transfer from the HOMO of TTF to the LUMO of PCBM. Consequently, the HOMO of TTF and LUMO of PCBM become partially filled, and TTF and PCBM are charged positively and negatively, respectively. Therefore, carriers are generated, and the device exhibits a sharp increase in electrical conductivity associated with the electric field-induced CT process.

Another electronic device based on a hybrid material containing 1,4-dibenzyl C_{60} (DBC) and zinc phthalocyanine (ZnPc) doped in the polystyrene matrix has been reported to exhibit memory effect based on a stable negative differential resistance

(NDR) (Lin et al., 2007). Electric field-induced CT between the ZnPc donor and DBS acceptor is believed to induce the electrical bistability.

Memory effect has also been observed in a memory device with C_{60} molecules as the charge storage medium dispersed in an insulating poly(vinyl phenol) (PVP) matrix (Paul et al., 2006). This simple device exhibits distinct electrical hysteresis with low- and high-conductivity states. Charge transfer and retention in the C_{60} molecules are proposed to account for the electrical switching. By implementing a small organic molecule (8-hydroxyquinline, 8HQ) to combine with the C_{60} molecules, a more significant electrical hysteresis can be obtained (Paul, 2007).

2.3.4.3 Carbon Nanotubes Based CT Complex

Carbon Nanotubes (CNTs) are another kind of material possessing intense π-conjugation and strong electron-withdrawing ability. Functionalized CNTs show good solubility in organic solvents and can form homogeneous films with regioregular P3HT as the matrix material (Pradhan et al., 2006). Reproducible electrical bistability can be observed in device based on the P3HT:CNT film. Device with only the pristine P3HT, however, cannot exhibit any change in conductance during the electrical sweeps. Thus, the electrical switching is attributed to CT from the CNTs to the LUMO of P3HT. The current magnitudes for both the OFF and ON states, as well as the ON/OFF current ratio, increase along with the increase in CNTs concentration in the

P3HT matrix.

The composite material of CNTs and a conjugated copolymer of 9,9-didodecylfluorene and 4-triphenylamino-2,6-bis(phenyl)pyridine (F12TPN) has been reported to show a more desirable electrical bistability (Liu et al., 2007). When operated alone, memory device based the F12TPN thin film exhibited an unconspicuous electrical switching at around -2.3 V, with the ON/OFF current ratio being only about 10. When doping the F12TPN layer with about 1wt% of CNTs, electric field-induced CT occurs from the CNTs to the conjugated polymer chains, resulting in a significantly increased ON/OFF current ratio (10^5) and a reduced switch-on threshold voltage (-1.7 V). The improvement in memory behavior is believed to arise from the strong electron-withdrawing ability of the CNTs.

2.3.4.4 Au Nanoparticles Based CT Complex

Programmable electrical bistability has been observed in a device made from Au Nanoparticles capped with 1-dodecanethiol (AuNP-DT) and 8HQ dispersed in the polystyrene matrix (Ouyang et al., 2004). The device displays an abrupt transition from the OFF state to the ON state under an external bias, with an ON/OFF ratio of about 10^4. Applying an opposite bias can return the device back to the OFF state. In this composite film, 8HQ and AuNP act as the electron donor and acceptor, respectively. Initially, there is no interaction between the AuNP-DT and 8HQ, and the

film exhibits a low conductivity. At the switching threshold voltage, electrons on the HOMO of 8HQ may gain enough energy to tunnel into the AuNP through the capping DT layer. Consequently, 8HQ and the AuNP are positively and negatively charged, respectively. Carriers are generated, and the device exhibits a sharp increase in conductivity. A reverse electric field can transfer the electrons from AuNP back to the HOMO of 8HQ, resulting in the recovery of the OFF state. Other materials have also been studied for their effect on device performance. When 8HQ is replaced by 9,10-dimethylanthracene (DMA) or the polystyrene matrix is replaced by the PMMA matrix, similar electrical bistability can be observed (Ouyang et al., 2005). However, in the absence of 8HQ or any other conjugated organic compound, no significant electrical switching is observed, indicating the key role of the organic donor materials.

If the capping molecule on the AuNP is changed from a saturated alkylthiol compound to an aromatic compound, the electrical behavior of the device will change significantly. For example, when the AuNP is capped with conjugated 2-naphthalenethiol (2NT), in which the covalently bonded naphthalene group acts as the electron donor, the device Al/AuNP-2NT:polystyrene/Al exhibits an non-rewritable WORM rather than rewritable flash type memory effect (Ouyang et al., 2005). Electrical switching from the OFF state to the ON state, with an ON/OFF ratio of 10^3, was observed. However, after the transition, the device cannot return to the OFF state by applying a reverse voltage. This electrical switching is attributed to the electric field-induced CT between the AuNP and the capping 2NT. After the CT, the

capping 2NT molecules are positively or negatively charged so that the film exhibits a high current and remain in the ON state.

Another non-volatile memory device based on the AuNP-DT and P3HT composite has been demonstrated (Prakash et al., 2006). Electrical switching between the OFF and ON states can be accomplished a thousand times with an ON/OFF ratio of about 10^3. The electronic transition is attributed to the electric field-induced CT between the P3HT donor and AuNP-DT acceptor. Although the electronic transition mechanism of this device is very similar to that for the Al/AuNP-DT:8HQ:polystyrene/Al device mentioned above (Ouyang et al., 2004), the electrical behaviors of the two devices do differ. The conduction mechanisms for the AuNP-DT:P3HT and AuNP-DT:8HQ:polystyrene devices in the ON state are Poole-Frenkel emission and Fowler-Nordheim tunneling, respectively. Presumably, this difference is due to the different charge transport processes through the polymer or organic materials. Charge transport through P3HT is via charge hopping among the polymer chains, while charge transport through 8HQ dispersed in the inert polystyrene matrix is via probably charge tunneling among the molecules.

In addition, rewritable and non-volatile electrical switching behaviors have been observed in another memory device based on the AuNP-DT and PVK (Song et al., 2007). In this device, PVK serves both as the matrix for AuNP and the electron donor, while AuNP serves as the electron acceptor. When a high electric field is applied to

the device, CT between PVK and AuNP occurs, leading to the formation of a conductive CT complex and the electrical switching to the ON state. A reverse bias can dissociate CT complex and reset the device to the initial OFF state.

2.3.4.5 Functional Polyimide Based CT Complex

A functional polyimide (TP6F-PI), containing single bond linked triphenylamine and phthalimide moieties, has been synthesized and studied for its memory behavior (Ling et al., 2006). Electronic device based on TP6F-PI exhibits volatile electrical switching and is able to write, read, erase, and refresh the electrical states, thus fulfilling the functionality of a DRAM. The mechanism underlying the electrical switching is probably similar to that of the photoinduced CT in photoconductive polyimides. In TP6F-PI, the triphenylamine group acts as the electron donor, while the phthalimide acts as the electron acceptor. At the switching threshold voltage, CT can occur from the triphenylamine donor to the phthalimide acceptor, forming the conductive CT states. Under an electric field, the charges can be further segregated and delocalized to the conjugated triphenylamine, thus stabilizing the CT state to some extent. However, the ON state of the TP6F-PI device could not be sustained due to limited delocalization in the triphenylamine moieties. A reverse bias or removal of the electric field can dissociate the CT complex and return the device to the initial OFF state. As a result, a volatile and rewritable electrical switching was observed in the TP6F-PI device.

CHAPTER 3

ELECTRICAL SWITCHING AND MEMORY EFFECTS IN FUNCTIONAL POLYIMIDES CONTAINING DIFFERENT ELECTRON DONOR MOIETIES

3.1 Introduction

Aromatic polyimides are a class of high-performance polymers possessing the cyclic imide and aromatic groups in the main chains. They constitute an important class of materials due to their many desirable characteristics, such as good thermal stability, superior mechanical properties, low dielectric constant, high breakdown voltage, high radiation resistance, inertness to solvents, and long-term stability (Ghosh and Mittal, 1996). In view of their unique properties, polyimides have found a wide range of applications in advanced technologies, such as integrated electronic circuits, microelectronics, optoelectronics, and aerospace industries (Kirby, 1996).

The first commercial polyimide is Kapton (molecular structure shown in Figure 3.1), which was developed by DuPont in the 1960s (Hasegawa and Horie, 2001). Since then this field has blossomed, and hundreds of polyimides have become available with different characteristics to satisfy requirements for various applications. However, most of them have high melting temperatures, low optical transparencies or poor solubilities in organic solvents (Liaw et al., 2007). These disadvantages make them generally intractable and difficult to process, thus limiting their applications. In order to overcome these drawbacks, special structures, such as bulky lateral substituents, flexible alkyl side chains, and unsymmetric, alicyclic or kinked structures, have been introduced into the polyimide chains (Imai, 1995; Liaw et al., 2005; de Abajo and de la Campa, 1999). In recent years, polyimides with good organic solubility have

attracted wide research efforts, which have been focused on synthesizing new rigid

diamines that can result in soluble and processable polyimides without deteriorating

their positive properties (Wang et al., 2008; Jung et al., 2006).
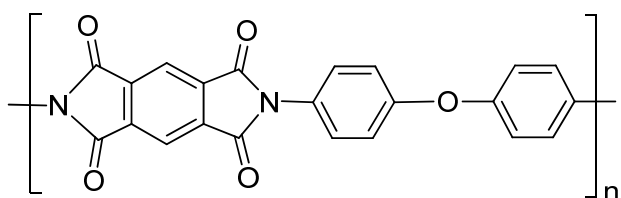
Figure 3.1 Molecular structure of Kapton

In addition to being adopted as insulating and dielectric materials in traditional

electronic devices, polyimides have also been investigated for applications in organic

electronics, such as photovoltaics (Rumyantsev et al., 2005; Lozano et al., 2007),

light-emitting diodes (Shin et al., 20003; Hsu et al., 2007), xerography (Wang et al.,

1998), and polymer memories (Takimoto et al., 1992; Cai et al., 2008; Hahm et al.,

2008). In the pioneer work, Ling et al. have synthesized a solution-processable

functional polyimide (TP6F-PI, molecular structure shown in Figure 3.2) containing

both electron-donor (triphenylamine) and electron-acceptor (phthalimide) moieties,

and studied its switching effects under electrical sweeps (Ling et al., 2006). Switching

device based on TP6F-PI was able to switch between the low-conductivity (OFF) and

high-conductivity (ON) state and exhibit a volatile and rewritable dynamic random

access memory (DRAM) behavior. In the following work (Ling et al., 2007), they

have synthesized another functional polyimide (PP6F-PI, molecular structure shown

in Figure 3.2), which contains the same phthalimide acceptor moiety but different

donor moiety (pyrene-substituted diphenylpyridine). Due to this change in molecular structure, electronic device based on PP6F-PI was found to exhibit a different non-volatile and rewritable flash type memory effect. The results indicate that electrical switching behaviors and memory effects of the functional polyimides are dependant to a large extent on their molecular structures. To study the effect of different donor moieties on the resultant memory behaviors, a series of solution-processable functional polyimides (molecular structures shown in Figure 3.2), containing the same electron-acceptor moiety but different electron-donor moiety, were designed and studied for their electrical switching and memory effects in this chapter. Electronic devices were fabricated based on solution-cast thin film of the polyimide sandwiched between an indium-tin oxide (ITO) bottom electrode and an Al top electrode. Under the electrical sweeps, all the devices were able to exhibit electrical switching and memory effects. However, the volatility of the ON state, switching threshold voltages, and ON/OFF current ratios were varied with different polyimides. The variation in electrical switching effects arises probably from the difference in molecular conformations, polarities, and stability of the charge transfer (CT) state, associated with the difference in their molecular structures. Experimental characterizations and molecular simulations were carried out to investigate the mechanisms underlying the molecular structure-dependent memory effects.

TP6F-PI

PP6F-PI

OXTA-PI

AZTA-PI

AZTA-PEI

P(BPPO)-PI

Acceptor   **Donor**
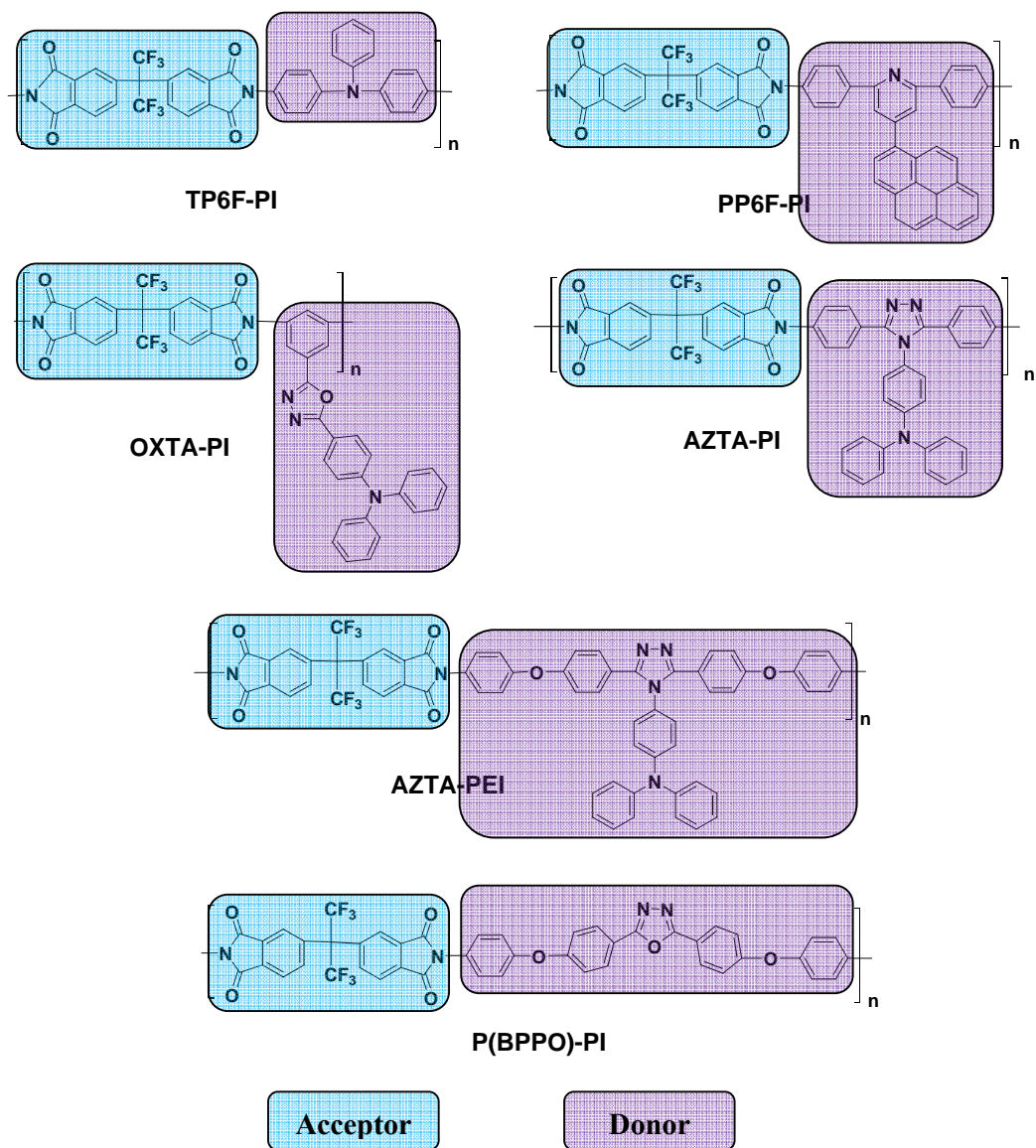
Figure 3.2 Molecular structures of the functional polyimides studied in this chapter

3.2 Experimental Section

3.2.1 Materials

10% Palladium on activated carbon (Pd/C) was purchased from Merck Chemical Co. and used as received. 4-(*N,N*-Diphenylamino)benzaldehyde and *p*-fluorobenzoic acid were purchased from Sigma-Aldrich Chemical Co. and used as received. 4,4'-Hexafluoroisopropylidenediphthalic anhydride (6FDA) was purchased from Chriskev Chemical Co. and sublimated before use. Diphenylamine, 4-aminophenol, 4-fluorobenzoyl chloride, 4-nitrobenzoyl chloride, 4-fluoronitrobenzene, acetic anhydride, and pyridine were purchased from Acros Chemical Co. and used as received. Phosphorus pentachloride, hydrazine monohydrate, and potassium carbonate were purchased from Riedel-de Haën Chemical Co., Alfa Aesar Chemical Co., and Showa Chemical Co., respectively, and were used as received. *N*-Methyl-2-pyrrolidinone (NMP), *N,N*-dimethylacetamide (DMAc), dimethyl sulfoxide (DMSO), and toluene were purchased from Tedia Chemical Co. Tetrahydrofuran (THF) and *N,N*-dimethylformamide (DMF) were purchased from Echo Chemical Co. 1,3-Dimethyl-3,4,5,6-tetrahydro-2(1H)-pyrimidinone (DMPU) was purchased from Sigma-Aldrich Chemical Co. All the solvents were purified by distillation over calcium hydride and stored over 4 Å molecular sieves.

3.2.2 Instrumentation

FT-IR spectra of the synthesized monomers and polymers dispersed in KBr, as well as of the polymer films, were recorded in the wavenumber range of $400 \sim 4000$ cm^{-1} on a Bio-Rad Digilab FTS-3500 spectrometer. NMR spectra were measured on a Bruker Avance 500 spectrometer. Elemental analysis was carried out on a Perkin-Elmer 2400 elemental analyzer. The inherent viscosity of the polymer solution was measured with an Ubbelohde viscometer. Weight average molecular weight (M_w) and number average molecular weight (M_n) were determined by gel permeation chromatography (GPC) with four Waters (Ultrastyragel) columns (300×7.7 mm, guarded and packed with 10^5, 10^4, 10^3, and 500 Å gels) in series. THF (1 mL·min^{-1}) was used as the eluent which was monitored with a UV detector (JMST Systems, VUV-24, USA) at 254 nm. Monodispersed polystyrene samples were used as the molecular weight standards. Thermogravimetric analysis (TGA) was conducted on a TA Instrument Dynamic TGA 2950 thermogravimetric analyzer at a heating rate of 10°C·min^{-1} and under a nitrogen flow rate of 50 cm^3·min^{-1}. Differential scanning calorimetry (DSC) analysis was performed on a TA Instrument TA 910 differential scanning calorimeter at a heating rate of 10°C·min^{-1} and under a nitrogen flow rate of 50 cm^3·min^{-1}. UV-visible absorption and photoluminescence (PL) spectra were measured on a Shimadzu UV-NIR 1601 spectrophotometer and Shimadzu RF 5301PC luminescence spectrophotometer, respectively. Atomic force microscope (AFM) image of the cast polyimide film on the indium-tin oxide (ITO) coated glass substrate was measured on a Veeco Multimode Atomic Force Microscope loaded with a Nanosensors PPP-NCHR

Si tip.

3.2.3 Synthesis of the Functional Polyimides

The functional polyimides of OXTA-PI, AZTA-PI, AZTA-PEI and P(BPPO)-PI were prepared and characterized by Associate Prof. Wang Kun-Li, Mr. Huang Guo-Syun, Mr. Lee Jian-Wei and Mr. Shi I-Hao from National Taipei University of Technology.

3.2.3.1 Synthesis of OXTA-PI

The synthesis route of OXTA-PI is illustrated in Figure 3.3. Details on the preparation and characterizations are given below.

Synthesis of 5-(5-(4-(diphenylamino)phenyl)-1,3,4-oxadiazol-2-yl)benzene-1,3-diamine (OXTA): The **OXTA** diamine was prepared by four steps from 4-(*N,N*-diphenylamino)benzaldehyde. Compounds **1** and **2** were prepared according to the published method (Bing et al., 2004; Tamoto et al., 1997). Compound **2** was reacted with 3,5-dinitrobenzoyl chloride in pyridine to afford the orange compound **3,** followed by reduction with hydrazine monohydrate in ethanol in the presence of Pd/C at reflux temperature. The above mixture was then filtered to remove Pd/C and dried under reduced pressure to afford the crude product, which was recrystallized from THF to afford the yellow-white product (**OXTA,** yield: 27%). FT-IR (KBr, cm^{-1}):

3446, 3380, 3323, 3213 (-NH$_2$ stretch), 1592 (-C=N-). ^{1}H-NMR (d_6-DMSO, 500

MHz), δ(ppm): 5.10 (s, 4H, NH$_2$), 6.02 (d, J = 1.71 Hz, H), 6.52 (d, J = 1.8 Hz, 2H),

7.03 (d, J = 8.8 Hz, 2H), 7.17 (m, J = 6.2 Hz, 6H), 7.39 (t, J = 7.8 Hz, 4H), 7.87 (d, J

= 8.8 Hz, 2H). ^{13}C-NMR (d_6-DMSO), δ(ppm): 100.79, 102.46, 115.58, 120.47,

124.02, 124.64, 125.55, 127.73, 129.88, 149.87, 146.09, 150.31, 163.30, 164.51.

Anal. calcd. for C$_{26}$H$_{17}$N$_5$O (wt %): C 74.44, H 5.05, N 16.70; found: C 74.47, H 4.96,

N 16.73.
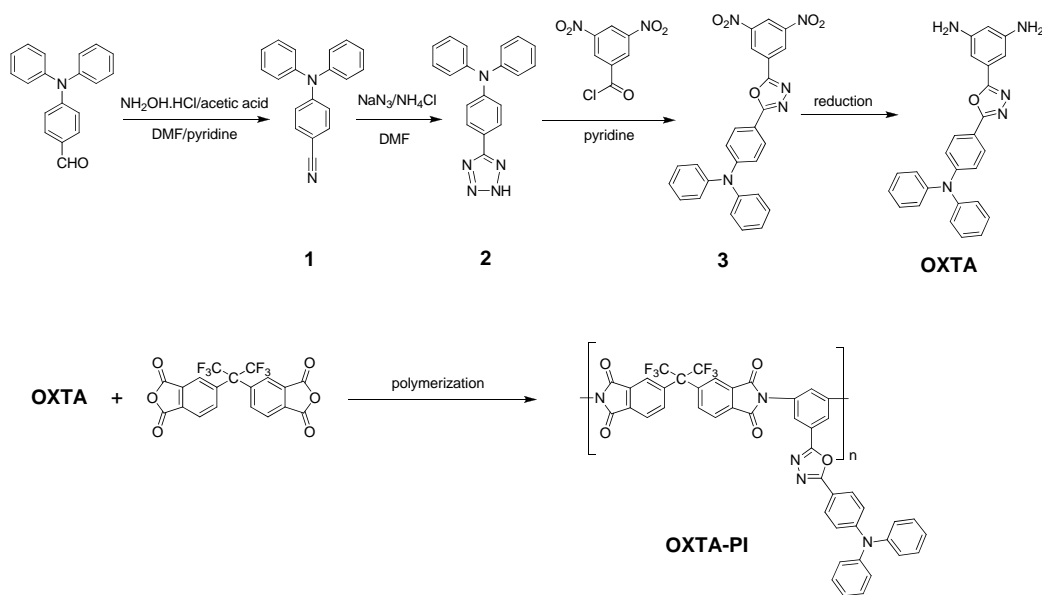
Figure 3.3 Synthesis routes for the monomers and the OXTA-PI polymer

Synthesis of OXTA-PI: 6FDA (0.05 mol) was added slowly, with stirring, to a NMP

solution of **OXTA** (0.05mmol). The mixture was stirred at ambient temperature for 4

h to form the poly(amic acid). Chemical imidization was carried out by addition of 1

mL acetic anhydride and 0.5 mL pyridine into the above-mentioned poly(amic acid)

solution, followed by heating the mixture at 120°C for 3 h. The polymer solution was

poured slowly into 300 mL of methanol with stirring. The precipitate was filtered, washed with hot methanol, and dried at 100°C under reduced pressure.

3.2.3.2 Synthesis of AZTA-PI and AZTA-PEI

The synthesis routes for the two polyimides are illustrated in Figure 3.4. Details on the preparation and characterizations are given below.

AZTAN and **AZTAF** were prepared according to the previously reported procedures (Wang et al., 2008), in which 4-nitrobenzoyl chloride and 4-fluorobenzoyl chloride were used as the initial reaction compound, respectively.

Synthesis of N-(4-(3,5-bis(4-aminophenyl)-4H-1,2,4-triazol-4-yl)phenyl)-N-phenylbenzenamine (AZTA). **AZTA** was prepared from **AZTAN** by general reduction reaction with hydrazine monohydrate in ethanol in the presence of Pd/C at reflux temperature. The mixture was then filtered to remove Pd/C and dried under reduced pressure to afford the crude product, which was recrystallized from THF to afford the yellow product (**AZTA,** yield: 83%). FT-IR (KBr, cm^{-1}): 3369, 3461 (-NH$_2$). ^{1}H-NMR (d_6-DMSO 500 MHz), δ(ppm): 5.33 (s, 4H, NH$_2$), 6.52-6.53 (d, J=7.66Hz, 4H), 6.96-6.98 (d, J=8.6Hz, 2H), 7.03-7.05 (d, J=7.8Hz, 4H), 7.09-7.10 (m, 6H), 7.14-7.16 (d, J=8.68Hz, 2H), 7.32-7.35 (t, J=7.78Hz, 4H). ^{13}C-NMR (d_6-DMSO), δ(ppm): 113.2, 114.1, 122.7, 123.8, 124.5, 129.2, 129.3, 129.5, 129.7, 146.6, 147.8, 149.8, 154.2. Anal. calcd. for C$_{32}$H$_{26}$N$_6$ (wt %): C 77.71, N 16.99, H 5.30; found: C

76.10, N 16.45, H 5.48.

Synthesis of N-(4-(3,5-bis(4-(4-aminophenoxy)phenyl)-4H-1,2,4-triazol-4 -yl)phenyl)-N-phenylbenzenamine (AZTAE). **AZTAF** was reacted with 4-aminophenol and potassium carbonate in NMP at 150°C, according to the method reported previously (Hamciuc et al., 1996), to produce the light-yellow product (**AZTAE**, yield: 48%). FT-IR (KBr, cm^{-1}): 1199 (-O-), 3359, 3454 (-NH$_2$). ^{1}H-NMR (*d$_6$*-DMSO, 500 MHz), δ(ppm): 5.03 (s, 4H, NH$_2$), 6.61-6.62 (t, *J*=8.64Hz, 4H), 6.74-6.76 (d, *J*=8.66Hz, 4H), 6.81-6.83 (d, *J*=8.79Hz, 4H), 6.88-6.90 (d, *J*=8.73Hz, 2H), 6.98-7.00 (d, *J*=7.79Hz, 4H), 7.04-7.07 (t, *J*=7.34Hz, 4H), 7.14-7.15 (d, *J*=8.725Hz, 2H), 7.24-7.27 (t, *J*=7.83Hz, 4H), 7.35-7.37 (d, *J*=8.78Hz, 4H) ^{13}C-NMR (*d$_6$*-DMSO), δ(ppm): 115.0, 115.9, 120.4, 121.4, 122.2, 124.1, 124.8, 128.0, 129.3, 130.0, 130.2, 144.6, 146.0, 146.4, 148.3, 153.9, 160.2. Anal. calac. for C$_{44}$H$_{34}$N$_6$O$_2$ (wt %):C 77.86, N: 12.38, H: 5.05; found: C 77.42, N: 2.23, H 5.08.

Synthesis of AZTA-PI and AZTA-PEI: 6FDA (0.05 mol) was added slowly, with stirring, to a NMP solution of **AZTA** or **AZTAE** (0.05mmol). The mixture was stirred at ambient temperature for 4 h to form the poly(amic acid). Chemical imidization was carried out by addition of 1 mL acetic anhydride and 0.5 mL pyridine into the above-mentioned poly(amic acid) solution, followed by heating the mixture at 120°C for 3 h. The polymer solution was poured slowly into 300 mL of methanol with stirring. The precipitate was filtered, washed with hot methanol, and dried at 100°C

under reduced pressure.
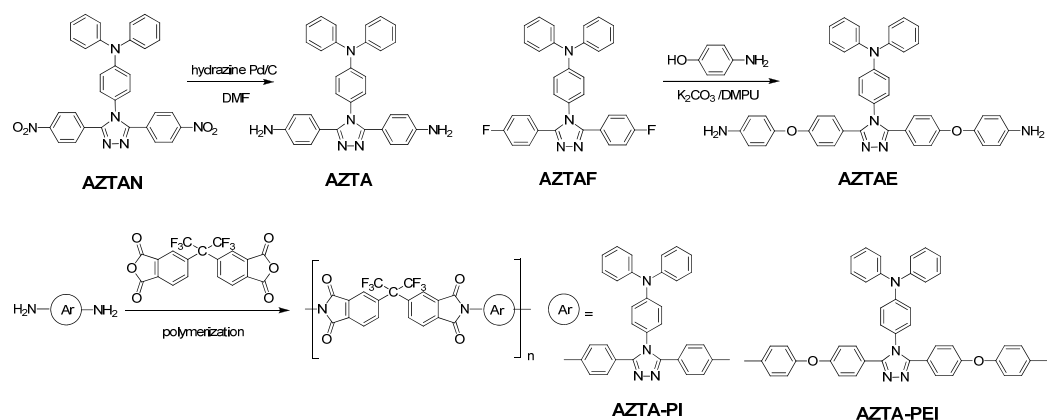
Figure 3.4 Synthesis routes for the monomers and the AZTA-PI and AZTA-PEI polymers

3.2.3.3 Synthesis of P(BPPO)-PI

The synthesis route of P(BPPO)-PI is illustrated in Figure 3.5. Details on the preparation and characterization are given below.

Synthesis of 2,5-bis(4-fluorophenyl)-1,3,4-oxadiazole (BFOXD): 2,5-bis(4-fluorophenyl)-1,3,4-oxadiazole (BFOXD) was synthesized according to the published method (Hwang and Chen, 2000). After the reaction of *p*-fluorobenzoic acid (2 mol) and hydrazine hydrate (1 mol) in polyphosphoric acid (PPA), the mixture was recrystallized twice from ethanol, giving rise to small needle-like white crystals. FT-IR (KBr pellet): 1610 cm^{-1} (-C=N-). ^{1}H NMR (CDCl$_3$, 500 MHz), δ(ppm): 7.97-8.00 (m, 4H), 7.28-7.32 (t, J= 8.87 Hz, 4H).

*Synthesis of 2,5-bis(p-aminophenoxy-phenyl)-1,3,4-oxadiazole (**BAOXD**):* BFOXD was reacted with 4-aminophenol and potassium carbonate in NMP at 150°C, according to the method reported previously (Hamciuc et al., 2007), to produce the diamine. This method is based on the nucleophilic displacement of the activated fluoro-substituents by potassium phenoxide in polar aprotic solvent. FT-IR (KBr, pellet): 3454 and 3373 cm^{-1} (NH$_2$), 1612 cm^{-1} (-C=N-), 1240 cm^{-1} (-O-). ^{1}H NMR (d_6-DMSO, 500 MHz), δ(ppm): 8.01-8.03 (d, J=8.79 Hz, 4H), 7.02-7.04 (d, J=8.79 Hz, 4H), 6.82-6.84 (d, J=8.67 Hz, 4H), 6.61-6.63 (d, J=8.71 Hz, 4H), 5.08 (s, 4H).

Synthesis of P(BPPO)-PI: 6FDA (0.509 g) was added slowly, with stirring, to 4 mL of DMAc containing 0.5 g of BAOXD at 0°C. The mixture was stirred at ambient temperature for 24 h under a nitrogen atmosphere to form the poly(amic acid). Chemical imidization was carried out by adding 1 mL of acetic anhydride and 0.5 mL of pyridine into the poly(amic acid) solution, followed by heating the mixture at 140°C for 6 h. The polymer solution was poured slowly into 300 mL of methanol with stirring. The precipitate was filtered, washed with methanol, and dried at 100°C under reduced pressure. FT-IR (film): 1784, 1724, 1376 cm^{-1} (imide). ^{1}H NMR (d_6-DMSO, 500 MHz), δ(ppm): 8.10-8.20 (6H), 7.95-7.98 (2H), 7.68-7.88 (2H), 7.45-7.58 (4H) , 7.25-7.38 (8H).
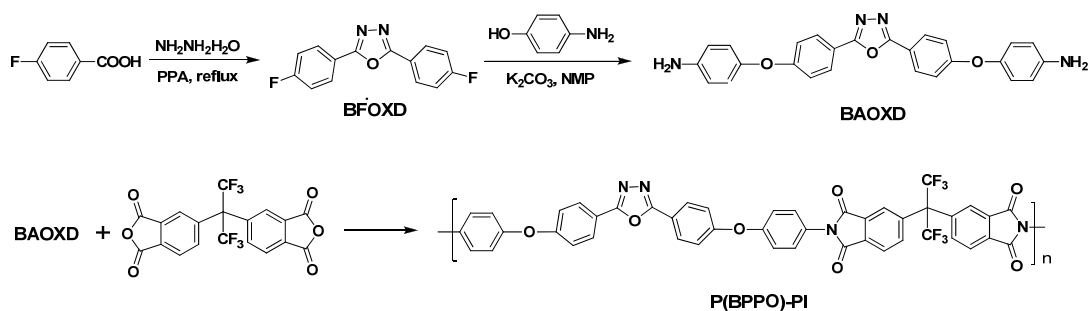
Figure 3.5 Synthesis routes for the monomers and the P(BPPO)-PI polymer

3.2.4 Fabrication and Characterization of the Memory Devices

The ITO coated glass substrate was pre-cleaned sequentially with deionized water, acetone, and isopropanol in an ultrasonic bath for 15 min. A 10 mg·mL^{-1} DMAc solution of the polyimide was spin-coated onto the ITO substrate, followed by solvent removal in a vacuum chamber at 10^{-5} Torr and 60°C for 12 h. The thickness of the polymer layer was determined by the AFM step profile. Finally, an Al top electrode of 400 nm in thickness was thermally deposited onto the polymer layer through a shadow mask at a pressure of about 10^{-7} Torr. The measurements of electrical properties were carried out on devices of 0.4×0.4 mm^2, 0.2×0.2 mm^2 and 0.15×0.15 mm^2 in size, under ambient conditions, using an Agilent 4155C semiconductor parameter analyzer equipped with an Agilent 41501B pulse generator. The current density-voltage (*J-V*) data reported are based on device units of 0.4×0.4 mm^2 in size, unless stated otherwise. ITO was maintained as the ground electrode during the electrical measurements.

3.2.5 Molecular Simulation

Molecular simulations of the polyimides were carried out with the Gaussian 03 (Revision E. 01) program package on an Intel Xeon EM64T workstation. The calculations for the ground and excited states were carried out with 1 CPU and 2GByte memory, and 4 CPUs and 8GByte memory, respectively. Electronic properties of the polyimides at the ground state, including molecular orbitals, electrostatic potential (ESP) surface, and dipole moment, were calculated from the density function theory (DFT), using the Becke's three-parameter functional with the Lee, Yang and Parr correlation functional method (B3LYP) and the basis set 6-31G with d function added to heavy atoms (in short, DFT B3LYP/6-31G(d)) (Frisch et al., 2004). Based on the ground state optimized geometry, the optimized geometry, dipole moment and ESP surface of the first excited state were calculated with configuration interaction involving single electron excitations (CIS) method (Foresman et al., 1992). For both molecular simulations, vibrational frequencies were calculated analytically to ensure that the optimized geometries really correspond to the total energy minima.

3.3 Results and Discussion

3.3.1 Characterizations of the Functional Polyimides

The solubilities of the functional polyimides in common organic solvents are summarized in Table 3.1. Due to "fluorine effect" of 6FDA (Wang et al., 2008), all the functional polyimides exhibit good solubility in common solvents, such as DMF, DMAc, NMP, DMSO and chloroform, at room temperature. In comparison to the traditional polyimides that are insoluble in common solvents, e.g., Kapton, the present polyimides are more desirable for fabricating electronic devices via solution process (Hasegawa and Horie, 2001).

Table 3.1 Solubilities of the functional polyimides in common organic solvents

Polymer	Solubility[a]					
	DMAc	DMF	NMP	DMSO	CHCl$_3$	THF
OXTA-PI	++	++	++	++	++	++
AZTA-PI	++	++	++	++	++	+-
AZTA-PEI	++	++	++	++	++	++
P(BPPO)-PI	++	++	++	++	++	++

[a]Solubility measured in concentration of 1 mg·mL^{-1}
++: Soluble at room temperature
+-: Partially soluble on at room temperature

The inherent viscosities, molecular weights, and thermal properties of the functional polyimides are summarized in Table 3.2. In comparison to OXTA-PI, P(BPPO)-PI with similar molecular structure exhibits a much lower glass transition temperature (250°C for P(BPPO)-PI *vs* 317°C for OXTA-PI), probably arising from its more

flexible molecular chain due to the incorporation of the phenoxyl group (Jin et al., 2004). The similar phenomenon is also elucidated by the lower glass transition temperature of AZTA-PEI (273°C) containing an additional phenoxyl group than that of AZTA-PI (304°C).

Table 3.2 Inherent viscosities, molecular weights and thermal properties of the functional polyimides

Polymer	η (g·dL^{-1})[a]	Molecular weights[b]		Thermal properties	
		M_n	M_w	T_{d10}(°C)[c]	T_g(°C)[d]
OXTA-PI	0.25	2.5×10^4	3.8×10^4	476	317
AZTA-PI	0.44	3.2×10^4	5.6×10^4	515	304
AZTA-PEI	0.88	8.0×10^4	1.7×10^5	526	273
P(BPPO)-PI	0.35	6.6×10^4	9.5×10^5	566	250

[a]Inherent viscosity was measured in DMAc at a concentration of 0.5g·L^{-1} at 30 °C
[b]Molecular weights were measured by GPC in DMF using polystyrene as standard
[c]T_{d10} is 10% weight loss temperature measured by TGA in nitrogen
[d]T_g is the glass transition temperature measured by DSC in nitrogen

Figure 3.6 shows the UV-visible absorption spectra of OXTA-PI, AZTA-PI, AZTA-PEI and P(BPPO)-PI in chloroform. The concentration of P(BPPO)-PI was about 5×10^{-7} M. The concentrations of the rest three polyimides were adjusted to have the same number of repeating units as that of P(BPPO)-PI. All the absorption spectra are normalized to the maximum absorption peak of P(BPPO)-PI for ease of comparison. As shown in Figure 3.6, P(BPPO)-PI exhibits a maximum absorption peak at 301 nm, which is attributed to the $\pi \rightarrow \pi^*$ transition of the π electrons delocalized along the 2,5-bis(4-phenoxyphenyl)-1,3,4-oxadiazole (BPPO) moieties

(Wolarz et al., 2007). In comparison to P(BPPO)-PI, an additional triphenylamine group is incorporated into the OXTA-PI molecule, which significantly enhance the intramolecular CT and thus induces a CT absorption band at 364 nm (Tao et al., 2009). When the oxadiazole group in OXTA-PI is substituted by the triazole group in AZTA-PI, a nearly orthogonal dihedral angle is formed between the triazole and triphenylamine groups (Strukelj et al., 1995), which inhibits the intramolecular CT and blue-shifts the maximum absorption to 290 nm. Incorporation of the flexible phenoxyl group into the AZTA-PEI molecule limits the conjugation of the polymer chain and induces a further blue-shift to 282 nm in the maximum absorption.
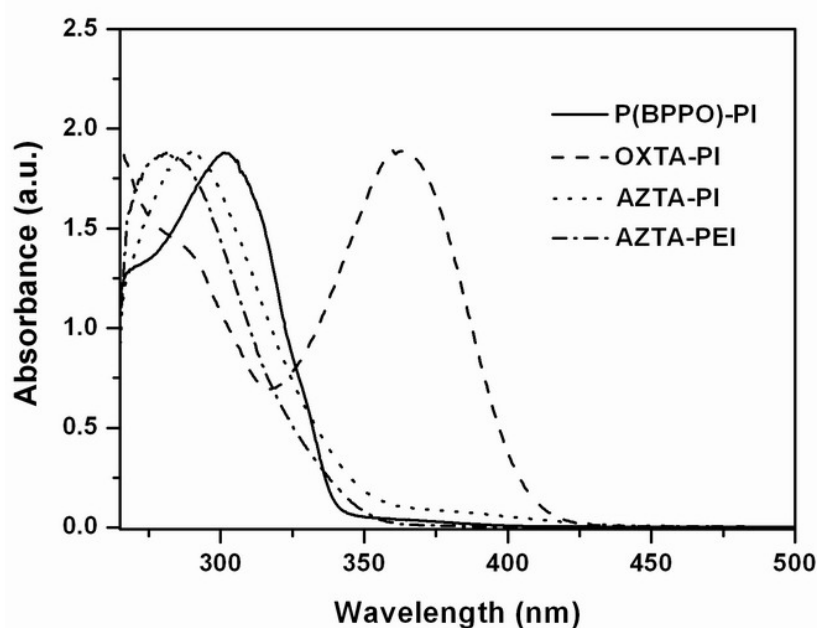
Figure 3.6 UV-visible absorption spectra of OXTA-PI, AZTA-PI, AZTA-PEI and P(BPPO)-PI in chloroform. The concentration of P(BPPO)-PI was about 5×10^{-7} M. The concentrations of the rest three polyimides were adjusted to have the same number of repeating units as that of P(BPPO)-PI. All the absorption spectra are normalized to the maximum absorption peak of P(BPPO)-PI for ease of comparison.

The PL spectra of OXTA-PI, AZTA-PI, AZTA-PEI in chloroform and P(BPPO)-PI in

DMAc are shown in Figure 3.7. The PL spectra of the corresponding monomers, OXTA, AZTA and BFOXD were employed as the references. The concentrations of OXTA-PI, AZTA-PI, AZTA-PEI and P(BPPO)-PI in solution were 6.7×10^{-7} M, 5.2×10^{-7} M, 2.1×10^{-7} M and 1.0×10^{-8} M, respectively. The concentrations of the monomers were adjusted to have the same number of repeating units as their corresponding polymers. All the emission spectra were obtained with the excitation wavelength of 280 nm. As shown in Figure 3.7(a), the OXTA monomer exhibits an intense emission peak at 436 nm, which is red-shifted by 87 nm in comparison to the emission of 2,5-diphenyl-1,3,4-oxadiazole (Franco et al., 2006). This large red-shift probably arises from the intense CT between the triphenylamine and oxadiazole groups in OXTA. The PL quantum yield (Φ_{PL}) of the OXTA monomer in chloroform was estimated by comparison with the PL of standard 9,10-diphenylanthracene. The PL quantum yield of OXTA was 23.6%. The fluorescence of OXTA-PI, however, was significantly quenched, indicating considerable decay of the excited singlet state of the OXTA moiety, either by charge or energy transfer between the OXTA and phthalimide moieties (Shibano et al., 2006; Lukas et al., 2002). The poor match between the emission spectrum of OXTA and the absorption spectrum of 6FDA rules out the possibility of energy transfer (Gómez et al., 2005). CT between the OXTA and phthalimide moieties is thus accountable for the fluorescence quenching in OXTA-PI. For the AZTA modal materials, the orthogonal conformation between the triphenylamine and triazole group largely limits the intramolecular CT, resulting in a blue-shift of 18 nm in the emission peak in comparison to the emission of OXTA
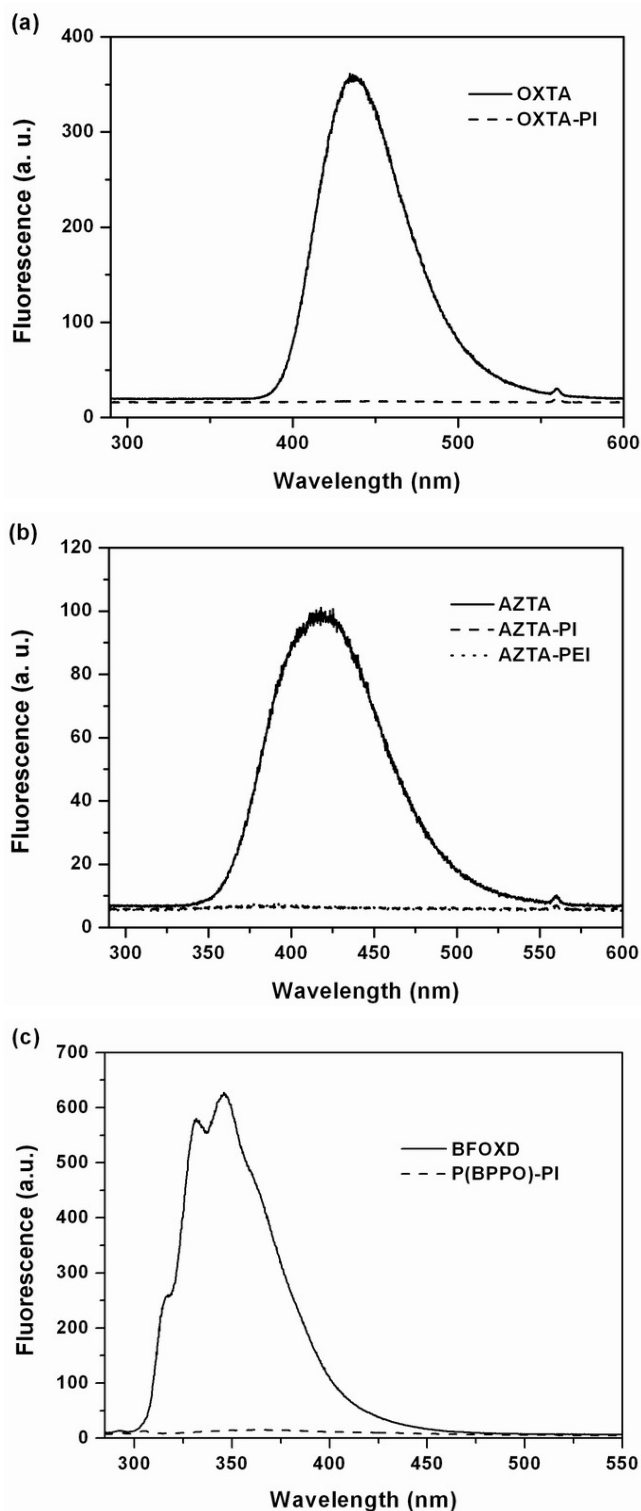
Figure 3.7 PL spectra of (a) OXTA-PI, (b) AZTA-PI and AZTA-PEI in chloroform, and (c) P(BPPO)-PI in DMAc. The corresponding monomers, OXTA, AZTA and BFOXD, were employed as the references. All the emission spectra were obtained with the excitation wavelength of 280 nm.

(Figure 3.7(b)). Similar to OXTA-PI, the fluorescence quenching effects in AZTA-PI and AZTA-PEI are also induced by CT process between the AZTA and phthalimide moieties. The similar fluorescence quenching phenomenon was also observed in P(BPPO)-PI when compared to its monomer BFOXD (Figure 3.7(c)).

3.3.2 Electrical Switching and Memory Effects of the Functional Polyimides

In this section, memory behaviors of all the functional polyimides are described, along with that of the previously reported TP6F-PI. As can be seen from the molecular structures of the polyimides (Figure 3.2), all the polyimides are based on TP6F-PI, which has the simplest structure, i.e., single bond-linked phthalimide and triphenylamine moieties. For the rest polyimides, the phthalimide moiety is preserved, while the triphenylamine moiety is replaced by some more complicated groups. Thus, this section is organized as follows, as shown in Figure 3.8. Firstly, the volatile and rewritable DRAM type memory effect of TP6F-PI is described. For OXTA-PI and AZTA-PI, an additional mediator group, i.e., oxadiazole and triazole groups, respectively, is incorporated between the phthalimide and triphenylamine moieties. Non-volatile write-once read-many times (WORM) type memory effect is observed for the OXTA-PI and AZTA-PI devices. In comparison to AZTA-PI, an additional phenoxyl group is incorporated between the phthalimide and triazole moieties in AZTA-PEI. A similar WORM type memory effects with larger switching threshold voltage is observed in the AZTA-PEI device. For P(BPPO)-PI, the same phenoxyl group is incorporated between the phthalimide and oxadiazole moieties while the

triphenylamine moiety is removed. This change in molecular structure results in a volatile static random access memory (SRAM) type memory effect in the P(BPPO)-PI device. In the following parts, electrical switching and memory effects of the five functional polyimides will be elaborated in detail, which are demonstrated by the *J-V* characteristics of their respective ITO/polymer/Al sandwich device.
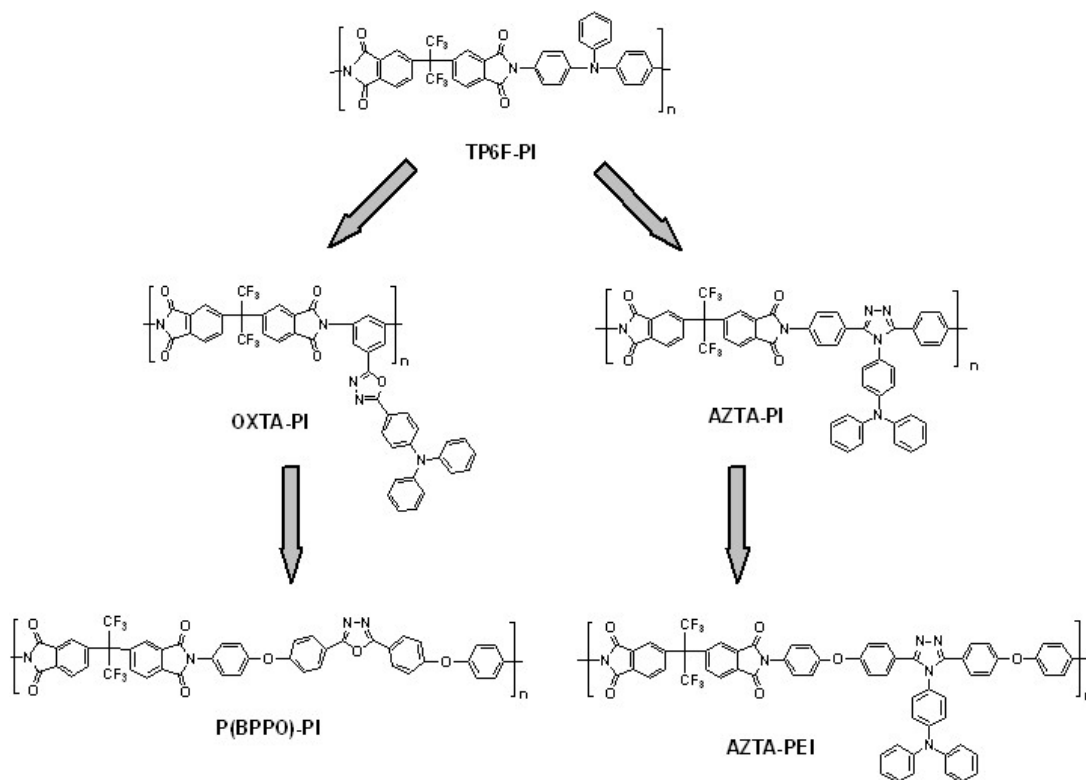
Figure 3.8 Differentiation of the structure scheme in the functional polyimides

Figure 3.9 shows the *J-V* characteristics of the TP6F-PI device under ambient conditions. In the 1st sweep from 0 to 4 V (with Al as the anode and ITO as the cathode), the device was initially in the low-conductivity (OFF) state and exhibited an abrupt increase in the current density at the switching threshold voltage of about 3.2 V, indicating the device transition from the OFF state to the high-conductivity (ON) state. This transition corresponds to the "writing" process in a digital memory. The device

remained in this high-conductivity state during the subsequent positive sweep (the 2nd sweep). The distinct conductivity states in the voltage range of 0 to 3.2 V allowed a voltage (e.g., 1.0 V) to read the OFF state or ON state. In the 3rd sweep from 0 to -4 V, an abrupt decrease in current density was observed at about -2.1 V, indicating the device transition from the ON state back to the OFF state. This transition is equivalent to the "erasing" process in a digital memory. The device remained in the OFF state after this erasing process, as indicated by the subsequent negative sweep (the 4th sweep). The OFF state can be further written to the ON state when the switching threshold voltage was reapplied, indicating that the memory device was rewritable (the 5th and 6th sweeps). The 7th sweep was conducted after turning off the power for about 1 min. It was found that the ON state had relaxed to the steady OFF state without an erasing process. The short retention time of the ON state indicated that the memory device was volatile. However, the device could be reprogrammed to the ON state (the 7th and 8th sweeps). The unstable ON state could be electrically sustained by a refreshing voltage pulse of 1 V (1 ms duration) in every 5 s (the 9th trace). The ability to write, read, erase and refresh the electrical states determines the DRAM behavior of the TP6F-PI device.
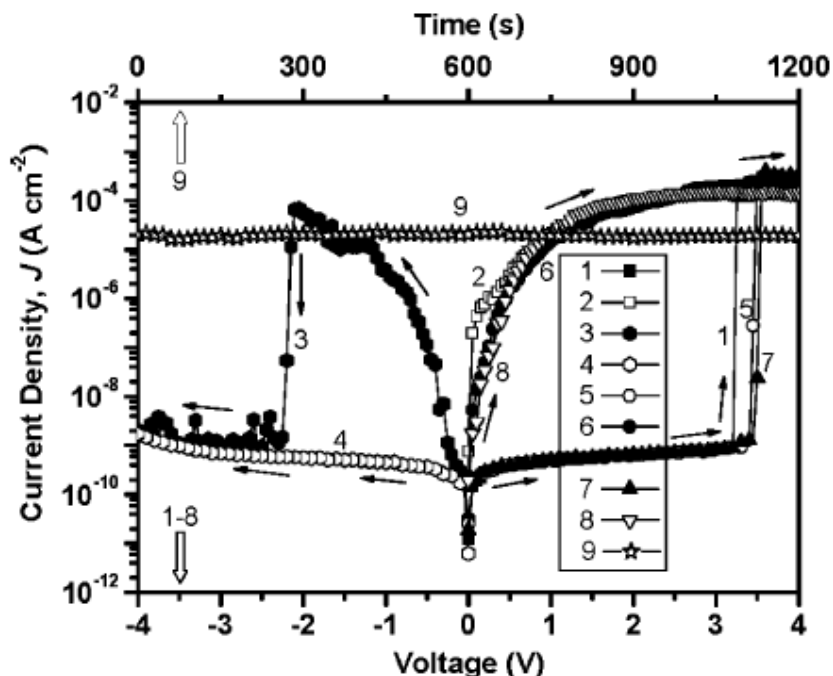
Figure 3.9 *J-V* characteristics of the ITO/TP6F-PI/Al device under ambient conditions. The sequence and direction of each sweep are indicated by the respective number and arrow. The 7th and 8th sweeps were conducted sequentially about 1 min after turning off the power. The ON state was sustained by a refreshing voltage pulse of 1 V (1 ms duration) in every 5 s (the 9th trace).

The variations in switching threshold voltages indicate that conformational relaxations of the polymer chains lack behind the corresponding change in electric field (Ling et al., 2007; Liu et al., 2009). Except for the slight variations in switching threshold voltages, the *J-V* characteristics and the ON-OFF switching behavior were found to have good reproducibility. In addition, the current magnitudes of the devices in both states showed linear dependence on the device area, indicating that the current density is independent on the device area. The rewritability, good reproducibility, volatile nature of the ON state, and area-independent current density, rule out the possibility of filament effect (Henisch and Smith, 1974), metal diffusion (Lim et al., 1998; Ma et al., 2000), and dielectric breakdown.

In comparison to TP6F-PI, an oxadiazole mediator group is incorporated between the phthalimide and triphenylamine moieties in OXTA-PI. Due to this change in molecular structure, non-volatile and non-rewritable WORM type memory effects were observed in the OXTA-PI device. Figure 3.10(a) shows the J-V characteristics of the OXTA-PI device under ambient conditions. During the 1st negative sweep (with Al as the cathode and ITO as the anode) from 0 to -3 V, the device switched from the initial OFF state to the ON state at about -1.8 V, with the ON/OFF current ratio on the order of 10^5 at -1 V. Afterwards, the device exhibited good stability in the ON state during the subsequent negative and positive sweeps. It did not return to the OFF state even after turning off the power (the 2nd sweep) or upon applying a reverse sweep (the 3rd sweep). The non-volatile and non-rewritable nature of the ON state determines the WORM type memory effects of the OXTA-PI device. In addition, the OXTA device can also exhibit electrical switching if the initial electrical sweep is positive. As shown in Figure 3.10(b), the device was initially swept positively from 0 to 3 V. An abrupt increase in the current density was observed at the switching threshold voltage of 1.8 V, which is comparable in magnitude to the negative switching threshold voltage of -1.8 V. The results indicate that the OXTA device can be switched bi-directionally, with comparable positive and negative switching threshold voltages.
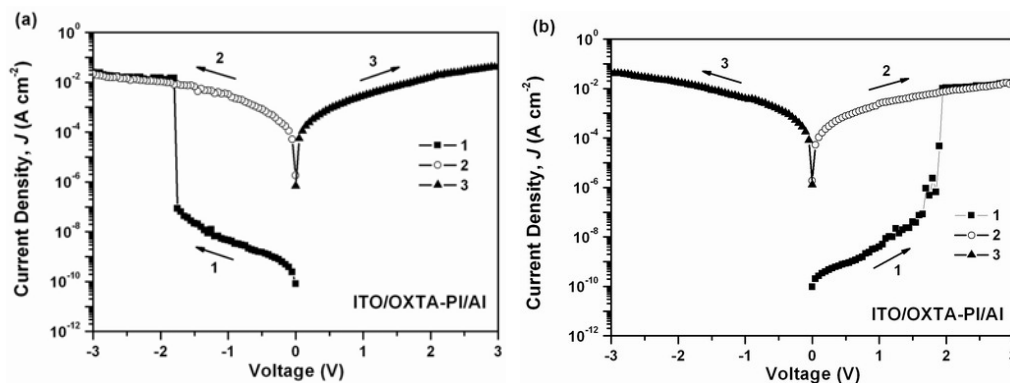
Figure 3.10 *J-V* characteristics of the ITO/OXTA-PI/Al device under ambient conditions. The sequence and direction of each sweep are indicated by the respective number and arrow. (a) Negative electrical switching of the OXTA-PI device. (b) Positive electrical switching of the OXTA-PI device.

In the AZTA-PI molecule, the oxadiazole mediator group is replaced by the triazole group. A similar WORM type memory effects was observed in the AZTA-PI device, except for the slightly higher switching threshold voltage (±2.5 V). As shown in Figure 3.11, the AZTA-PI device could be switched from the initial OFF state to the ON state bi-directionally, with the ON/OFF current ratio on the order of 10^5 at ±1 V. Afterwards, the device was able to retain in the ON state and could not be switched back to the OFF state by a reverse bias. The higher switching threshold voltage for AZTA-PI is probably attributed to the orthogonal conformation between the triazole and pendant triphenylamine moieties, which introduces a higher energy barrier for the intramolecular CT (Cacelli et al., 2006; Cacelli et al., 2007). A larger electrical field is thus required to overcome the energy barrier and trigger the electrical switching.
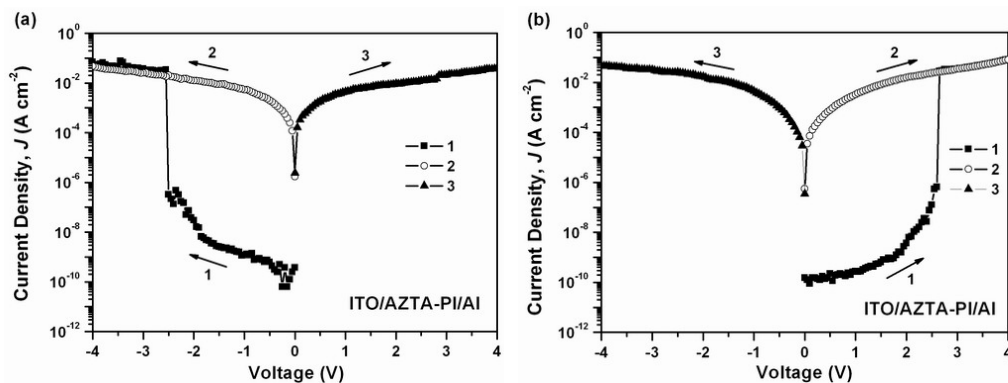
Figure 3.11 *J-V* characteristics of the ITO/AZTA-PI/Al device under ambient conditions. The sequence and direction of each sweep are indicated by the respective number and arrow. (a) Negative electrical switching of the AZTA-PI device. (b) Positive electrical switching of the AZTA-PI device.

In comparison to AZTA-PI, an additional phenoxyl group is introduced between the phthalimide and triazole moieties in AZTA-PEI. Similar to the OXTA-PI and AZTA-PI devices, the non-volatile and rewritable WORM type memory effect was also observed in the AZTA-PEI device. However, as the flexible phenoxyl group enhances intramolecular twisting of the AZTA-PEI molecule, the energy barrier for intramolecular CT is further increased. As a result, an even larger switching threshold voltage (±3.2 V) is observed for the AZTA-PEI device, as shown in Figure 3.12.
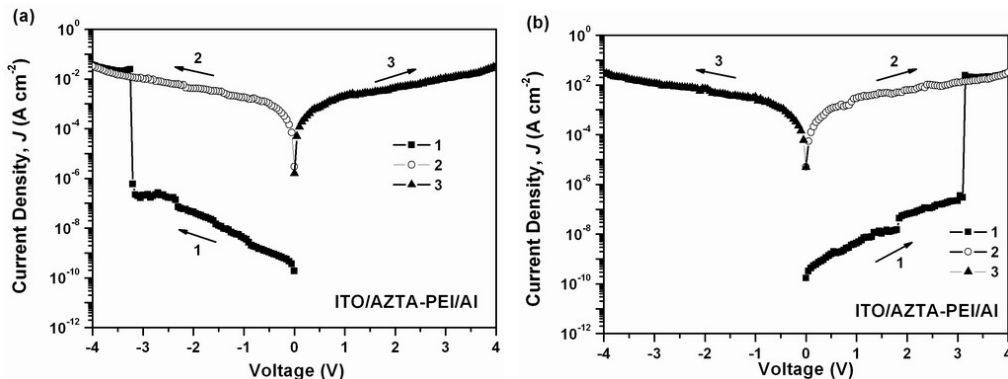
Figure 3.12 *J-V* characteristics of the ITO/AZTA-PEI/Al device under ambient conditions. The sequence and direction of each sweep are indicated by the respective number and arrow. (a) Negative electrical switching of the AZTA-PEI device. (b) Positive electrical switching of the AZTA-PEI device.

In comparison to OXTA-PI, an additional phenoxyl group is introduced into the P(BPPO)-PI molecule between the phthalimide and oxadiazole moieties, while the pendant triphenylamine moiety is removed. This change in molecular structure results in. a volatile SRAM type memory effect for the P(BPPO)-PI device. The J-V characteristics of the P(BPPO)-PI device under ambient conditions are shown in Figure 3.13. During the 1st positive sweep from 0 to 4 V, the device switched from the initial OFF state to the ON state at 2.3 V. The device remained in the ON state when the positive voltage sweep was repeated (the 2nd sweep). The memory device cannot be reset to the initial OFF state by the application of a reverse sweep (the 3rd sweep) and is thus irreversible. The ON state can be retained for a period of about 4 min after turning off the power, after which the device relaxed back to the OFF state, indicating the 'remanent', yet volatile, nature of the ON state. The device can be switched to the ON state again when the reverse threshold voltage was applied (-2.5 V in the 4th sweep). It remained in the ON state when the negative sweep was repeated (the 5th sweep). The results suggest that the P(BPPO)-PI device can be written bi-directionally at positive and negative switching threshold voltages of comparable magnitude. The 6th sweep was conducted about 4 min after turning off the power. The device was found to have relaxed to the OFF state again without any erasing process. The ON state can be re-programmed when the reverse threshold voltage (-2.4 V in the 6th sweep) was reapplied. The volatile ON state can be electrically sustained by a refreshing voltage pulse of -1 V (1 ms duration) in every 5 s (the 'rf' trace in Figure 3.13). The 'remanent', yet volatile, nature of the ON state, as well as the randomly

accessible ON and OFF states in the P(BPPO)-PI device, shares the common features

of a SRAM.
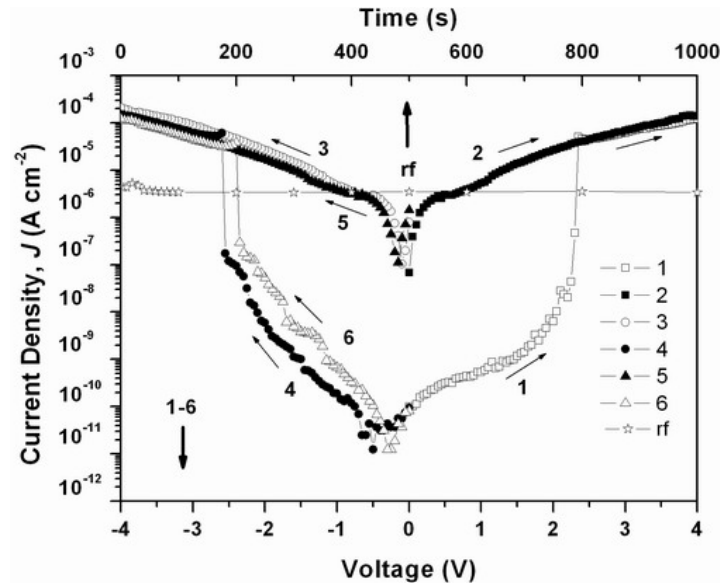
Figure 3.13 *J-V* characteristics of the ITO/P(BPPO)-PI/Al device under ambient conditions. The sequence and direction of each sweep are indicated by the respective number and arrow. The 4th and 6th sweeps were conducted about 4 min after turning off the power. The ON state was sustained by a refreshing pulse of -1 V (1 ms duration) in every 5 s, as shown by the "rf" trace.

3.3.3 Memory Performances of the Functional Polyimides

In addition to the memory effect, some other parameters, such as stability and read

cycles, are of equal importance to the performance of a memory device. All of these

parameters were evaluated under ambient conditions.
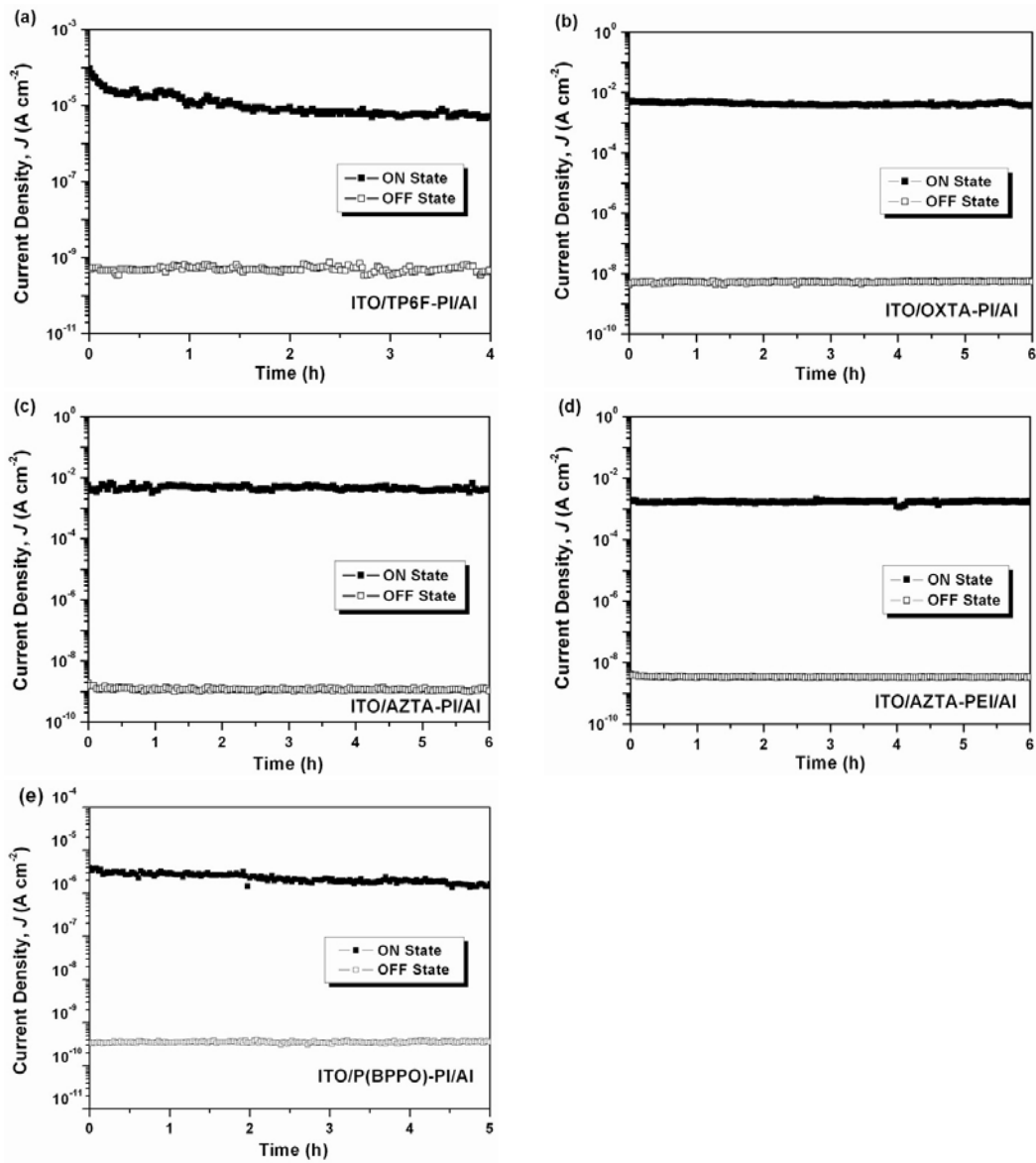
Figure 3.14 Effect of operation time on the ON and OFF state currents of (a) ITO/TP6F-PI/Al device, (b) ITO/OXTA-PI/Al device, (c) ITO/AZTA-PI/Al device, (d) ITO/AZTA-PEI/Al device, and (e) ITO/P(BPPO)-PI/Al device, under a constant stress of -1 V.

Fig. 3.14(a)~(e) show the effect of operation time on the stability of the polyimide devices. Under a constant stress of -1 V, no obvious degradation in current density was observed for both the ON and OFF state currents of the polyimide devices over several hours.
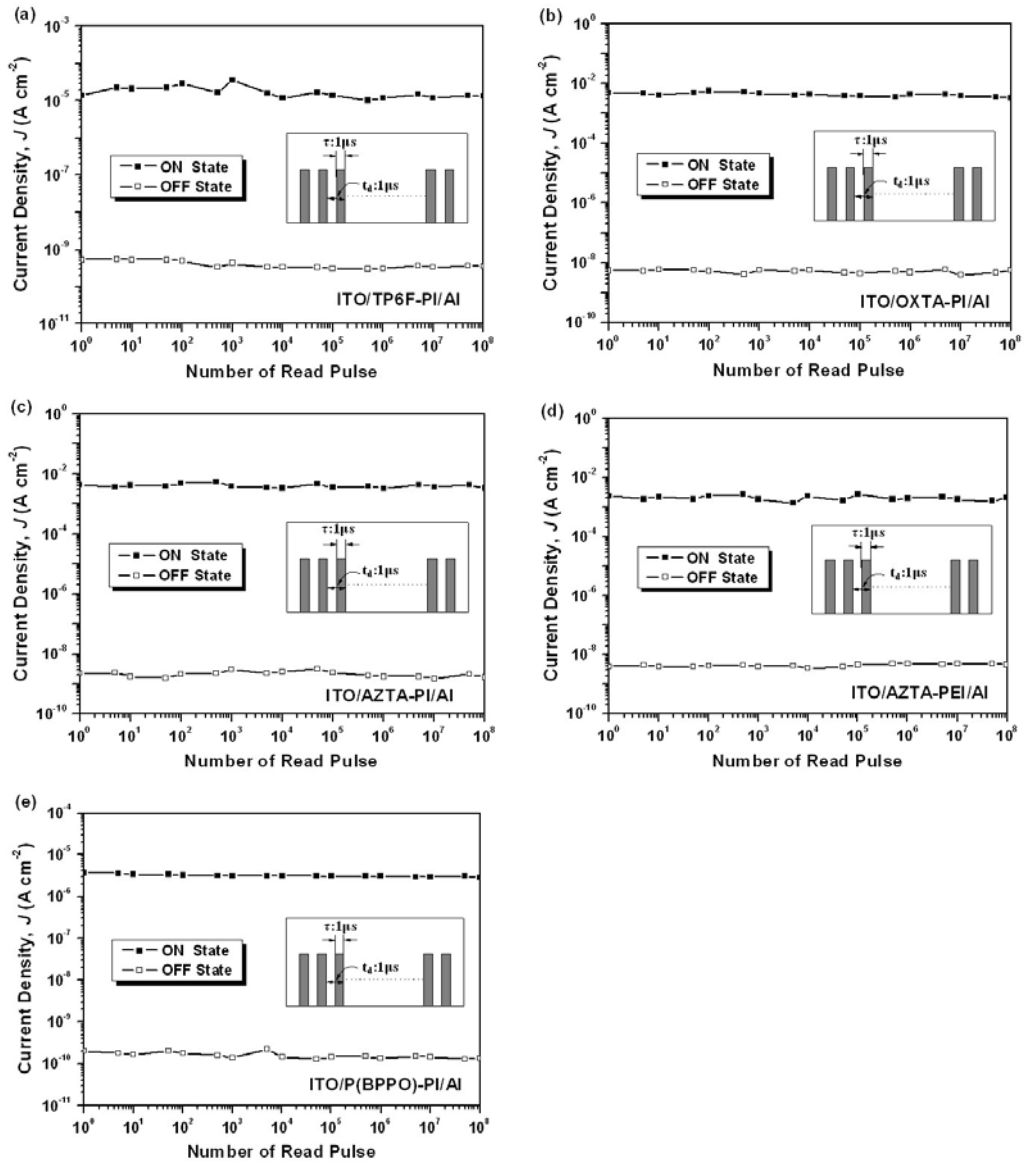
Figure 3.15 Effect of read pulses of -1 V on the ON and OFF state currents of (a) ITO/TP6F-PI/Al device, (b) ITO/OXTA-PI/Al device, (c) ITO/AZTA-PI/Al device, (d) ITO/AZTA-PEI/Al device, and (e) ITO/P(BPPO)-PI/Al device. The insets of (a) ~ (e) show the pulse used for measurement.

The effect of continuous read cycles on the ON and OFF states was also investigated, as shown in Figure 3.15. After more than one hundred million (10^8) read pulses of -1 V, no degradation in current densities was observed for both the ON and OFF state current, indicating that the memory device is stable and insensitive to the read pulses.
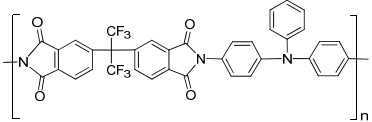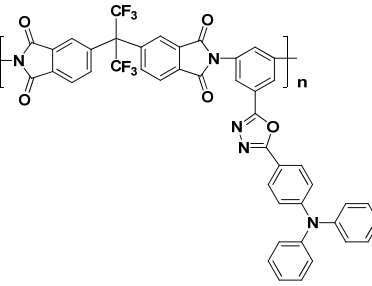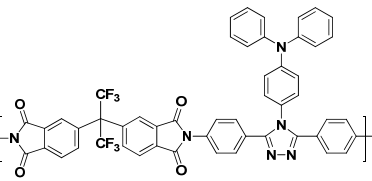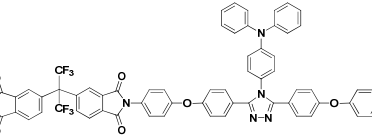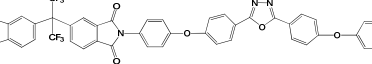
3.3.4 Switching Mechanism

To compare the memory effects of the functional polyimides clearly, the molecular structures of the five polyimides and their respective memory effects are summarized in Table 3.3. In the following sections, mechanisms underlying the various memory effects of the functional polyimides will be studied with the aid of molecular simulation and experimental characterizations. The variation in memory effects are found to arise from the different molecular conformations, polarities, and stability of the CT states, associated with the different electron donor moieties.

3.3.4.1 Switching Mechanism of TP6F-PI

To understand the switching behavior of the TP6F-PI memory device, the electronic properties of TP6F-PI in the ground state were studied by density function theory (DFT). Calculations of the molecular orbitals, dipole moment and ESP surface of the basic unit (BU), taking into account the two functional moieties, i.e., the phthalimide and triphenylamine moieties, were carried out at the B3LYP/6-31G(d) level with Gaussian 03 program package (Frisch et al., 2004). The trifluoromethyl groups of

Table 3.3 Summary of the memory effects of all the five functional polyimides

Material	Molecular Structure	Memory Effect	Write	Read	Erase	Refresh	Volatile
TP6F-PI		DRAM	√	√	√	+	√
OXTA-PI		WORM	√	√	×	o	×
AZTA-PI		WORM	√	√	×	o	×
AZTA-PEI		WORM	√	√	×	o	×
POXD-PI		SRAM	√	√	×	+	√

√ - Yes or able; × - No or unable; + - Necessary; o - Unnecessary

TP6F-PI were not included in the calculation because they probably do not significantly affect the electronic properties of the BU (LaFemina, 1989). The highest occupied molecular orbital (HOMO) and lowest unoccupied molecular orbital (LUMO) of the BU, as well as the plausible electronic transitions under excitations, are demonstrated in Figure 3.16. As can be seen, the HOMO is located mainly on the triphenylamine moieties, while the LUMO is located on the phthalimide moieties,

indicating that in the polyimide, the triphenylamine moiety acts as the electron donor and the phthalimide moiety acts as the electron acceptors. In addition, the two higher excited energy levels, LUMO2 and LUMO3, are located on the phthalimide and triphenylamine moieties, respectively. Under excitations with sufficient energy, electrons in the ground state of TP6F-PI can transit to the various excited states.

Figure 3.16 Molecular orbitals of the TP6F-PI BU and the plausible electronic transitions under the electric field

When the applied electric field reaches the switch-on voltage, some electrons at the HOMO of TP6F-PI accumulate sufficient energy and transit to LUMO3 within the triphenylamine to form the locally excited state. Excitation of the triphenylamine moiety leads to a decrease in ionization potential and thus facilitates the CT at the excited state. CT can occur indirectly from LUMO3 to LUMO2, then to LUMO

located at the phthalimide moieties, or directly from HOMO to LUMO, to form the conductive CT state. Under the electric field, the generated holes can delocalize to the conjugated triphenylamine groups, giving rise to an open channel in the HOMO of TP6F-PI for the charge carriers (holes) to migrate through. As a result, the current density increases rapidly to switch the device to the ON state. The conduction process dominated by hole migration through the HOMO is consistent with the widely known applications of aromatic polyimides with donor moieties as hole transporting layers in electroluminescence devices (Wang et al., 1998; Wang et al., 2000). As the TP6F-PI chains are non-conjugated, charge carriers probably do not move along the polymer backbone. Instead, they probably hop between neighboring triphenylamine moieties (either in the same or neighboring polymer chains) (Freilich, 1987; Lee et al., 1998; Oh-e et al., 2002; Grazulevicius et al., 2003).

However, the ON state of TP6F-PI could not be sustained due to the limited charge delocalization in the propeller-like triphenylamine moieties (Chen et al., 2007). A reverse bias of about -2.1 V, or removal of the electric field, can dissociate the CT complex and return the device to the initial OFF state. A volatile and rewritable ON state is thus observed in the TP6F-PI device.

Molecular simulation of TP6F-PI in the excited state was also carried out to further demonstrate the above CT process. Optimized geometry, ESP surface, and dipole moment of the TP6F-PI BU in the excited state were studied at the CIS/6-31G(d)

level with the Gaussian 03 program package. The corresponding electronic properties

of BU in the ground state were employed as the reference. Figure 3.17 summarizes

the molecular simulation results of both the ground and excited states. From the ESP

surfaces, it can be seen that TP6F-PI at both states consist mainly of positive ESP

region, with some minor negative ESP regions arising from the sp^2 hybridized O

atoms in the phthalimide group. As ESP is the potential energy of a proton at a

particular location of a molecule, it can reflect the local electron density. Accordingly,

the negative ESP regions in TP6F-PI suggest concentrated local electron densities

around the phthalimide moiety which possess certain electron-withdrawing ability

(Aleksandrova et al., 2001). In comparison to TP6F-PI in the ground state, TP6F-PI in

the excited state exhibits larger negative regions around the phthalimide moiety,

indicating that under excitation, electron will transfer to the phthalimide moiety from

other parts in the molecule. This electronic process is consistent with the electric field

induced electron transfer process from the triphenylamine moieties to the phthalimide

moieties, as mentioned above. The electron transfer process can also supported by the

enhanced dipole moment of TP6F-PI in the excited state (2.34 Debye) in comparison

to that in the ground state (2.06 Debye) (Kishore et al., 2008).

Following the above electron transfer process, the TP6F-PI molecule also undergoes a

small conformational change under the applied electric field, as indicated by the

different optimized geometries of the BU in the ground and excited states (Figure

3.17). Due to the steric effect of the carbonyl groups in the phthalimide moieties,

TP6F-PI exhibits a pre-twisted conformation, with the dihedral angle between the phthalimide and triphenylamine moieties (θ_I) being 42.1°. Upon excitation, this dihedral angle undergoes a slight increase to 43.9°. However, when some mediator group, such as the oxadiazole, triazole or phenoxyl group, is incorporated into the polyimide molecule, much more significant molecular twisting will be observed, with change in dihedral angle between the phthalimide plane and the adjacent benzene ring being 13.8° ~ 17.4°, which will be demonstrated by the molecular simulation results of OXTA-PI, AZTA-PI, AZTA-PEI and P(BPPO)-PI in the following sections. The larger chain twisting in these polyimide molecules is probably due to the fact that incorporation of the mediator group increases the free volume in the polymer matrix (Brar and Markanday, 2005), making the polymer chain more flexible and easier to undergo conformational change under the electric field. For the TP6F-PI molecule, the relatively small dihedral angle in the excited state cannot place a sufficient energy barrier for dissociation of the CT complexes (Cacelli et al., 2006). As a result, the conductive CT complexes can be dissociated either by a reverse bias or turning off the power. In addition, due to the absence of any mediator group, the dipole moment of the TP6F-PI molecule is relatively small (2.06 Debye for the ground state and 2.34 Debye for the excited state), which cannot hold the conductive CT state effectively. Thus, the volatile and rewritable DRAM type memory effect was observed in the TP6F-PI device.
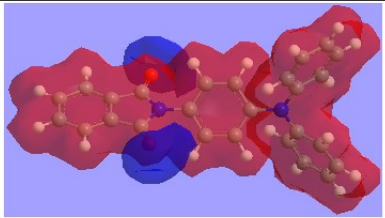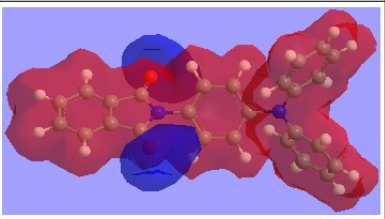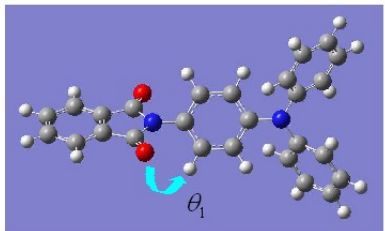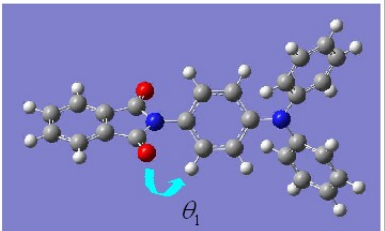
Properties	Ground State	Excited State
Dipole Moment	2.06 Debye	2.34 Debye
ESP Surface		
Optimized Geometry	θ_1	θ_1
Dihedral Angle	$\theta_1 = 42.1°$	$\theta_1 = 43.9°$

Figure 3.17 Dipole moments, ESP surfaces, optimized geometries of the TP6F-PI BU, and dihedral angles (θ_1) between the phthalimide and adjacent benzene ring planes in the ground and excited state. For ESP surfaces, the positive ESP regions are in red, whereas the negative ESP regions are in blue.

3.3.4.2 Switching Mechanism of OXTA-PI

The electronic properties of OXTA-PI were also studied at the B3LYP/6-31G(d) level with the Gaussian 03 program package. The HOMO and LUMOs of the BU, as well as the plausible electronic under excitations, are demonstrated in Figure 3.18. The HOMO of OXTA-PI is located mainly on the triphenylamine moieties, while the first LUMO (LUMO1) is located on the phthalimide moieties, indicating that in this copolymer, the triphenylamine moiety acts as the main electron donors and the phthalimide moiety acts as the electron acceptors. In addition to LUMO1, the two higher LUMOs, i.e., LUMO2 and LUMO3, distribute on the oxadiazole moieties,

suggesting that the oxadiazole moieties can serve as the mediators to facilitate the intramolecular CT. Upon excitation, electrons at HOMO can transit locally to LUMO4 on the triphenylamine moieties, and then relax to LUMO1 via the intermediate LUMO2 and LUMO3, or transit directly to LUMO1, giving rise to the CT state. Under the electric field, the generated holes can delocalize among the triphenylamine donor moieties, generating an open channel in the HOMO for the charge carriers (holes) to migrate through. Thus, the current density increases rapidly to switch the device to the high-conductivity (ON) state.
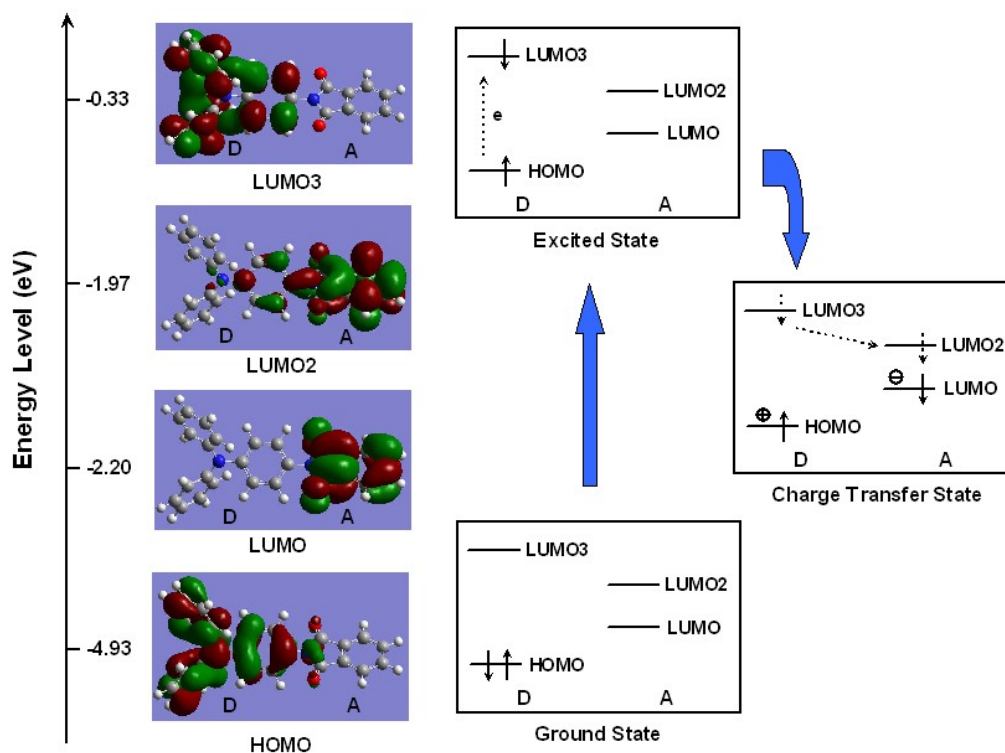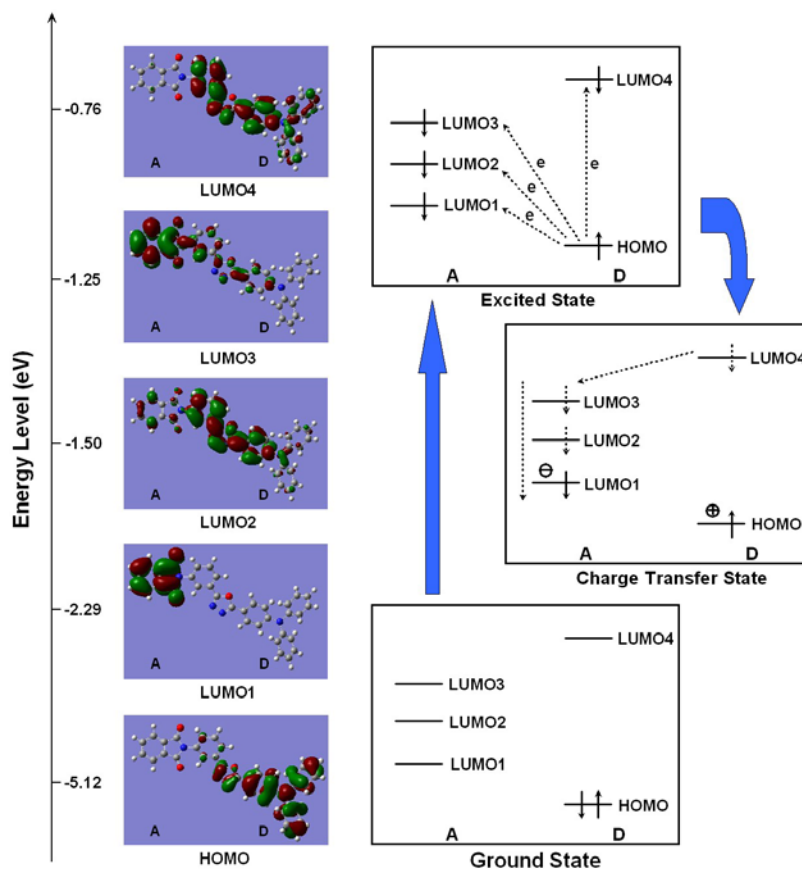

Figure 3.18 Molecular orbitals of the OXTA-PI BU and the plausible electronic transitions under the electric field

The possibility that the electrical switching arises from charge (hole) injection process

can be eliminated by the symmetrical bi-directional switching, with comparable positive and negative switching threshold voltages, in the ITO/OXTA-PI/Al device (Figure 3.10). If the hole injection process plays the dominant role, the device should exhibit asymmetrical switching or uni-directional switching phenomenon (Ling et al., 2007) due to the difference in energy barriers for hole injection under different applied biases (0.84 eV for hole injection into the HOMO from Al under positive electrical sweep and 0.32 eV for hole injection into the HOMO from ITO under negative electrical sweep).

Molecular simulation of OXTA-PI in the excited state was also carried out to further elucidate the above CT process, as shown in Figure 3.19. In comparison to TP6F-PI, the negative ESP surfaces of OXTA-PI also arise from the sp^2 hybridized N atoms in the oxadiazole group, in addition to the sp^2 hybridized O atoms in the phthalimide group. Upon excitation, the negative ESP regions around the phthalimide group become larger while the negative region around the oxadiazole becomes smaller, indicating electron transfer from the oxadiazole moiety to the phthalimide moiety. This electronic process is consistent with the electric field induced CT from the oxadiazole-substituted triphenylamine donor moieties to the phthalimide acceptor moieties, as shown in Figure 3.18. The electron transfer process can also be supported by the enhanced dipole moment of OXTA-PI in the excited state (5.39 Debye) in comparison to that in the ground state (4.00 Debye).
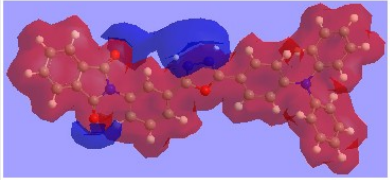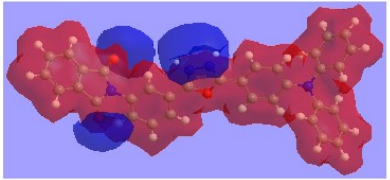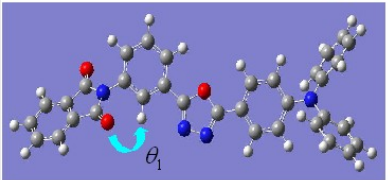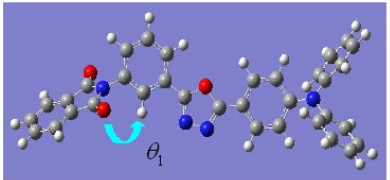
Properties	Ground State	Excited State
Dipole Moment	4.00 Debye	5.39 Debye
ESP Surface		
Optimized Geometry		
Dihedral Angle	$\theta_1 = 42.2°$	$\theta_1 = 58.8°$

Figure 3.19 Dipole moments, ESP surfaces, optimized geometries of the OXTA-PI BU, and dihedral angles (θ_1) between the phthalimide and adjacent benzene ring planes in the ground and excited state. For ESP surfaces, the positive ESP regions are in red, whereas the negative ESP regions are in blue.

In comparison to TP6F-PI, OXTA-PI has larger free volumes in the polymer matrix, due to presence of the oxadiazole mediator and pendant triphenylamine moiety. As a result, the OXTA-PI molecule is easier to undergo chain twisting under the electric field, following the above CT process. This conformational change can be demonstrated by the different optimized geometries of the OXTA-PI BU in the ground and excited states. Upon excitation, the dihedral angle between the phthalimide plane and the adjacent benzene ring (θ_1) is found to exhibit an increase from 42.2° to 58.8°, which is much more significant than that occurs in the TP6F-PI molecule. The more twisted conformation in the excited state decouples the triphenylamine-substituted oxadiazole donor and phthalimide acceptor moieties, and generates an energy barrier which prevents dissociation of the CT complexes. As a result, the conductive CT

states can be sustained, and the ON state is retained. Even a reverse bias of the same magnitude cannot overcome the energy barrier and dissociate the CT complexes. In addition, the relatively large excited state dipole moment (5.39 Debye) of OXTA-PI can also help to stabilize the CT state. Thus, non-volatile and non-rewritable WORM type memory effect was observed in the OXTA-PI device.

Forrest et al. have reported WORM memory devices based on poly(ethylene dioxythiophene) (PEDOT):polystyrene sulfonic acid (PSS) films (Möller et al., 2003; Smith and Forrest, 2004). The switching of the PEDOT:PSS film from the ON state to the OFF state was explained by a simple un-doping process. Thermal effects arising from Joule heating play a significant role in destabilizing the PEDOT:PSS complex formed by CT interaction (Smith and Forrest, 2004). To further understand the switching phenomenon in OXTA-PI, thermal effects on the OXTA device were investigated. The switching behavior of a device before and after heating is shown in Figure 3.20(a). The device was initially in the OFF state and exhibited abrupt switching to the ON state at -1.8 V (the 1st sweep). Afterwards, it retained in the ON state during the subsequent negative and positive sweeps (the 2nd and 3rd sweeps). However, after being heated at 150°C for 10 min under vacuum and then cooled to room temperature, the device was found to have relaxed from the ON state back to the OFF state (the 4th sweep). This switch-off phenomenon is probably because at elevated temperature, the polyimide molecule becomes more flexible and tends to relax to its initial less twisted conformation. As a result, the energy barrier for

dissociation of the CT complexes disappears, and electrons transfer back to the donor moieties from the acceptor moieties, switching the device back to the OFF state. This phenomenon is similar to the conductivity decrease by thermal un-doping of PEDOT at elevated temperature reported previously (Pei et al., 1994).

In addition, the ON state current at different testing temperatures was also studied. As shown in Figure 3.20 (b), the ON state current density increases slightly with increase in temperature. According to filamentary theory (Segui et al., 1976; Henisch and Smith, 1974), the ON state current exhibits metallic current-voltage characteristics and will increase as the temperature is decreased. Thus, the filamentary conduction effect can be excluded from the electrical switching phenomena in the present device.
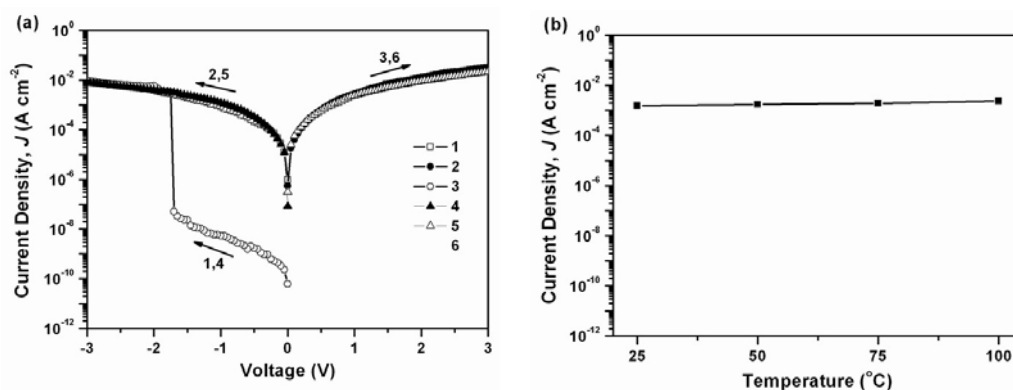
Figure 3.20 (a) *J-V* characteristics of an ITO/OXTA-PI/Al device. The sequence and direction of each sweep are indicated by the respective number and arrow. The 4th ~ 6th sweeps were conducted sequentially after heating the device at 150°C for 10 min under vacuum. (b) ON state current density measured at -1 V under different temperatures.

3.3.4.3 Switching Mechanism of AZTA-PI

The molecular orbitals, dipole moment, and ESP surface of the AZTA-PI BU, were

also studied with the Gaussian 03 software. The HOMO and LUMOs of AZTA-PI, as well as the plausible electronic transition under the electric field, are demonstrated in Figure 3.21.
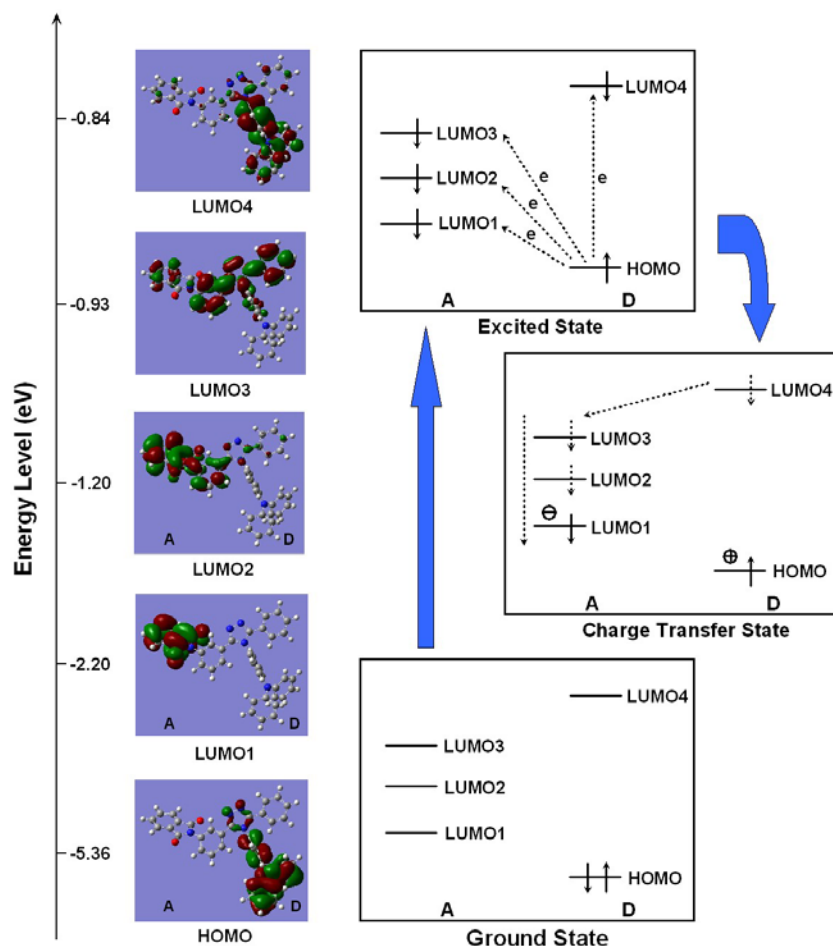
Figure 3.21 Molecular orbitals of the AZTA-PI BU and the plausible electronic transitions under the electric field

Similar to OXTA-PI, the HOMO and LUMO1 of AZTA-PI are also located on the triphenylamine and phthalimide moieties, respectively, indicating that these two moieties act as the electron-donor and -acceptor, respectively. The triazole group serves as the mediator to facilitate the intramolecular CT, similar to the effect of oxadiazole group in OXTA-PI. Upon excitation, electron transfer occurs from HOMO

to LUMO1, either directly or indirectly via the intermediate LUMO2, LUMO3 and LUMO4, giving rise to the conductive CT state. This electronic transition can be supported by the enhanced negative ESP region around the phthalimide group and diminished negative ESP region around the triazole group, as well as the increased dipole moment, in the excited AZTA-PI molecule, as shown in Figure 3.22.
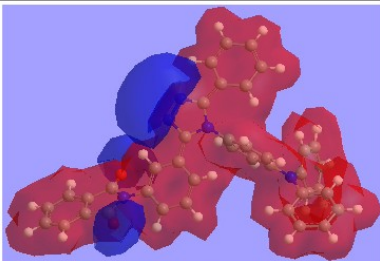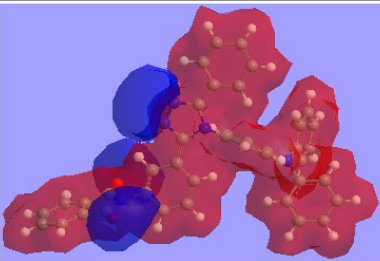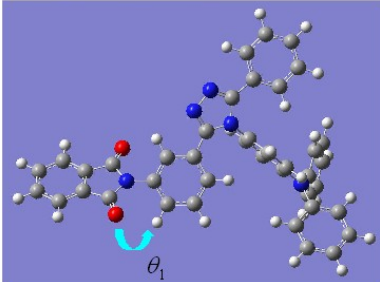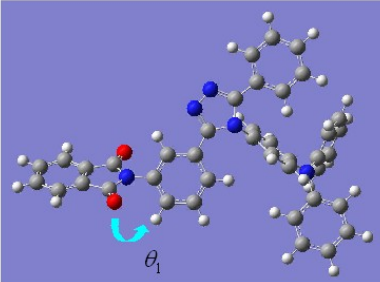
Properties	Ground State	Excited State
Dipole Moment	6.05 Debye	8.39 Debye
ESP Surface		
Optimized Geometry		
Dihedral Angle	$\theta_1 = 42.9°$	$\theta_1 = 60.3°$

Figure 3.22 Dipole moments, ESP surfaces, optimized geometries of the AZTA-PI BU, and dihedral angle (θ_1) between the phthalimide and adjacent benzene ring planes in the ground and excited state. For ESP surfaces, the positive ESP regions are in red, whereas the negative ESP regions are in blue.

Following the above CT process, the AZTPA-PI also undergoes chain twisting under the applied electric field, as indicated by the increase in dihedral angle between the phthalimide plane and the adjacent benzene ring (θ_1) from 42.9° in the ground state to

60.3° in the excited state (Figure 3.22). The enhanced dihedral angle in the excited state generates an energy barrier for dissociation of the CT complexes, and results in the non-rewritable feature of the ON state. In addition, the large excited state dipole moment (8.39 Debye) can stabilize the conductive CT state effectively, making the ON state non-volatile.

As shown in Figure 3.10 and 3.11, the AZTA-PI device exhibits a larger switching threshold voltage (±2.5 V) than that of the OXTA-PI device (±1.8 V). As the oxadiazole and triazole groups possess comparable ionization potential (*IP*) and electron affinity (*EA*) (Chen and Chen, 2005; Jansson et al., 2006), their effects on the intramolecular CT are similar, ruling out their possibility to affect the switching threshold voltage. As indicated by the optimized geometries of OXTA-PI and AZTA-PI (Figure 3.19 and 3.22), the main difference consists in the torsional angles between the pendant triphenylamine moiety and the oxadiazole/triazole moiety. The larger torsional angle (85.7°) in AZTA-PI in comparison to that (1.7°) in OXTA-PI can place a much higher energy barrier for the intramolecular CT, accounting probably for the larger switching threshold voltage of the AZTA-PI device. To figure out the above assumption, molecular orbitals and potential energies were calculated for the oxadiazole-triphenylamine (OXZ-TPA) and triazole-triphenylamine (TAZ-TPA) modal materials (molecular structures shown in Figure 3.23), of which the dihedral angles were set the same as those of the corresponding segments in OXTA-PI (1.7°) and AZTA-PI (85.7°), respectively. Another triazole-triphenylamine modal material

(TAZ-TPA-R) with the same dihedral angle as that of OXZ-TPA (1.7°) was studied as the reference. As shown in Figure 3.23, OXZ-TPA and TAZ-TPA-R with similar planar conformation are found to possess comparable HOMO and LUMO energy levels and thus the HOMO-LUMO energy gaps (3.66 eV and 3.67 eV, respectively), further suggesting similarity in the electronic properties of the oxadiazole and triazole groups. The HOMO-LUMO energy gap of TAZ-TPA (4.42 eV), however, is much larger, due to its nearly orthogonal conformation. As the HOMOs of the modal materials are mainly located at the triphenylamine moiety, and the LUMOs are located at the oxadiazole/triazole moiety, the HOMO-LUMO energy gap corresponds to the energy barrier for intramolecular CT between the triphenylamine donor and the oxadiazole/triazole acceptor moieties. Accordingly, the larger HOMO-LUMO energy gap of TAZ-TPA indicates that a larger energy is required to trigger the corresponding intramolecular CT. Thus, a larger switching threshold voltage is observed in the AZTA-PI device. In addition, the HOMO-LUMO energy gap of TAZ-TPA is 0.76 eV larger than that of OXZ-TPA, which is consistent with the 0.7 V larger switching threshold voltage of the AZTA-PI device in comparison to that of the OXTA-PI device.
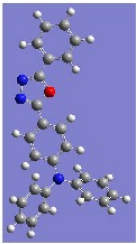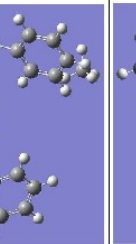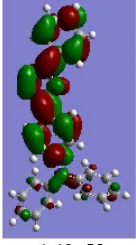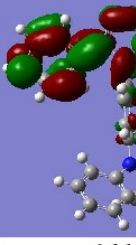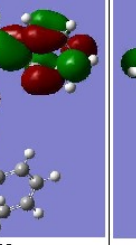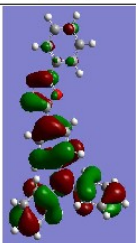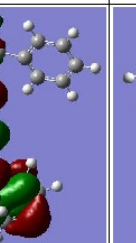
Properties	OXZ-TPA	TAZ-TPA	TAZ-TPA-R
Molecular Structure			
LUMO	-1.48 eV	-0.96 eV	-1.43 eV
HOMO	-5.14 eV	-5.38 eV	-5.10 eV

Figure 3.23 Molecular orbitals and energy levels of the OXZ-TPA, TAZ-TPA and TAZ-TPA-R modal materials. The dihedral angle between the triphenylamine and oxadiazole/triazole moieties in OXZ-TPA and TAZ-TPA are set the same as those of the corresponding segments in OXTA-PI and AZTA-PI, respectively, while the dihedral angle of TAZ-TPA-R is set the same as that of OXZ-TPA.

3.3.4.4 Switching Mechanism of AZTA-PEI

In comparison to AZTA-PI, the AZTA-PEI molecule has a similar molecular structure,

except for an additional phenoxyl group between the triazole and phthalimide

moieties. The similarity in the molecular structures determines that the AZTA-PEI

device exhibits a similar WORM type memory effect as the AZTA-PI device, as

shown in Figure 3.12. In addition, similar electronic excitations are believed to occur

in the AZTA-PEI molecule under the electric field, as demonstrated in Figure 3.24. This electric field-induced CT process can also be supported by changes in the dipole moment and the size of negative ESP regions upon excitation (Figure 3.25).
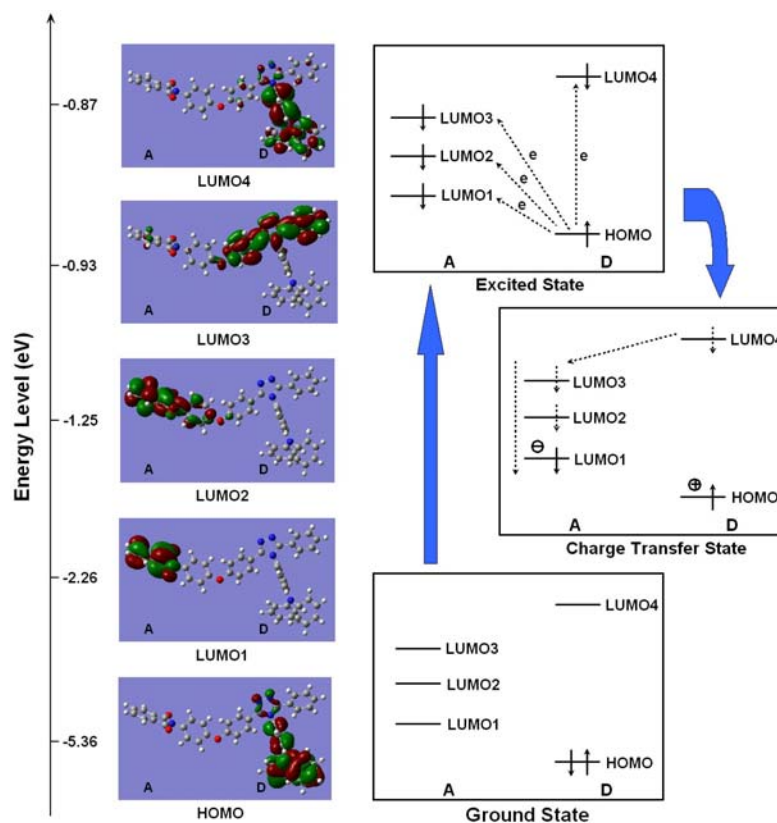
Figure 3.24 Molecular orbitals of the AZTA-PEI BU and the plausible electronic transitions under the electric field

Similar to OXTA-PI and AZTA-PI, the AZTPA-PEI molecule also undergoes electric field-induced conformation twisting, following the above CT process. As demonstrated in Figure 3.25, the dihedral angles between the phthalimide plane and the adjacent benzene ring (θ_1) increases from 41.1° to 54.9° upon excitation. Moreover, an additional twisting between the phenoxyl plane and the triazole plane is also observed, with the dihedral angle (θ_2) increasing from 66.7° in the ground state to

72.8° in the excited state. The more twisted conformation in the excited state helps to stabilize the conductive CT (ON) state.
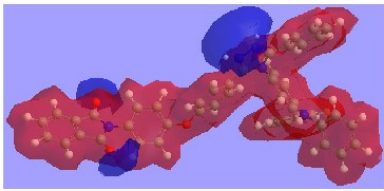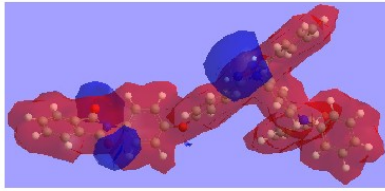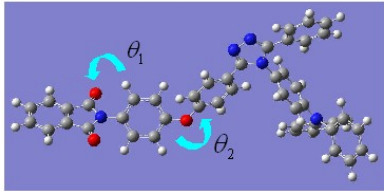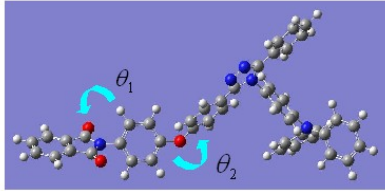
Properties	Ground State	Excited State
Dipole Moment	5.04 Debye	6.61 Debye
ESP Surface		
Optimized Geometry		
Dihedral Angle	$\theta_1 = 41.1°$, $\theta_2 = 66.7°$	$\theta_1 = 54.9°$, $\theta_2 = 72.8°$

Figure 3.25 Dipole moments, ESP surfaces, and optimized geometries of the AZTA-PEI BU in the ground and excited states. θ_1 denotes the dihedral angle between the phthalimide and adjacent benzene ring planes, and θ_2 denotes the dihedral angle between the triazole and adjacent benzene ring planes. For ESP surfaces, the positive ESP regions are in red, whereas the negative ESP regions are in blue.

The only difference between the memory effects of AZTA-PI and AZTA-PEI consists in their switching threshold voltages, with the value of AZTA-PEI (±3.2 V) being larger than that of AZTA-PI (±2.5 V). The larger switching threshold voltage of AZTA-PEI probably arises from incorporation of the additional flexible phenoxyl group, which increases the twisting degree of the molecules and introduces an additional energy barrier for the intramolecular CT. As a result, a larger bias is required to overcome the extra energy barrier, resulting in the larger switching threshold voltage for the AZTA-PEI device.

3.3.4.5 Switching Mechanism of P(BPPO)-PI

In comparison to OXTA-PI, an additional phenoxyl group is introduced into the P(BPPO)-PI molecule between the phthalimide and oxadiazole moieties, while the pendant triphenylamine moiety is removed. This change in molecular structure results in a significant change in the memory effect. Different from the nonvolatile WORM type memory effect of OXTA-PI, P(BPPO)-PI exhibits a volatile SRAM type memory effect, as shown in Figure 3.13. In order to better understand this novel memory effect, molecular simulation and experimental characterization were carried out to study the electronic properties of P(BPPO)-PI.

Figure 3.26 demonstrates the HOMO and LUMOs of the P(BPPO)-PI BU, taking into account the phthalimide, 2,5-bis(4-phenoxyphenyl)-1,3,4-oxadiazole (BPPO), and phenoxyl mediator moieties. As can be seen, the HOMO is located mainly on the BPPO moieties, while the first LUMO (LUMO1) is located on the phthalimide moieties, indicating that in the copolymer, the BPPO moiety acts as the electron donor and the phthalimide moiety acts as the electron acceptor. In addition, the two higher excited energy levels (LUMO2 and LUMO3) are distributed over all the BU. Under excitations, similar electronic excitations occur in the P(BPPO)-PI molecule as those happen in the above OXTA-PI, AZTA-PI and AZTA-PEI molecules. When the applied electric field reaches the switch-on voltage, some electrons at the HOMO of P(BPPO)-PI accumulate sufficient energy and transit to the LUMO2 and LUMO3, due to overlapping of the HOMO with these LUMOs at the oxadiazole moieties, to

result in the excited state. As the LUMO2 and LUMO3 are distributed over the entire BU, the excited electrons on the oxadiazole moieties can delocalize readily to the phthalimide moieties, which has a higher electron affinity and where they can relax to the lowest excited singlet state via internal conversion. As a result, CT complexes between the BPPO and phthalimide moieties are formed. In addition to the indirect CT process, CT can also occur via direct electron transition from the HOMO to the LUMO. As the CT state is conductive, the current density increases rapidly to switch the P(BPPO)-PI device to the ON state. Although the oxadiazole derivatives are widely used as electron-transporting materials in electroluminescence devices, they do not possess high hole-blocking properties (Kidoe et al., 1994). It is reported that holes can migrate successfully through a 2-(4-biphenylyl)-5-(4-*tert*-butylphenyl)-1,3,4-oxadiazole (PBD) film with thickness as high as 30 nm (Kido et al., 1993). Thus, it is reasonable that the BPPO moieties in P(BPPO)-PI can act as a hole-transporting pathway, albeit not as efficient as some strong electron donor species.
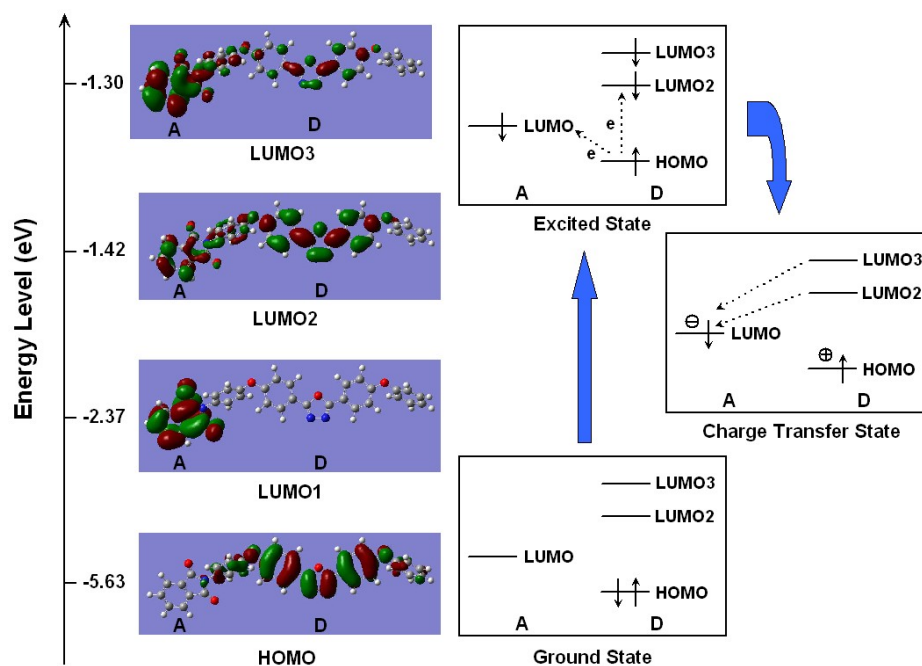
Figure 3.26 Molecular orbitals of the P(BPPO)-PI BU and the plausible electronic transitions under the electric field

Molecular simulation of P(BPPO)-PI in the excited state was also carried out to study the above electronic transition. As shown in Figure 3.27, upon excitation, the dipole moment of the P(BPPO)-PI molecule was increased, and the negative ESP region at the phthalimide group was enhanced, further supporting the electronic transfer from the oxadiazole donor moiety to the phthalimide acceptor moiety via the phenoxyl mediator (Huang et al., 2002). Thereafter, the P(BPPO)-PI molecule undergoes electric field-induced conformation twisting, similar to those happen in the OXTA-PI, AZTA-PI and AZTA-PEI molecules. As shown in Figure 3.27, upon excitation, the dihedral angle between the phthalimide plane and the phenoxyl plane (θ_1) is found to increase from 40.1° to 54.6°, and the dihedral angle between the phenoxyl plane and the oxadiazole plane (θ_2) increases from 67.1° to 72.7°. The increased torsional displacement between the oxadiazole and phthalimide moieties in the excited state

reduces the effective conjugation of the π electrons between neighboring aromatic moieties, and generate an intramolecular energy barrier for dissociation of the CT complexes. As a result, the conductive CT state can be sustained, and the ON state is retained. Even a reverse bias cannot dissociate the CT complexes and reset the ON state to the initial OFF state. Nevertheless, the polymer relaxes to its original conformation sometime after removal of the applied electric field. The dihedral angles between the component aromatic moieties decrease to their initial levels and the energy barrier disappears (Cacelli et al., 2006). As determined from the molecular simulation results, the dipole moment of P(BPPO)-PI in the excited state is only 3.06 Debye, which is probably not high enough to retain the CT states. As a result, the conductive CT states are not stable and dissociate after sometime upon removal of the electric field, resulting in the eventual loss of the ON state and the volatile nature of the memory effect.
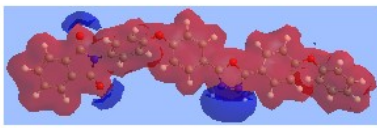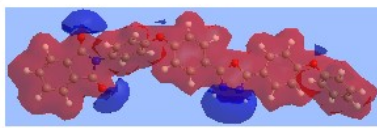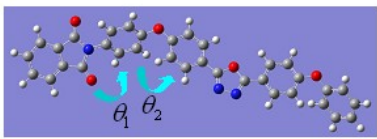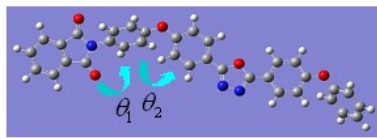
Properties	Ground State	Excited State
Dipole Moment	2.82 Debye	3.06 Debye
ESP Surface		
Optimized Geometry		
Dihedral Angle	$\theta_1 = 40.1°$, $\theta_2 = 67.1°$	$\theta_1 = 54.6°$, $\theta_2 = 72.7°$

Figure 3.27 Dipole moments, ESP surfaces, and optimized geometries of the P(BPPO)-PI BU. θ_1 denotes the dihedral angle between the phthalimide and adjacent benzene ring planes, and θ_2 denotes the dihedral angle between the oxadiazole and adjacent benzene ring planes. For ESP surfaces, the positive ESP regions are in red, whereas the negative ESP regions are in blue.

To elucidate the above conformation-coupled CT processes experimentally, UV-visible absorption spectrum of the solid state P(BPPO)-PI film with and without the applied electric field was studied. A liquid Hg droplet was employed as the top electrode in place of the Al contact. After an electrical sweep from 0 to -4 V (with ITO as the ground electrode), the Hg electrode was removed and the resultant UV-visible absorption spectrum was compared with the pristine spectrum before the electrical sweep. In Figure 3.28, OFF-1, ON-1 and OFF-2 denote, respectively, the absorption spectra of P(BPPO)-PI film spin-coated on ITO substrate measured before, immediately after, and 3 h after the electrical sweep. The P(BPPO)-PI film was found to exhibit a broad absorption band between 500 nm ~ 700 nm and an absorption shoulder at 360 nm (OFF-1 spectrum), which are associated, respectively, with the absorption of CT complexes in the ground state (Benson-Smith et al., 2007) and the formation of π-π stacks of the oxadiazole units (Lee et al., 2006; Paul et al., 2008). Upon excitation by an applied electric field, the intensities of both absorption bands are enhanced (ON-1 spectrum). The increase in intensity of the CT absorption band is consistent with an increase in concentration of the CT state, arising from the conformation-coupled CT induced by the applied electric field. The increase in concentration of the conductive CT state leads to the switching of the P(BPPO)-PI device from the OFF state to the ON state. Due to CT from the oxadiazole donors to the phthalimide acceptors, the oxadiazole groups become positively charged. Driven by the applied electric field, the charged oxadiazole groups have the tendency to interact with the neighboring neutral oxadiazole groups, forming the partial or full

face-to-face conformation (Teo et al., 2006). Thus, the π-π stacking of the oxadiazole groups is enhanced, as indicated by the increase in intensity of the absorption shoulder at about 360 nm. The increased extent of face-to-face conformation of the conjugated oxadiazole groups also facilitates the migration of charge carriers and sustains the ON state. Sometime after removal of the electric field, the conformation of the polymer chain relaxes to its initial state and the induced intramolecular CT disappears. Thus, the concentration of CT complexes decreases to the initial level, and the extent of face-to-face conformation of the oxadiazole moieties also relaxes to the initial level. As a result, the original OFF-state absorption spectrum is recovered (OFF-2 spectrum). The effect of applied electric field on the absorption spectrum of P(BPPO)-PI film provides further support to the conformation-coupled CT process in P(BPPO)-PI. The CT absorption band is located at around 560 nm, indicating that the CT process occurs with the highest probability at about 2.2 eV. This energy value is comparable to the switching threshold voltage (~ 2.3 V) in the *J-V* characteristics, consistent with the threshold voltage-induced CT process.
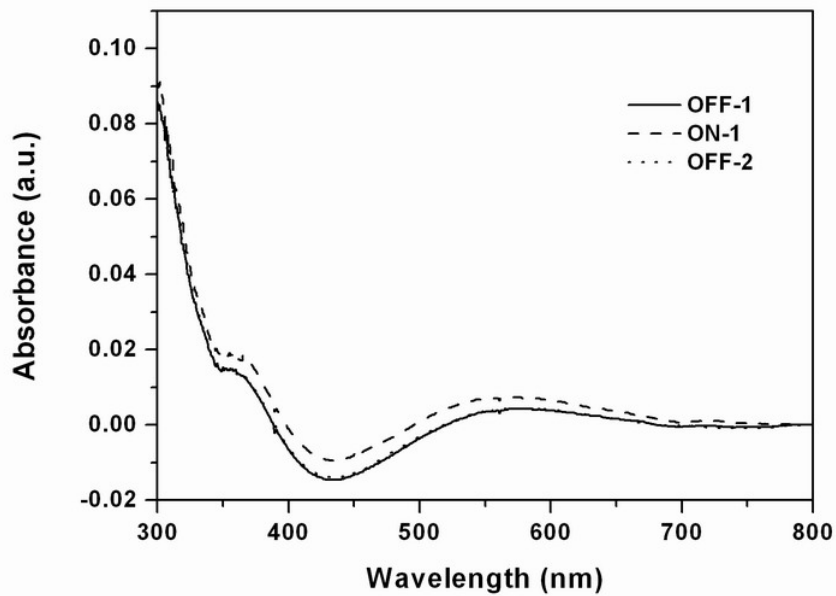
Figure 3.28 UV-visible absorption spectra of the P(BPPO)-PI film spin-coated on ITO substrate. OFF-1, ON-1, and OFF-2 denote, respectively, the absorption spectra of the P(BPPO)-PI films measured before, immediately after, and 3 h after an electrical sweep (0 to -4 V, with a removable Hg droplet as the working electrode and ITO as the ground electrode).

In the above mentioned OXTA-PI, AZTA-PI and AZTA-PEI molecules, the pendant triphenylamine group possesses strong electron-donating ability and can significantly enhance the hole delocalization (Redecker et al., 1999). It can also enhance the polarity of the three polyimide molecules. The molecular simulation results show that the dipole moment of OXTA-PI, AZTA-PI and AZTA-PEI in excited state are 5.39 Debye, 8.39 Debye and 6.61 Debye, respectively, much larger than that of P(BPPO)-PI (3.06 Debye). The effective charge delocalization and large excited state dipole moment help to stabilize the conductive CT state. As a result, the ON states of the OXTA-PI, AZTA-PI and AZTA-PEI devices are non-volatile and can survive even after turning off the power. However, for the P(BPPO)-PI molecule, due to the absence of the strong triphenylamine donor group, the dipole moment is relatively

small (3.06 Debye in the excited state), which cannot hold the conductive CT state effectively. In addition, the hole delocalization in the weak oxadiazole donor group is limited, making the CT state unstable. As a result, the ON state of P(BPPO)-PI will relax to the initial OFF state sometime after turning off the power, when the polyimide molecule relaxes to its initial less twisted conformation and the energy barrier for dissociation of the CT complexes disappears. SRAM type memory effect with volatile ON state is thus observed in the P(BPPO)-PI device. In addition, the ON state current densities for the P(BPPO)-PI device is lower than those of the OXTA-PI, AZTA-PI and AZTA-PEI devices by about two orders, further evidencing the poor hole-delocalizing and -transporting feature of the oxadiazole group in comparison to that of the triphenylamine group (Khan et al., 2007).

3.4 Conclusion

A series of solution-processable functional polyimides, OXTA-PI, AZTA-PI, AZTA-PEI and P(BPPO)-PI, containing both electron-donor and -acceptor moieties, were designed and studied for their bistable electrical switching and memory effects. Memory devices based on the four polyimides are all able to exhibit bi-directional electrical switching from the initial OFF state to the ON state. The molecular simulation results indicate that electric field-induced CT between the donor and acceptor moieties accounts for the observed electrical switching. In comparison to the previously reported TP6F-PI molecule, oxadiazole or triazole group is incorporated into these four polyimides. This change in molecular structure increases the polymer flexibility and facilitates the electric field-induced conformational change, which can introduce an energy barrier for dissociation of the conductive CT complexes. As a result, more stable ON states were observed in the four memory devices, in comparison to that of the TP6F-PI device. Memory devices based OXTA-PI, AZTA-PI and AZTA-PEI exhibited similar WORM type memory effects, with comparable ON and OFF current densities. The only difference is in their switching threshold voltages, with those of the OXTA-PI, AZTA-PI and AZTA-PEI device being ±1.8 V, ±2.5 V, and ±3.2 V, respectively. The larger switching threshold voltage of AZTA-PI than that of OXTA-PI arises probably from the large energy barrier for intramolecular CT placed by the orthogonal conformation between the triazole and triphenylamine moieties. The further increase in threshold voltage in

AZTA-PEI is associated with the additional energy barrier for intramolecular CT introduced by the flexible phenoxyl group. For P(BPPO)-PI, due to absence of the strong triphenylamine donor group, the dipole moment is relatively small and the charge delocalization in the weak oxadiazole donor moiety is limited, resulting in an unstable conductive CT state. Volatile SRAM type memory effect is thus observed in the P(BPPO)-PI device, different from the non-volatile WORM type memory effects observed in the OXTA-PI, AZTA-PI and AZTA-PEI devices. The results indicate that memory effects of the functional polyimides are dependant to a large extent on their molecular structures. Thus, it is possible to tune the memory properties of functional polyimide via molecular design and synthesis.

CHAPTER 4

ELECTRICAL SWITCHING AND MEMORY EFFECTS IN POLYFLUORENE COPOLYMERS CONTAINING DIFFERENT ELECTRON ACCEPTOR MOIETIES

4.1 Introduction

Polyfluorene derivatives are an important class of electroactive materials (Leclerc, 2001; Ohmori et al., 1991). The facile substitution at the remote C_9 site can improve the solubility and processability of the polymers (Lemmer et al., 1995; Jenekhe and Osaheni, 1994). Polyfluorenes have many desirable characteristics for application as the active constituents in polymer-based electronic devices. For example, they can be chemically tuned to give electroluminescence emission across the full visible spectrum, from blue to red, with high luminescence quantum efficiency, allowing for the fabrication of efficient polymer light-emitting diodes (PLEDs) (Grice et al., 1998; Becker et al., 2002; Scherf and List, 2002; Babel and Jenekhe, 2003; Lee et al., 2005). In addition, polyfluorenes have large optical gains (Heliotis et al., 2002; Xia et al., 2003) and can be readily processed from solution onto etched silica gratings to produce low-threshold, distributed-feedback lasers (Heliotis et al., 2003; Lemmer et al., 1995). In addition to the above areas, applications in other domains, such as photovoltaic devices (Svensson et al., 2003; Benson-Smith et al., 2007), transistors (Zaumseil, et al., 2006), and memory devices (Lei et al., 2009; Kim et al., 2008), are also emerging in recent years.

In this chapter, two fluorene-based copolymers, TPATz-F8 and TPATz-F8BT, (molecular structures shown in Figure 4.1), containing both hole-transporting unit (triphenylamine moiety) and electron-transporting unit (triazole, or triazole and

benzothiadiazole, moiety), were studied for their electrical switching and memory effects. In these two copolymers, the hole-transporting moiety acts as the electron donor, while the electron-transporting moiety acts as the electron acceptor. Under the electric field, conformation-coupled charge transfer (CT) occurs between the donor and acceptor moieties, giving rise to a conductive CT state. As a result, conducting channels for both holes and electrons are generated, switching the polymer memory devices abruptly from the initial low-conductivity (OFF) state to the high-conductivity (ON) state. Molecular simulations of the TPATz-F8 molecule in both ground and excited states (the OFF and ON states of the device) were carried out to better understand the mechanism underlying the electrical switching phenomenon.

4.2 Experimental Section

4.2.1 Materials

Bromine (Acros), benzoyl chloride (Alfa Aesor), phosphorus pentachloride (Riedel-de Haën), 4-nitrofluorobenzene (Acros), *N*-bromosuccinimide (Acros), tin(II) chloride anhydrous (Showa Denko), hydrazine monohydrate (Alfa Aesar), heptanoyl chloride (Acros), tetrakis (triphenylphosphine) palladium(0) (Acros), 9,9-dioctylfluorene-2,7-diboronic acid bis(1,3-propanediol) ester (Sigma-Aldrich), aluminum chloride (Acros), and 2,1,3-benzothiadiazole (Sigma-Aldrich) were used as received. *N*-methyl-2-pyrrolidinone (NMP), *N,N*-dimethylacetamide (DMAc), and dimethyl sulfoxide (DMSO) were purchased from TEDIA Chemical Co., while *N,N*-dimethylformamide (DMF) and tetrahydrofuran (THF) were purchased from ECHO Chemical Co. All the solvents were purified by distillation over calcium hydride and stored over 4 Å molecular sieves. The surfactant trioctylmethylammonium chloride (Aliquat 336) was purchased from Tokyo Chemical Industry (TCI) Co., Ltd. and used as received.

4.2.2 Instrumentation

FT-IR spectra of the synthesized monomers and polymers were recorded on a Perkin-Elmer GX FTIR spectrophotometer. Thermogravimetric analysis (TGA) was conducted on a Perkin-Elmer Pyris 6 TGA thermogravimetric analyzer at a heating

rate of 20 °C·min^{-1} and under a nitrogen flowing rate of 20 cm^3·min^{-1}. Differential scanning calorimetric analysis was performed on a Perkin-Elmer Pyris 6 differential scanning calorimeter (DSC) at a heating rate of 10 °C·min^{-1} and under a nitrogen flow rate of 20 cm^3·min^{-1}. Cyclic voltammetry (CyV) measurements were carried out on an Autolab potentiostat/galvanostat system using a three-electrode cell under an argon atmosphere. The TPATz-F8 film deposited on a platinum disk electrode (working electrode) was scanned anodically and cathodically at a rate of 0.1 V·s^{-1} in a 0.1 M acetonitrile solution of tetrabutylammonium hexafluorophosphate (n-Bu$_4$NPF$_6$). Ag/AgCl and a platinum wire were employed as the reference electrode and counter electrode, respectively. A solution of ferrocene in toluene (0.01 M) was used as the external standard. Other instruments used in this chapter are the same as in Chapter 3.

4.2.3 Synthesis of the Monomers and Polymers

The two polyfluorene copolymers were prepared and characterized by Associate Prof. Wang Kun-Li and Mr. Hsieh Li-Ga from National Taipei University of Technology. The synthesis routes for the monomers and copolymer are shown in Figure 4.1. The detailed preparation procedures are given below.

Benzoyl chloride (9.8 g, 0.07 mol) and hydrazine monohydrate (1.8 g, 0.035 mol) were mixed in 170 mL NMP and allowed to react at room temperature for 5 h. The product was precipitated from deionized water, rinsed with ethyl acetate, and dried

under vacuum, to give the white solid of monomer **1** (yield: 5.5 g, 66%). Under a nitrogen atmosphere, a mixture of monomer **1** (5.0 g, 0.021 mol) and phosphorus pentachloride (9.4 g, 0.045 mol) was dissolved in 50 mL toluene and stirred at 120°C for 3 h. After removal of the solvent under reduced pressure, the residue was rinsed with deionized water and recrystallized from ethanol to afford the yellow crystal of monomer **2** (yield: 2.7 g, 47.7%). Diphenylamine (20 g, 0.12 mol) and 1-fluoro-4-nitrobenzene (18.3 g, 0.13mol) were added sequentially to 230 mL 1 M DMSO solution of sodium hydride. The mixture was then heated to 130°C and stirred for 24 h, followed by cooling to room temperature. The crude product was precipitated from deionized water and recrystallized from ethanol to afford the yellow crystal of monomer **3** (yield: 21.9 g, 63%). Under a nitrogen atmosphere, a 24 mL DMF solution of *N*-bromosuccinimide (NBS) (8.0 g, 0.045 mol) was added drop-wise to a 42 mL DMF solution of monomer **3** (6.1 g, 0.021 mol)**.** The mixture was then stirred for 48 h. The product was precipitated from deionized water and dried under vacuum to afford the orange solid of monomer **4** (yield: 9.2 g, 97.7%). A mixture of monomer **4** (9.0 g, 0.02 mol) and tin chloride (27 g, 0.12 mol) was dissolved in 300 mL ethanol and refluxed for 24 h. After removal of the solvent under reduced pressure, 200 mL 0.1 M NaOH aqueous solution was added to the residue maintained in an ice bath. The precipitate was then extracted with ethyl acetate, followed by concentration of the ethyl acetate solution, to afford monomer **5** (yield: 7.6 g, 91%). Monomer **2** (1.9 g, 0.007 mol) and **5** (5.9 g, 0.014 mol) were mixed in 60 mL *p*-xylene and stirred at 160°C for 3 days. After removal of the solvent under reduced pressure, the crude

product was recrystallized from ethanol to afford monomer **6** (yield: 3.1 g, 71%). A solution of Br_2 (1.13 mL) in HBr (10 mL) was added dropwise to a mixture of 2,1,3-benzothiadiazole (1.0 g) and HBr (15 mL, 48%), which was then refluxed for 6 h. After the solution was cooled to room temperature, an excess amount of saturated solution of $NaHSO_3$ was added to completely consume any unreacted Br_2. The mixture was rinsed with deionized water and cold ether to give the crude product, which was further purified by recrystallization from ethanol to afford monomer **7** (yield: 0.77 g, 35.5%).

The polymerization of **TPATz-F8** was carried out, under argon atmosphere, by the Suzuki coupling reaction between monomers **6** (1 g, 1.61 mmol) and fluorene derivative **8** (0.925 g, 1.65 mmol), in the presence of Aliquat 336 (several drops), $Pd(PPh_3)_4$ (0.037 g, 0.032 mmol), 6.7 mL 2 M K_2CO_3 aqueous solution, and 10 mL THF. The mixture was heated to 65 °C and stirred for 96 h, followed by pouring into deionized water and methanol. The precipitate was purified by dissolving in chloroform and reprecipitating from deionized water and methanol for several times. The product was further purified by Soxhlet extraction in acetone for 24 h to afford the final **TPATz-F8** copolymer (yield: 1.37 g, 94%). FTIR spectroscopy (KBr, cm^{-1}): 1508 (C=N), 2851, 2924 (alkyl group). ^{1}H NMR (CDCl$_3$, 500 MHz), δ(ppm): 0.67-0.81 (m, 10H), 1.07-1.19 (m, 20H), 2.05 (s, 4H), 7.04-7.05 (d, 2H, J=8.46 Hz), 7.18-7.19 (d, 2H, J=8.50 Hz), 7.26–7.28 (t, 4H), 7.33-7.49 (m, 6H), 7.57-7.60 (t, 8H), 7.65-7.67 (d, 4H, J=8.29 Hz), 7.77–7.79 (d, 2H, J=7.87 Hz). ^{13}C NMR (CDCl$_3$, 125

MHz), δ(ppm): 14.0, 22.5, 23.7, 29.1, 29.9, 31.7, 40.4, 55.2, 120.0, 120.9, 122.6, 125.3, 125.7, 126.5, 127.1, 127.8, 128.2, 128.4, 128.6, 128.7, 128.9, 129.8, 137.4, 139.0, 139.9, 145.6, 148.7, 151.6, 154.7. Anal Calac for $C_{61}H_{64}N_4$: C, 85.87; N, 6.57; H, 7.56. Found: C, 84.85; N, 6.49; H, 7.47.
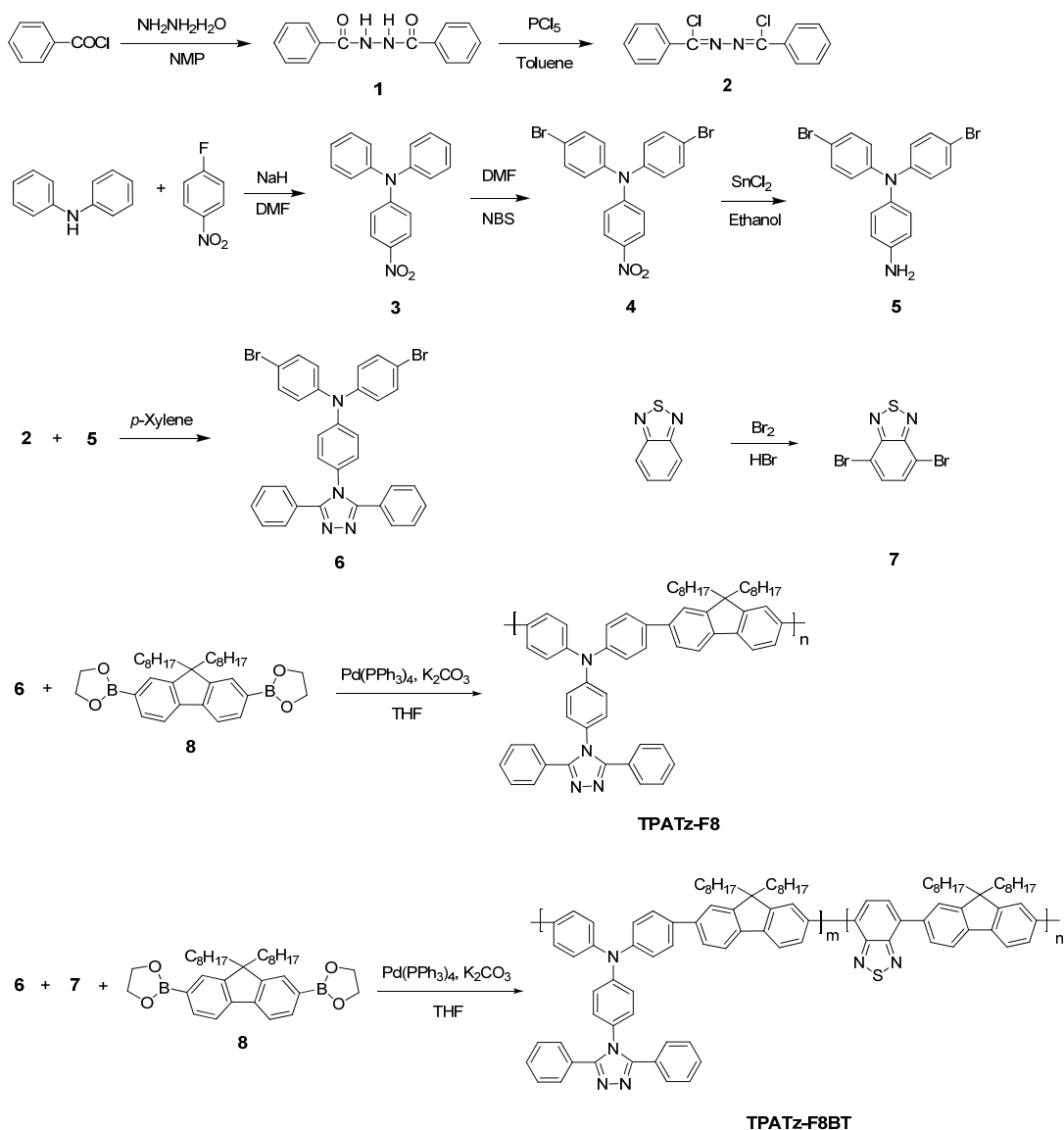
Figure 4.1 Synthesis routes for the monomers and the TPATz-F8 and TPATz-F8BT copolymers

The copolymer **TPATz-F8BT** was prepared by a similar Suzuki coupling reaction between monomer **6**, **7**, and **8**. Under argon atmosphere, Aliquat 336 (several drops), Pd(PPh$_3$)$_4$ (0.074 g, 0.064 mmol), 13.4 mL 2 M K$_2$CO$_3$ aqueous solution, and 20 mL THF were added to a mixture of monomer **6** (1 g, 1.61 mmol), monomer **7** (0.47 g, 1.61 mmol) and fluorene derivative **8** (1.85 g, 3.30 mmol). The mixture was heated to 65 °C and stirred for 96 h, followed by pouring into deionized water and methanol. The precipitate was purified by dissolving in chloroform and reprecipitating from deionized water and methanol for several times. The product was further purified by Soxhlet extraction in acetone for 24 h to afford the final **TPATz-F8BT** product (yield: 1.66 g, 75%). FTIR spectroscopy (KBr, cm^{-1}): 1508 (C=N), 2845, 2924 (alkyl group). ^{1}H NMR (CDCl$_3$, 500 MHz), δ(ppm): 0.80-1.26 (m, 60H), 2.06-2.16 (d, 8H), 7.06 (s, 2H), 7.19-7.28 (m, 6H), 7.42-7.46 (m, 6H), 7.59-7.68 (m, 12H), 7.78-8.08 (m, 10H). Anal Calac for C$_{96}$H$_{106}$N$_6$S: C, 83.80; N, 6.11; H, 7.76. Found: C, 83.42; N, 6.21; H, 7.89.

4.2.4 Fabrication and Characterization of the Memory Devices

The indium-tin oxide (ITO) coated glass substrate was pre-cleaned sequentially with deionized water, acetone and isopropanol in an ultrasonic bath for 15 min. A 100 μL DMAc solution of the copolymer (10 mg·mL^{-1}) was spin-coated onto the ITO substrate at a spinning rate of 1200 rpm, followed by solvent removal in a vacuum oven at 10^{-5} Torr and 60°C for 10 h. The thickness of the polymer layer was about 50 nm, as determined by the AFM edge profiling. Finally, an Al top electrode of about

400 nm in thickness was thermally deposited onto the polymer surface through a shadow mask at a pressure of about 10^{-7} Torr. Electrical property measurements were carried out on devices of 0.4×0.4 mm^2, 0.2×0.2 mm^2, and 0.15×0.15 mm^2 in size, under ambient conditions, using an Agilent 4155C semiconductor parameter analyzer equipped with an Agilent 41501B pulse generator. The current density-voltage (*J-V*) data reported were based on device units of 0.4×0.4 mm^2 in size, unless stated otherwise. ITO was maintained as the ground electrode during the electrical measurements.

4.3 Results and Discussion

4.3.1 Characterizations of the Polyfluorene Copolymers

The solubilities of the polyfluorene copolymers in common organic solvents are summarized in Table 4.1. Due to the presence of long aliphatic *n*-octyl substituent at the C_9 position of fluorene group, the two polymers exhibit good solubilities in common solvents, such as DMAc, NMP, THF, chloroform and dichloromethane, at room temperature. As a result, they can be easily cast into uniform films from solutions by spin-coating.

Table 4.1 Solubilities of the polyfluorene copolymers in common organic solvents

Polymer	Solubility[a]					
	DMAc	NMP	THF	CHCl$_3$	CH$_2$Cl$_2$	Toluene
TPATz-F8	++	++	++	++	++	+-
TPATz-F8BT	++	++	++	++	++	+-

[a]Solubility measured in concentration of 1 mg·mL^{-1}
++: Soluble at room temperature
+-: Partially soluble at room temperature

The molecular weights and thermal properties of the two polymers are summarized in the below Table 4.2. The weight-average (M_w) and number-average (M_n) molecular weights of TPATz-F8 are 3.3×10^4 and 2.1×10^4, respectively, with a polydispersity index (PDI) of 1.57, while those for TPATz-F8BT are 3.8×10^4 and 2.4×10^4, respectively, with a PDI of 1.58. The glass transition temperatures (T_g) of TPATz-F8 and TPATz-F8BT are 135°C and 155°C, respectively, which are much higher than that

of poly-(9,9-dioctylfluorene) (75°C). It is evident that incorporation of the triphenylamine and triazole moieties has significantly enhanced the rigidity of the polymer chain. The thermal gravimetric analysis reveals 5% and 10% weight loss temperatures of 428°C and 455°C for TPATz-F8, and 433°C and 456°C for TPATz-F8BT, respectively, in nitrogen. In addition, from the ^{1}H NMR spectrum, the segment ratio (m/n) of triphenylaminetriazole to 2,1,3-benzothiadiazole unit in TPATz-F8BT is 3/2.

Table 4.2 Molecular weights and thermal properties of the copolymers

Polymer	Molecular weight[a]			Thermal properties[c]		
	M_n	M_w	PDI[b]	$T_g(^oC)$	$T_{d5}(^oC)$	$T_{d10}(^oC)$
TPATz-F8	2.1×10^4	3.3×10^4	1.57	317	428	476
TPATz-F8BT	2.4×10^4	3.8×10^4	1.58	304	433	515

[a]Molecular weight was measured by GPC in THF using polystyrene as standards
[b]PDI: polydispersity index = (M_w/M_n)
[c]T_g is the glass transition temperature measured by DSC. T_{d5} and T_{d10} are 5% and 10% weight loss temperatures, respectively, measured by TGA in nitrogen.

Figure 4.2 shows the UV-visible absorption spectra of TPATz-F8 and TPATz-F8BT in chloroform, along with that of poly(9,9'-dihexylfluorene) (PF6) as the reference. The concentration of TPATz-F8 was about 4×10^{-7} M. The concentrations of TPATz-F8BT and PF6 were adjusted to have the same number of repeating units as that of TPATz-F8. The absorption spectra were cut off at 250 nm because of the strong interference from the solvent in the short wavelength region. The absorption spectra of TPATz-F8 and TPATz-F8BT were normalized to the maximum absorption of PF6 at 388 nm for ease of comparison. As shown in Figure 4.2, TPATz-F8 exhibits a

maximum absorption at 372 nm. By comparing the absorption spectrum of TPATz-F8 with that of PF6 and considering the conjugated backbone of TPATz-F8, this absorption peak probably arises from $\pi \rightarrow \pi^*$ transition of the TPATz-F8 backbones (Shi et al., 2009; Jiang et al., 2009; Zhang et al., 2009). It is similar to the characteristic $\pi \rightarrow \pi^*$ transition of the conjugated backbone of PF6 (Wu et al., 2005). In comparison to PF6, the maximum absorption of TPATz-F8 has blue-shifted by about 16 nm. This blue-shift is reported to be induced by the incorporation of twisted triphenylamine segments in the TPATz-F8 backbone, which reduces the planarity, and thus the degree of effective conjugation of the polymer main chain (Wu et al., 2005). Besides the main absorption peak, TPATz-F8 also exhibits an additional weak absorption in the short wavelength region (250 nm ~ 300 nm), which arises from absorption of the triazole moieties in the side chain (Chen et al., 2007). In comparison to that of TPATz-F8, the maximum absorption of TPATz-F8BT is further blue-shifted to 348 nm, attributable probably to the fact that the electron-deficient benzothiadiazole moieties weaken the electronic conjugation of the polymer main chain (Wu et al., 2006). An absorption shoulder in the long-wavelength region (440 nm) is also observed for the TPATz-F8BT solution, which arises from the intramolecular CT between the fluorene and benzothiadiazole units (Liu et al., 2007).
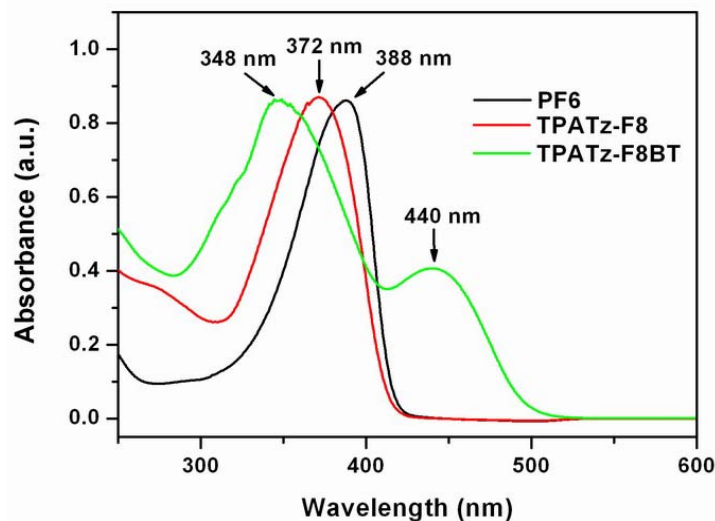
Figure 4.2 UV-visible absorption spectra of TPATz-F8, TPATz-F8BT and the PF6 model compound in chloroform solution. The concentration of TPATz-F8 was about 4×10^{-7} M. The concentrations of TPATz-F8BT and PF6 were adjusted to have the same number of repeating units as that of TPATz-F8. The absorption spectra of TPATz-F8 and TPATz-F8BT were normalized to the maximum absorption of PF6 at 388 nm for ease of comparison.

The PL spectra of TPATz-F8, TPATz-F8BT and PF6 in chloroform are shown in Figure 4.3. The concentration of TPATz-F8 is 1.7×10^{-7} M, while the concentrations of TPATz-F8BT and PF6 were adjusted to have the same number of repeating units as that of TPATz-F8. All the emission spectra were obtained with the excitation wavelength of 370 nm. As shown in Figure 4.3, the PL spectrum of PF6 is characterized by a series of well-resolved vibronic features located at 416 nm, 440 nm, 471 nm and 507 nm, which are assigned, respectively, to the $S_1 \rightarrow S_0$ 0-0, 0-1, 0-2 and 0-3 intrachain singlet transitions (Azuma et al., 2006; Li et al., 2004). TPATz-F8 exhibits, however, a less intense emission spectrum, in comparison to PF6. The partial fluorescence quenching in TPATz-F8 is probably attributed to the charge transfer and/or energy transfer between the three component moieties under photoexcitation (Shibano et al., 2006; Lukas et al., 2002). In addition, the vibronic structure of

110

TPATz-F8 becomes much less resolved, which results from the lack of intrachain ordering due to the presence of twisted triphenylamine segments in the copolymer backbone (Jiang et al., 2009). The fluorene emission in TPATz-F8BT is, however, significantly quenched, with the appearance of a green emission centered at about 540 nm, which is attributed to the Förster energy transfer from the excited fluorene segments to the vicinity of the benzothiadiazole segments (Wu et a;., 2007).
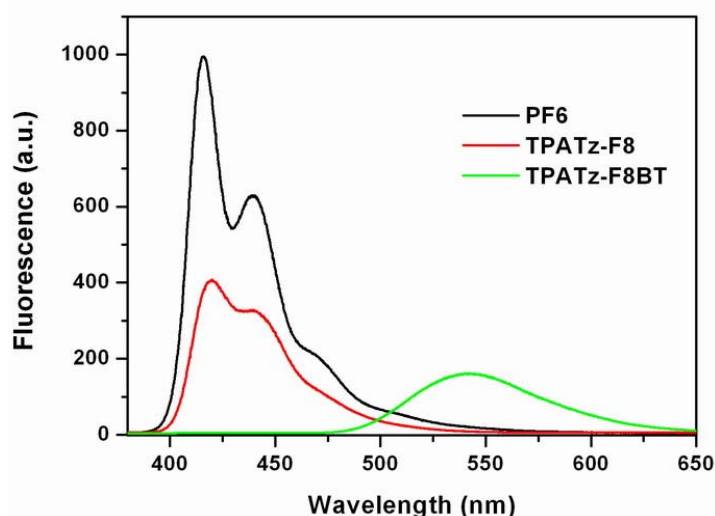
Figure 4.3 PL spectra of TPATz-F8, TPATz-F8BT and the PF6 model compound in chloroform solution. The concentration of TPATz-F8 is 1.7×10^{-7} M. The concentrations of TPATz-F8BT and PF6 were adjusted to have the same number of repeating units as that of TPATz-F8. All the emission spectra were obtained with the excitation wavelength of 370 nm.

4.3.2 Electrical Switching and Memory Effects of the Polyfluorene Copolymers

The memory switching effects of TPATz-F8 are demonstrated by the *J-V* characteristics of an ITO/TPATz-F8/Al sandwich device, as shown in Figure 4.4(a). Initially, the device was in the low-conductivity (OFF) state. During the 1st negative sweep (with Al as the cathode and ITO as the anode) from 0 to -3 V, an abrupt

increase in current density was observed in the device at -2.8 V, indicating device switching from the initial OFF state to the high-conductivity (ON) state. This electrical switching is equivalent to the "writing" process in a digital memory cell. The ON/OFF current ratio is in the order of 10^5 at -1 V. The device exhibited good stability in the ON state when the negative voltage sweep was repeated (the 2nd sweep). It remained in the ON state even after turning off the power (the 3rd sweep), indicating the non-volatile nature of the electrical bistability. One prominent feature of the present polymer memory is that the ON state can be reset to the initial OFF state by applying a reverse voltage of about +2.0 V, as shown in the 4th sweep. This switch-off process is equivalent to the "erasing" process of a digital memory cell. The device is thus reversible and allows for application in a rewritable data storage system. The subsequent 5th and 6th sweeps show the J-V characteristics of the device right after the application of an erasing sweep and 5 min after turning off the power, respectively. The device was found to exhibit good stability in the OFF state. The ability to write, read and erase the electrical states, as well as the non-volatile nature of the ON and OFF states, fulfill the functionality of a rewritable memory. As indicated by the subsequent 7th to 14th sweeps, the above write-read-erase-read switching cycles can be repeated with good accuracy, except for the slight variations in switching threshold voltages, associated probably with conformational relaxation of the polymer chain (Ling et al., 2007; Liu et al., 2009). In addition, devices with different active areas of 0.4×0.4 mm^2, 0.2×0.2 mm^2, and 0.15×0.15 mm^2 show almost the same J-V characteristics, indicating that the current density is independent on the

device areas. The rewritable electrical states, good reproducibility, and area-independent current density, rule out the possibility of filament conduction (Henisch and Smith, 1974), metal diffusion (Lim et al., 1998; Ma et al., 2000), and dielectric breakdown in the present devices.

Figure 4.4(b) shows the effect of operation time voltage stress on the stability of the TPATz-F8 device. Under a constant stress of -1 V, no obvious degradation in current density was observed for both the ON and OFF states over a 6 h period. In addition, the two electrical states were also stable up to 10^8 read pulses of -1 V, as shown in Figure 4.4(c).

The memory effects of TPATz-F8BT are demonstrated by the *J-V* characteristics shown in Figure 4.4(d). The TPATz-F8BT device exhibited similar rewritable memory effects as the TPATz-F8 device, except for a slightly lower ON state current, attributable probably to incorporation of the electron-deficient benzothiadiazole groups in the polymer backbone. The underlying switching mechanisms will be elucidated in next section. Figures 4.4(e) and 4.4(f) show that the TPATz-F8BT device is stable in both ON and OFF states under a continuous stress of -1 V or read pulses of -1 V.
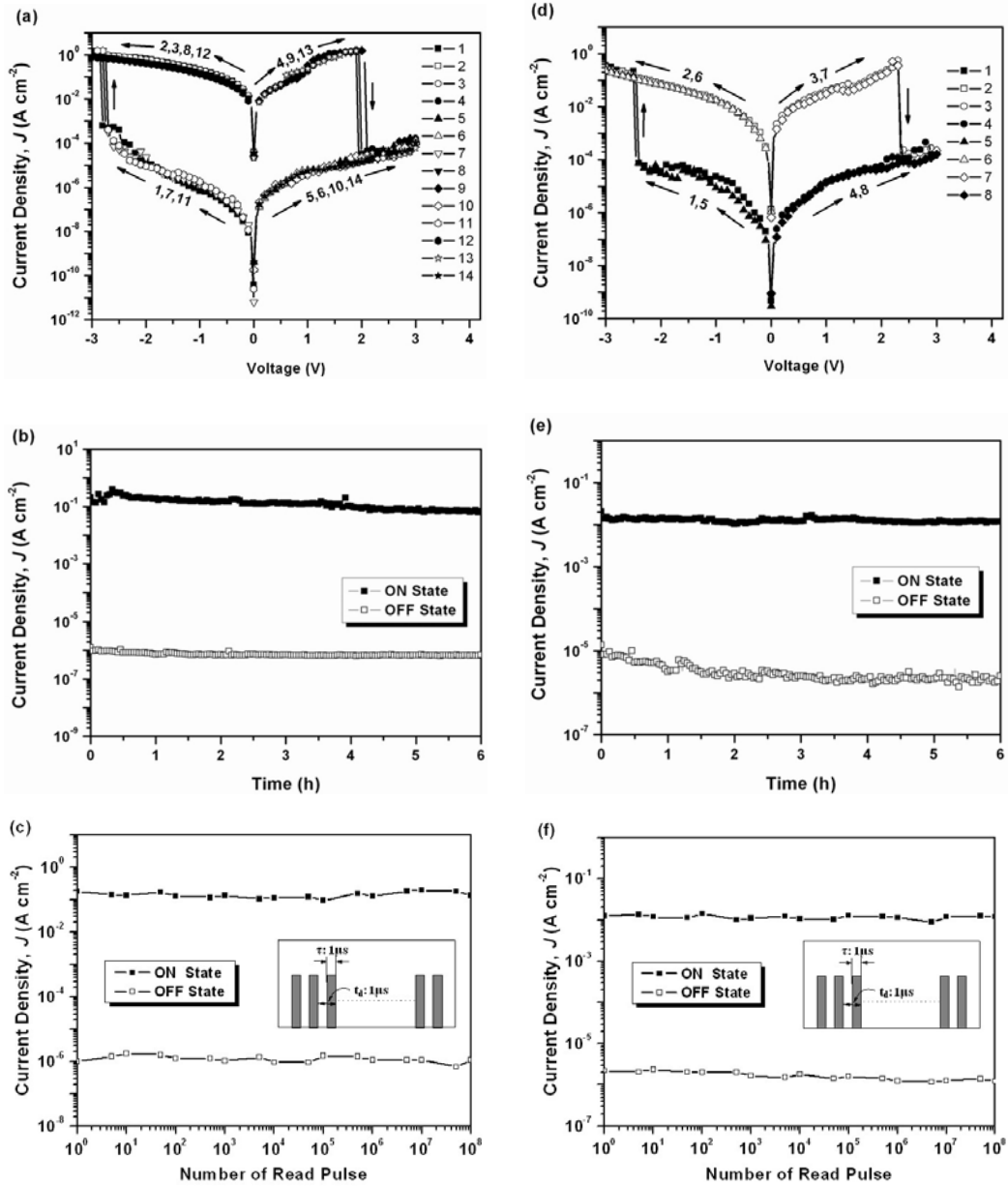
Figure 4.4 (a) *J-V* characteristics of a 0.4×0.4 mm^2 ITO/TPATz-F8/Al device. The sequence and direction of each sweep are indicated by the respective number and arrow. The 3rd and 6th sweeps were conducted about 5 min after turning off the power. (b and c) Stability of the ON and OFF states of the TPATz-F8 device under a constant stress of -1 V and read pulses of -1 V. (d) *J-V* characteristics of a 0.4×0.4 mm^2 ITO/TPATz-F8BT/Al device. The sequence and direction of each sweep are indicated by the respective number and arrow. (e and f) Stability of the ON and OFF states of the TPATz-F8BT device under a constant stress of -1 V and read pulses of -1 V. The insets of (c) and (f) show the pulse used for measurement.

4.3.3 Switching Mechanism

As the two copolymers possess similar molecular structures and exhibit similar rewritable memory effects, the mechanisms underlying their memory effects are probably similar. For simplicity, only the switching mechanism of TPATz-F8 is analyzed with theoretical molecular simulation and experimental characterization in this chapter.

To better understand the switching behavior of the TPATz-F8 memory device, electronic properties of TPATz-F8 in the ground state were studied by the DFT method. Calculations of the molecular orbitals and ESP surfaces of the basic units (BU), taking into account of all the three functional moieties, i.e., the fluorene, triphenylamine and triazole moieties, were carried out at the B3LYP/6-31G(d) level with the Gaussian 03 program package. The alkyl chains attached to the fluorene chromophore were not included in the calculation since they probably do not significantly affect the electronic properties of the BU (Sancho-García et al., 2004). The highest occupied molecular orbital (HOMO) and the first two lowest unoccupied molecular orbitals (LUMO1 and LUMO2) of the BU, as well as the plausible electronic transitions under excitation, are shown in Figure 4.5. The HOMO is located mainly on the triphenylamine and fluorene moieties, indicating that these two moieties act as the electron donors in the TPATz-F8 molecules. Upon excitation, electrons in the triphenylamine moiety tend to transit to the first unoccupied molecular orbitals (LUMO1) located mainly on the fluorene moiety, indicating that

the triphenylamine group possesses stronger electron-donating ability than the fluorene group, and thus acts as the main electron donor. Upon further excitation, electrons will transit to the higher unoccupied molecular orbital (LUMO2) located exclusively on the triazole moiety, suggesting that the triazole moiety acts as the electron acceptor in the copolymer molecule, consistent with its well-known electron-withdrawing nature (Yasuda et al., 2005).
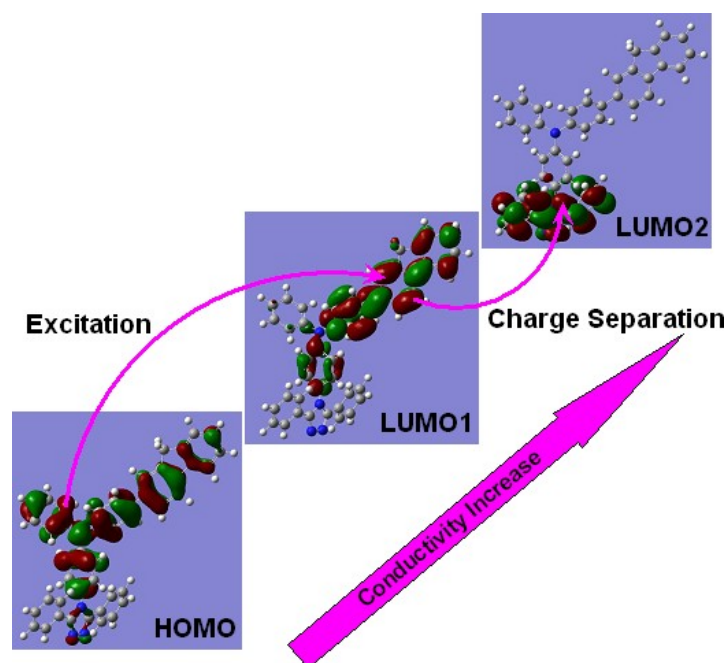
Figure 4.5 Molecular orbital surfaces of the TPATz-F8 BU and the plausible electronic transitions under the electric field

To identify the electron donor and acceptor groups experimentally, the electrochemical oxidation/reduction behavior of the TPATz-F8 molecule, along with PF6 and 4-(3,5-diphenyl-4*H*-1,2,4-triazol-4-yl)-*N,N*-diphenylaniline (TPATz) model compounds, were studied by cyclic voltammetry (CyV). Their HOMO and LUMO energy levels were estimated by the following equations (Lee et al., 2001),

$E_{HOMO} = -[(E_{Ox}(\text{onset})-E_{FOC})+4.8]$ (eV)

$E_{LUMO} = -[(E_{Red}(\text{onset})-E_{FOC})+4.8]$ (eV) $\qquad\qquad\qquad\qquad$ (1)

where E_{FOC} is the potential of the external standard, ferrocene/ferricenium ion (Foc/Foc$^+$) couple, measured under the same conditions. The CyV data, as well as the estimated HOMO and LUMO energy levels, are summarized in Table 4.2. The electrochemical oxidation and reduction processes of TPATz are found to start from 0.95 V and -1.65 V, respectively. As reported previously, the oxidation and reduction of TPATz arise from the triphenylamine and triazole moieties (Wu and Chen, 2009), respectively. The onset potentials for oxidation and reduction of PF6 are, however, much larger (1.38 V and -1.80 V, respectively). In comparison with these two model compounds, the onset potentials for oxidation and reduction of TPATz-F8 (0.98 V and -1.64 V, respectively) are much closer to those of TPATz, indicating that the electron donor and acceptor groups of TPATz-F8 arise mainly from the triphenylamine and triazole moieties, respectively.

Table 4.2 Electrochemical data of TPATz-F8, and the PF6 and TPATz model compounds, as well as their electrochemically determined energy levels

Molecule/ Polymer	$E_{Ox}(\text{onset})$ (V)	$E_{Ox}(\text{onset})$ (V)	E_{HOMO} (eV)[a]	E_{LUMO} (eV)[b]
PF6	1.38	-1.80	-5.79	-2.61
TPATz	1.03	-1.58	-5.45	-2.84
TPATz-F8	0.98	-1.64	-5.41	-2.79

[a] $E_{HOMO} = -[(E_{Ox}(\text{onset})-E_{FOC})+4.8]$ (eV)
[b] $E_{LUMO} = -[(E_{Red}(\text{onset})-E_{FOC})+4.8]$ (eV)

During the initial stage of the electrical sweep, electrons at HOMO are excited to LUMO1, due to significant overlapping of HOMO and LUMO1 at the triphenylamine and fluorene moieties. When the applied electric field reaches the switch-on threshold voltage, some of the excited electrons at LUMO1 acquire sufficient energy to overcome the energy barrier between the backbone and the pendant triazole moieties. Electrons are then excited to LUMO2 located at the triazole moiety, forming a CT state between the donor and acceptor moieties. Under the electric field, the generated holes at HOMO can delocalize among the conjugated backbone, forming an open channel for the charge carriers (holes) to migrate through. The holes can either move along the conjugated backbone or hop between neighboring molecules. On the other hand, the transferred electrons at LUMO2 can also migrate among the triazole moieties, due to the good electron-transporting property of the triazole derivatives (Yu and Chen, 2004). As the triazole groups are located at the side chains and separated from one another, the electrons migrate probably by hopping between the neighboring triazole moieties (either in the same or neighboring copolymer chains). As a result, conducting channels for both positive and negative charge carriers are formed in the TPATz-F8 molecules, resulting in the abrupt increase in current density and the electrical switching from the initial OFF state to the ON state.

To elucidate the above CT process, *in-situ* PL spectra of the TPATz-F8 film in an ITO/TPATz-F8/Al sandwich device under electrical biases were studied (Figure 4.6). The electrical biases were applied on the Al electrode, with ITO as the ground

electrode. All the emission spectra were obtained at the excitation wavelength of 370

nm. In Figure 4.6, OFF-1 denotes the PL spectrum of the TPATz-F8 film prior to the

application of electrical bias, corresponding to the initial OFF state in the *J-V*

characteristics of the memory device (Figure 4.4(a)). The PL spectrum exhibits a

maximum fluorescence at around 435 nm, which is attributed to the $S_1 \rightarrow S_0$ 0-0

transition of the fluorene chromophore (Heliotis et al., 2002). In comparison with the

dilute solution PL spectrum in Figure 4.3, the emission maximum in the solid state PL

spectrum of the TPATz-F8 film is red-shifted by about 15 nm, probably due to the

enhanced π-π stacking of the more planar segments of the backbone or increased

polarizability upon film formation (Shang et al., 2007; Kim et al., 2008). A vibrational

emission band at the longer wavelength (449 nm) is also observed, arising from the S_1

$\rightarrow S_0$ 0-1 transition of the fluorene chromophore (Jiang et al., 2009). In addition to the

above two intense emission features, the TPATz-F8 film also exhibits a less obvious,

structureless emission in the green region (around 530 nm), which is believed to result

from the inter-chain/inter-segmental interactions between the oxidation-induced

fluorenone defects (Sims et al., 2004).

When a negative bias (-4 V) larger than the switch-on threshold voltage (-2.8 V) is

applied on the TPATz-F8 device, electrical switching of the film from the OFF state to

the ON state is triggered. The corresponding PL spectrum (denoted by ON-1) exhibits

a decrease in intensity of all the three emission components. This partial fluorescence

quenching is associated with the decay of the excited singlet state of the fluorene

chromophore, resulting from the CT in the copolymer molecules (Shibano et al., 2006). Upon excitation by the electric field, electrons can transfer directly from the triphenylamine moiety to the adjacent triazole moiety, or indirectly from the fluorene moiety to the triphenylamine moiety, and then to the triazole moiety. Conductive CT states are thus formed in the TPATz-F8 molecules, resulting in the abrupt electrical switching of the device.
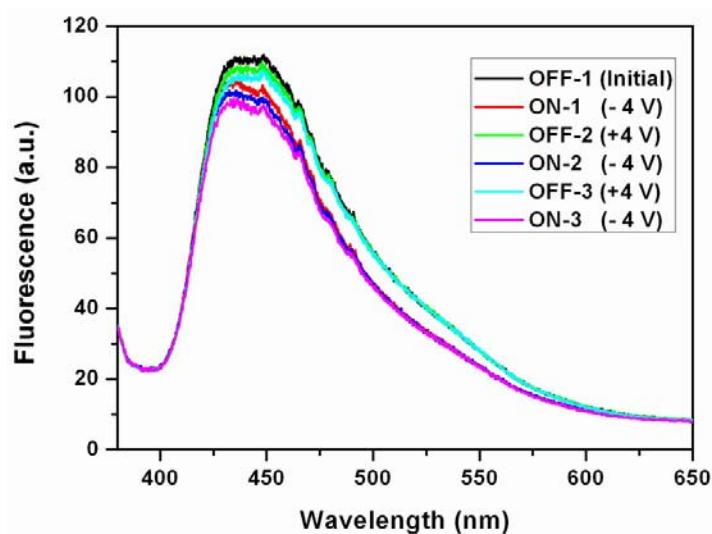
Figure 4.6 *In-situ* PL spectra of the TPATz-F8 film in an ITO/TPATz-F8/Al sandwich device under electrical biases. OFF-1 denotes the emission spectrum before applying any electric bias, while ON-1 to OFF-3 denote, respectively, the emission spectra after applying the electrical bias indicated in the bracket (with Al as the working electrode and ITO as the ground electrode).

In addition to the above fluorescence quenching, a redistribution of the oscillator strengths of the two main emission bands was also observed in the ON-1 spectrum, with the relative intensity of the 435 nm transition exhibiting a smaller decrease than that of the 449 nm transition. This phenomenon is similar to the previous report that a larger increase in relative intensity of the 0-0 PL peak than that of the 0-1 PL peak is observed in poly(9,9-dioctylfluorene) when the temperature decreases to 5 K (Ariu et

al., 2003). This redistribution is believed to be associated with the formation of a more planar polymer chain at low temperature. Accordingly, the electric field probably has also induced a more planar conformation in the excited TPATz-F8 molecule, which favors delocalization of the charge carriers in the conjugated backbone and stabilizes the conductive CT state. A non-volatile ON state is thus observed in the TPATz-F8 device.

Molecular simulation of the excited state TPATz-F8 molecule was carried out to further demonstrate the above conformation-coupled CT process. ESP surface and optimized geometry of the BU in the excited state were studied at the CIS/6-31G(d) level with the Gaussian 03 program package. The corresponding electronic properties of the BU in the ground state were employed as the reference. Figure 4.7 summarizes the molecular simulation results of both the ground and excited states. As shown by the ESP surfaces, TPATz-F8 at both states consists mainly of positive ESP region along the conjugated backbone, which permits migration of the charge carriers through this open channel. In addition, the molecule also exhibits some minor negative ESP regions arising from the sp^2 hybridized N atoms in the triazole group. As ESP is the potential energy of a proton at a particular location of a molecule, it can reflect the local electron density. Accordingly, the negative ESP region in TPATz-F8 suggests concentrated local electron densities in the triazole group, due to its electron-withdrawing nature (Yasuda et al., 2005). In comparison to TPATz-F8 in the ground state, TPATz-F8 in the excited state exhibits a larger negative region in the

triazole group, indicating that under excitation, electrons will transfer to the triazole

moiety from other parts of the molecule.
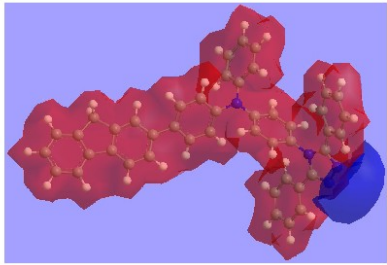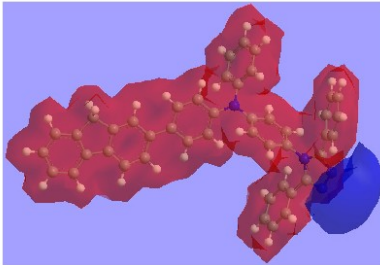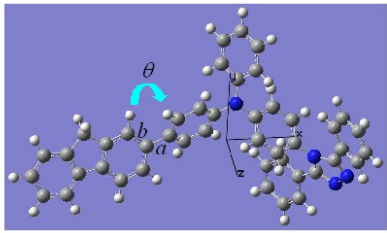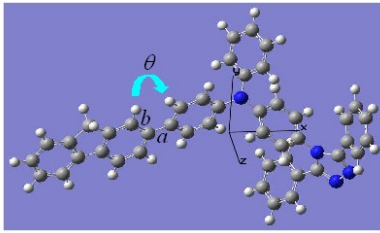
Properties	Ground State	Excited State
ESP Surface		
Optimized Geometry		
Bond Length	$a = 1.48\,\text{Å}, b = 1.41\,\text{Å}$	$a = 1.42\,\text{Å}, b = 1.44\,\text{Å}$
Dihedral Angle	$\theta = 35.8°$	$\theta = 7.5°$
Transition Dipole Moment (Debye)	—	x: 4.0760 y: 0.9808 z: -0.5721

Figure 4.7 ESP surfaces and optimized geometries of the TPATz-F8 BU in the ground and excited states, as well as the transition dipole moments along the three Cartesian axes. *a* and *b* denote, respectively, the inter-ring bond between the fluorene and adjacent benzene units and the nearby bond. *θ* denotes the dihedral angle between the fluorene and adjacent benzene planes. For the ESP surfaces, the positive ESP regions are in red, while the negative ESP regions are in blue.

Transition dipole moments along the three Cartesian axes are also calculated to

demonstrate the electronic transition orientation. As shown in Figure 4.7, the

transition dipole moment along the *x* axis (4.0760 Debye) is much larger than those

along the other two axes (0.9808 Debye for *y* axis and -0.5721 Debye for *z* axis,

respectively), indicating that the electrons have the largest tendency to transit along the *x* axis (Li et al., 2009), which orients approximately from the backbone to the pendant moiety.

Following the above electron transfer process, the conformation of TPATz-F8 molecule also undergoes changes under the applied electric field, as indicated by the different optimized geometries of TPATz-F8 in the ground and excited states. The inter-ring bond between the fluorene unit and the adjacent benzene ring (*a*) in the excited state (~ 1.42 Å) becomes shorter in comparison to that in the ground state (~ 1.48 Å), with the bond closest to it (*b*) becoming slightly longer (~ 1.44 Å in the excited state *vs* ~ 1.41 Å in the ground state). The shortening of the inter-ring bond length indicates that it changes from a single bond-like to a double bond-like character upon excitation, which is reported to be associated with the conversion from the aromatic isomer to the quinoid isomer (Gong and Lagowski, 2005; Gong and Lagowski, 2007). With the increase in double bond-like character of the inter-ring bond, the polymer chain becomes stiffer and rotation is restricted. As a result, the polymer assumes a more planar conformation, with the dihedral angle between the fluorene plane and the adjacent benzene ring (*θ*) decreasing from 35.8° in the ground state to 7.5° in the excited state. The conformational change is consistent with the previous report that polyfluorene molecules tend to change from a twisted conformation (torsional angle of 37.6°) to a more planar conformation (torsional angle of 8.1°) upon excitation (Liang et al., 2006). The double bond-like character of the

inter-ring bond and the more planar conformation in the excited TPATz-F8 molecule favor delocalization of charge carriers in the conjugated backbone. As a result, the conductive CT state is stabilized and the high-conductivity state can be retained, resulting in the non-volatile nature of the ON state.

When a positive electrical sweep is applied on the TPATz-F8 device, for example, the 4th sweep in Figure 4.4(a), the CT state is dissociated via back electron transfer and the polymer chain relaxes to the initial twisted conformation, switching the device back to the OFF state. The erasing of the ON state is supported by the recovery of the PL spectrum corresponding to the OFF state after the application of a positive bias of +4 V (OFF-2 spectrum). However, a slight decrease in intensity of the main emission bands is observed in the OFF-2 spectrum in comparison to that in the initial OFF-1 spectrum, probably due to the delay in conformational relaxation of the polymer chain under the applied electric field (Ling et al., 2007; Liu et al., 2009). The "ON-OFF" changes in PL spectra matches the write-erase process in the *J-V* characteristics of the TPATz-F8 device, and can be repeated with good accuracy, as indicated by the subsequent ON-2, OFF-3 and ON-3 spectra in Figure 4.6.

In comparison to TPATz-F8, TPATz-F8BT has a similar molecular structure, except for the presence of additional benzothiadiazole units in the backbone. Accordingly, similar rewritable memory effects were also observed in the TPATz-F8BT device, except for the lower (by about one order) ON state current, and thus lower ON/OFF current ratio, than that of the TPATz-F8 device. The phenomenon is probably

associated with the hole-blocking nature of the electron-deficient benzothiadiazole groups (Lim et al., 2006). The difference in ON state current is also consistent with the higher hole mobility of the fluorene-triphenylamine copolymer (in the order of 10^{-3} cm^2 V^{-1} s^{-1}) (Zaumseil et al., 2006) in comparison to that of the fluorene-benzothiadiazole copolymer (in the order of 10^{-4} cm^2 V^{-1} s^{-1}) (Redecker et al., 1999). The molecular structure-dependent memory effects also demonstrate that it is possible to tune the electrical switching behavior by tailoring the molecular structures of polymers.

4.4 Conclusion

Two solution-processable polyfluorene copolymers, TPATz-F8 and TPATz-F8BT, containing the fluorene, triphenylamine and triazole moieties, with TPATz-F8BT containing also the benzothiadiazole moieties, were characterized for their bistable electrical switching and memory effects. Devices based on the ITO/polymer/Al sandwich structure can be switched 'ON' and 'OFF' during the negative and positive electrical sweeps, respectively. The molecular simulation results and electrochemical measurement of TPATz-F8 indicate that the fluorene and triphenylamine groups act as the electron donors, while the triazole group acts as the electron acceptor. Electric field-induced CT from the donor moieties to the acceptor moiety gives rise to a conductive CT state, accounting for the electrical switching from the OFF state to the ON state. The more planar conformation of the TPATz-F8 molecule in the excited state stabilizes the conductive CT state and dictates the non-volatile nature of the ON state. The conformation-coupled CT was further elucidated from molecular simulation of the excited state TPATz-F8 molecule and *in-situ* changes in photoluminescence spectra of the TPATz-F8 film under electrical biases. The difference in electrical switching behavior associated with the difference in molecular structure of TPATz-F8 and TPATz-F8BT illustrate the possibility of tuning memory properties in polyfluorenes via molecular design and synthesis.

CHAPTER 5

ELECTRICAL SWITCHING AND MEMORY EFFECTS IN AZO POLYMERS CONTAINING DIFFERENT TERMINAL GROUPS IN THE PENDANT AZOBENZENE MOIETIES

5.1 Introduction

Azobenzene derivatives constitute a family of dye molecules which are characterized by the azo linkage (-N=N-) that bridges two phenyl rings (Kurihara et al., 2007; Ichimura, 2000). This extended aromatic structure gives rise to the intense optical absorption and unique optical properties of the azobenzene compounds. The most well-known optical property is their photochromic feature, which arises from the reversible *cis-trans* photoisomerizations (Diau, 2004; Ahonen et al., 2007; Murase et al., 2007). The *trans* configuration (also denoted as the E state) is thermally stable, while the *cis* configuration (also denoted as the Z state) is meta-stable (Yager and Barrett, 2006). Light within the broad *trans*-azobenzene absorption band will induce photochemical isomerization to the *cis* configuration (Zimmerman et al., 1958). The *cis* state will then typically relax thermally back to the *trans* state with a lifetime which depends on the nature of the substituents in the azobenzene. Irradiation of the *cis* state with light within its absorption band can also cause the isomerization back to the *trans* state. Due to this clean photochemistry and distinct changes in material properties under light irradiation, azobenzene derivatives have been investigated for a variety of applications, including non-linear optical devices (Natansohn and Rochon, 2002; Yesodha et al., 2004), holographic grating (Zhang et al., 2002), and optical switching (Ikeda and Tsutsumi, 1995). The reversible *trans-cis* photoisomerization of the azobenzene compounds has also been adopted for optical data storage (Kawata and Kawata, 2000). Besides optical manipulation, the isomerization can also be

controlled by an electric field (Alemani et al., 2006), suggesting the potential application of azobenzene compounds in electronic molecular switches. Moreover, a series of azobenzene molecules have been reported to exhibit good electrical bistability associated with the electric field-induced charge transfer (CT) (Wen et al., 2006; Hu et al., 2007; Jiang et al., 2008), providing a means for high-density data storage. In addition to the small azobenzene molecules, electrical bistability has also been observed in azobenzene-containing polymers (Attianese et al., 2008), where the *trans-cis* isomerization induced by the electric field is responsible for the electrical switching.

In this chapter, two azo polymers, AzoNEtCN and AzoNEt (molecular structures shown in Figure 5.1), with the pendant azobenzene chromophore attached by different terminal groups, were studied for their electrical switching and memory effects. Both memory devices were found to exhibit uni-directional electrical switching during the negative sweep. However, the volatility of their high-conductivity (ON) state is dependent on the terminal group in the pendant azobenzene moiety. The mechanism associated with the different memory effects were elucidated from molecular simulation results.

5.2 Experimental Section

5.2.1 Materials

Methacryloyl chloride was purchased from Haimen Best Fine Chemical Industry Co. and used after distillation. 2,2'-Azobisisobutyronitrile (AIBN, 97%) was purchased from Shanghai Chemical Reagent Co. and recrystallized from ethanol twice. Anisole and chloroform were purchased from Shanghai Chemical Reagent Co. as analytical regents and purified by distillation. Aniline (99%) and N-ethyl-N-2-hydroxyethyl-m-toluidine (99%) were purchased from Tokyo Kasei Kogyo Co. and used as received. 4-Aminobenzonitrile (98%) was purchased from Alfa Aesar, a Johnson Matthey Co. and used without further treatment. 2-cyanoprop-2-yl dithiobenzoate (CPDB) was synthesized according to the previous literature (Chong et al., 2003). Other materials were purchased from Shanghai Chemical Reagent Co. and purified according to the standard method.

5.2.2 Instrumentation

NMR spectra were obtained on an Inova 400 MHz spectrometer using $CDCl_3$ as the solvent. Weight average (M_w) and number average (M_n) molecular weights were determined on a Waters 1515 gel permeation chromatography (GPC) equipped with a refractive index detector. Tetrahydrofuran (THF) was used as the eluent and poly(methyl methacrylate) (PMMA) was employed as the molecular weight standard

sample. Other instruments used in this chapter are the same as in Chapter 3.

5.2.3 Synthesis of the Monomers and Polymers

The two azo polymers were prepared and characterized by Prof. Zhu Xiu-Lin and Mr. Cao Hai-Zhong from Soochow (Suzhou) University, China. The synthesis route of the azobenzene polymers are illustrated in Figure 5.1. Details on their preparations and characterizations are given below.

Synthesis of 4-{4-[ethyl-(2-hydroxy-ethyl)-amino]-2-methyl-phenylazo}-benzon-trile (1): 4-aminobenzonitrile (4.72 g, 40 mmol) was dissolved in an aqueous solution of sodium nitrite (3.38 g in 40 mL deionized water). The obtained solution was cooled to 0 ~ 5°C, followed by adding the hydrochloric acid solution (16 mL in 100 mL deionized water) slowly with stirring. After the above mixture was stirred for further 30 min, carbamide (0.48 g, 8 mmol) was added to demolish the residual sodium nitrite with tracking by starch-iodide paper. Then the diazonium salt solution was obtained. A solution of *N*-ethyl-*N*-2-hydroxyethyl-*m*-toluidine (8.78 g, 48 mmol), glacial acetic (15 mL), and deionized water (30 mL) were slowly added to the diazonium salt solution at 0 ~ 5°C. The mixture was vigorously stirred for 30 min in ice bath, and then the sodium hydroxide aqueous solution was added to adjust the pH to 5 ~ 7. The solution was heated to 40 ~ 50°C gradually and kept for 15 min. Afterwards, the solution was cooled with ice bath for 2 h. The resultant solid was filtered and dried under vacuum at room temperature. After recrystallized from ethanol/water mixture

(3/2 by volume), the compound **1** was obtained as a red crystal. ^{1}H NMR (CDCl$_3$, 400 MHz), δ(ppm): 7.84-7.94(d, 2H), 7.75-7.84(s, 1H), 7.65-7.78(d, 2H), 6.62(s, 2H), 3.88(s, 2H), 3.47-3.65(m, 3H), 2.68(s, 3H), 1.56(s, 2H), 1.18-1.30(t, 3H). Anal. Calcd. for C$_{18}$H$_{20}$N$_4$O: C 69.93, H 6.69, N 18.61; found: C 70.11, H 6.54, N 18.17.

Synthesis of 2-Methyl-acrylic-acid-2-{[4-(4-cyano-phenylazo)-3-methyl-phenyl]-ethyl-amino}-ethyl ester (MACP): Compound **1** (6.1 g, 20 mmol), dry THF (50mL), and triethylamine (2.8 mL) were added to a round-bottom flask and cooled with ice bath. Methacryloyl chloride (1.9 mL, 22 mmol) diluted in dry THF (10 mL) was added dropwise to the cool solution. The resultant mixture was vigorously stirred for 1 h at 0 ~ 5 °C and then for further 6 h at room temperature. The solution was filtered, and the solvent was removed by rotary evaporation. The crude product was dissolved in dichloromethane and washed with deionized water for three times, followed by drying with anhydrous magnesium sulfate overnight. Finally, the obtained crude product was purified by column chromatography (silicagel H) with petroleum ether/ethyl acetate mixture (10/1 by volume) as eluent to give a red crystal **MACP**. ^{1}H NMR (CDCl$_3$, 400 MHz), δ(ppm): 7.86-7.91(d, 2H), 7.78-7.82(d, 1H), 7.71-7.76(d, 2H), 6.62-6.64(t, 2H), 6.11(s, 1H), 5.59(s, 1H), 4.33-4.39(t, 2H), 3.66-3.78(t, 2H), 3.44-3.59(m, 2H), 2.69(s, 3H), 1.92-1.98(d, 3H), 1.22-1.29(t, 3H). Anal. Calcd. for C$_{22}$H$_{24}$N$_4$O$_2$: C 69.90, H 6.54, N 14.77; found: C 70.19, H 6.43, N 14.88.

Synthesis of 2-methyl-acrylic-acid-2-[ethyl-(4-phenylazo-3-methyl-phenyl)-ami-

no]-ethyl ester (MAEA): **MAEA** was synthesized using a similar procedure as **MACP**.

RAFT polymerization of MACP and MAEA: The following procedure is typical: a master batch of AIBN (4.1 mg, 0.025 mmol) and CPDB (33.2 mg, 0.15 mmol) were dissolved in anisole (10 mL). An aliquot of 1mL of the above solution was placed in 5 mL ampoules together with **MACP** (376.5 mg, 1.00 mmol). The mixture was purged with argon for approximately 20 min to eliminate the oxygen. Then, the ampoules were flame-sealed and placed in an oil bath held by a thermostat at 80°C to polymerize. After predetermined time, each ampoule was quenched in ice water and opened. The reaction mixture was diluted with 2 mL THF and poured slowly into 200 mL methanol. The precipitate was filtered, washed with methanol, and dried in vacuum at room temperature. The RAFT polymerization of **MAEA** was carried out with a similar procedure as that of **MACP**.
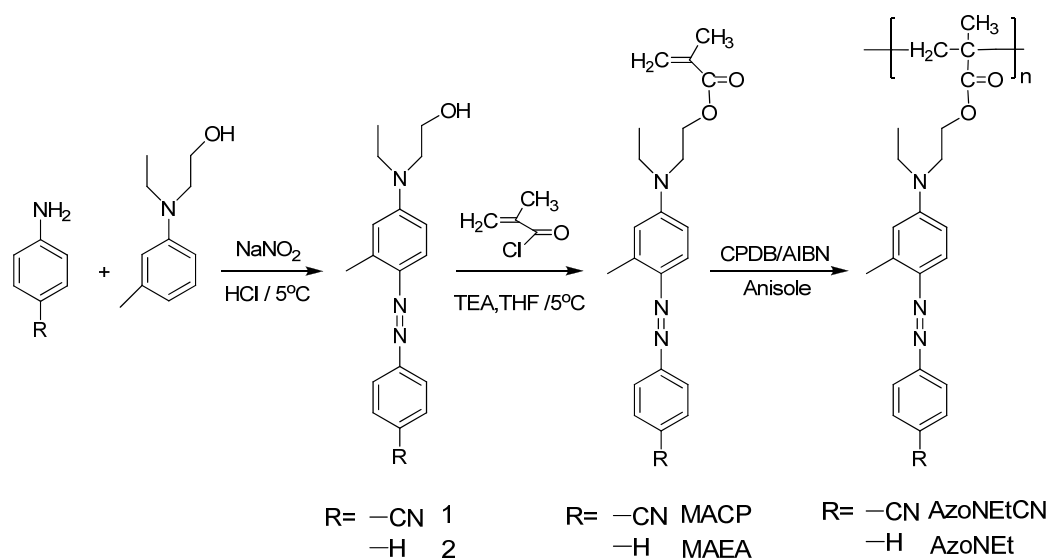
Figure 5.1 Synthesis routes for the monomers and the azo polymers

5.2.4 Fabrication and Characterization of the Memory Devices

The ITO coated glass substrate was pre-cleaned sequentially with deionized water, acetone, and isopropanol in an ultrasonic bath for 15 min. A *N,N*-dimethylacetamide (DMAc) solution of the azo polymer was spin-coated onto the ITO substrate, followed by solvent removal in a vacuum chamber at 10^{-5} Torr and 50°C for 10 h. The thickness of the polymer layer was about 50 nm, as determined by the AFM step profiling. Finally, an Al top electrode of 400 nm in thickness was thermally deposited onto the polymer layer through a shadow mask at a pressure of about 10^{-7} Torr. The electrical properties measurements were carried out on devices of 0.4×0.4 mm^2, 0.2×0.2 mm^2, and 0.15×0.15 mm^2 in size, under ambient conditions, using an Agilent 4155C semiconductor parameter analyzer equipped with an Agilent 41501B pulse generator. The current density-voltage (*J-V*) data reported are based on device units of 0.4×0.4 mm^2 in size, unless stated otherwise. ITO was maintained as the ground electrode during the electrical measurements.

5.3 Results and Discussion

5.3.1 Characterizations of the Azo Polymers

The solubilities of the azo polymers in common organic solvents are summarized in Table 5.1. The two azo polymers exhibit good solubilities in common solvents, such as DMAc, DMF, NMP, THF and chloroform, at room temperature. Thus, they can be easily cast into uniform thin film from solution by spin-coating. GPC measurement shows that M_n of AzoNEtCN and AzoNEt are 10743 and 3507, respectively, with the polydispersity indexes being 1.37 and 1.47.

Table 5.1 Solubilities of the azo polymers in common organic solvents

Polymer	Solubility[a]				
	DMAc	DMF	NMP	THF	CHCl$_3$
AzoNEt	++	++	++	++	++
AzoNEtCN	++	++	++	++	++

[a]Solubility measured in concentration of 1 mg·mL^{-1}
++: Soluble at room temperature

The UV-visible absorption spectra of the two azobenzene polymers in diluted DMAc solution are demonstrated in Figure 5.2. The concentrations of AzoNEt and AzoNEtCN are 5×10^{-6} mg·L^{-1} and 1.5×10^{-6} mg·L^{-1}, respectively. Both spectra exhibit two major absorption peaks. The absorption peak at the shorter wavelength originates from the $\pi\rightarrow\pi^*$ transition of the aromatic rings, while the absorption peak at the longer wavelength is due to the vibrational coupling between the $n\rightarrow\pi^*$ and $\pi\rightarrow\pi^*$ electronic transitions of the *trans*-azobenzene chromophore (Gore and Wheeler, 1961). The absorption spectrum of AzoNEt is characterized by a close energetic proximity of

the π→π* and n→π* absorption bands, as demonstrated in Figure 5.2(a). The maximum absorption peak at 423 nm arises from the π→π* electronic transition, while the absorption shoulder at about 465 nm arises from the n→π* electronic transition. In comparison to AzoNEt, AzoNEtCN has a cyano acceptor group attached to the azobenzene chromophore. The push-pull configuration between the amino donor and cyano acceptor groups greatly enhances the CT characteristic in AzoNEtCN. Thus, delocalization of the π electrons is significantly enhanced, resulting in a red-shift in the π→π* absorption band. As shown in Figure 5.2(b), the π→π* absorption band of AzoNEtCN red shifts to 460 nm, much longer than that of AzoNEt (424 nm). The weak n→π* absorption band is buried under the intense π→π* absorption band, and is thus not observable.
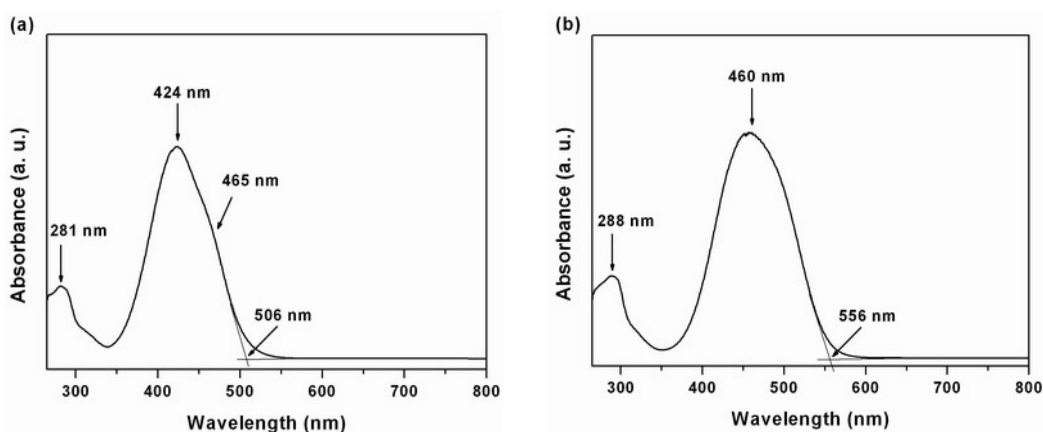
Figure 5.2 UV-visible absorption spectra of (a) AzoNEt and (b) AzoNEtCN in diluted DMAc solution, with their respective concentration being 5×10^{-6} mg·L^{-1} and 1.5×10^{-6} mg·L^{-1}, respectively.

5.3.2 Electrical Switching and Memory effects of the Azo Polymers

The electrical behaviors of AzoNEtCN under electrical sweeps are demonstrated by the *J-V* characteristics of an ITO/AzoNEtCN/Al sandwich device, as exemplified in Figure 5.3(a). Initially, the device was swept positively (with ITO as the cathode and Al as the anode) from 0 to 4 V (the 1st sweep). It remained in the low-conductivity (OFF) state without any abrupt increase in the current density. However, when it was swept negatively (with ITO as the anode and Al as the cathode) from 0 to -4 V (the 2nd sweep), the current density increased progressively with the applied bias, and exhibited an abrupt increase to the high-conductivity (ON) state at -3.4 V. Afterwards, the device remained in the ON state when the negative voltage sweep was repeated (the 3rd sweep). The ON state cannot be reset to the initial OFF state by the application of the positive sweep (the 4th sweep) and is thus irreversible. The device was able to remain in the ON state even after the power has been turned off. Thus, the AzoNEtCN device exhibits a non-volatile WORM type memory effect. Figure 5.3(b) shows the effect of operation time on the stability of the AzoNEtCN device. Under a constant stress of -1 V, no obvious degradation in current density was observed for both the ON and OFF states over a 6 h period. Figure 5.3(c) shows the effect of the reading pulses on the stability of the AzoNEtCN device. After 10^8 read pulses of -1 V, no degradation in current density was observed for both the ON and OFF states.

The *J-V* characteristics of the AzoNEt device under electrical sweeps are demonstrated in Figure 5.3(d). During the 1st positive sweep from 0 to 4 V, the device

remained in the OFF state, similar to the behavior of the AzoNEtCN device in the 1st positive sweep. During the subsequent negative sweep from 0 to -4 V (the 2nd sweep), the device switched to the ON state at -3.2 V. The device remained in the ON state during the subsequent negative sweep (the 3rd sweep). Similar to the AzoNEtCN device, the AzoNEt device cannot be reset to the initial OFF state by the reverse positive sweep (the 4th sweep). However, different from the stable ON state of AzoNEtCN, the ON state of AzoNEt was unstable and can be retained for a period of about 2 min, after turning off the power. The result indicates the volatile feature of the ON state of AzoNEt. Afterwards, when the negative threshold voltage was re-applied (-3.2 V in the 5th sweep), the device can be re-programmed to the ON state. The volatile ON state can be electrically sustained either by a refreshing voltage pulse of -1 V (1 ms duration) in every 5 s (the 'rf' trace in Figure 5.3(d)) or a continuous bias of -1 V (Figure 5.3(f)). Thus, the electrical behaviors of the AzoNEt device share the common characteristics with that of a SRAM, except for the relatively long retention time (about 2 min) of the ON state. Figure 5.3(e) and 5.3(f) show that the AzoNEt device is stable in both ON and OFF states under a continuous stress of -1 V or read pulses of -1 V.
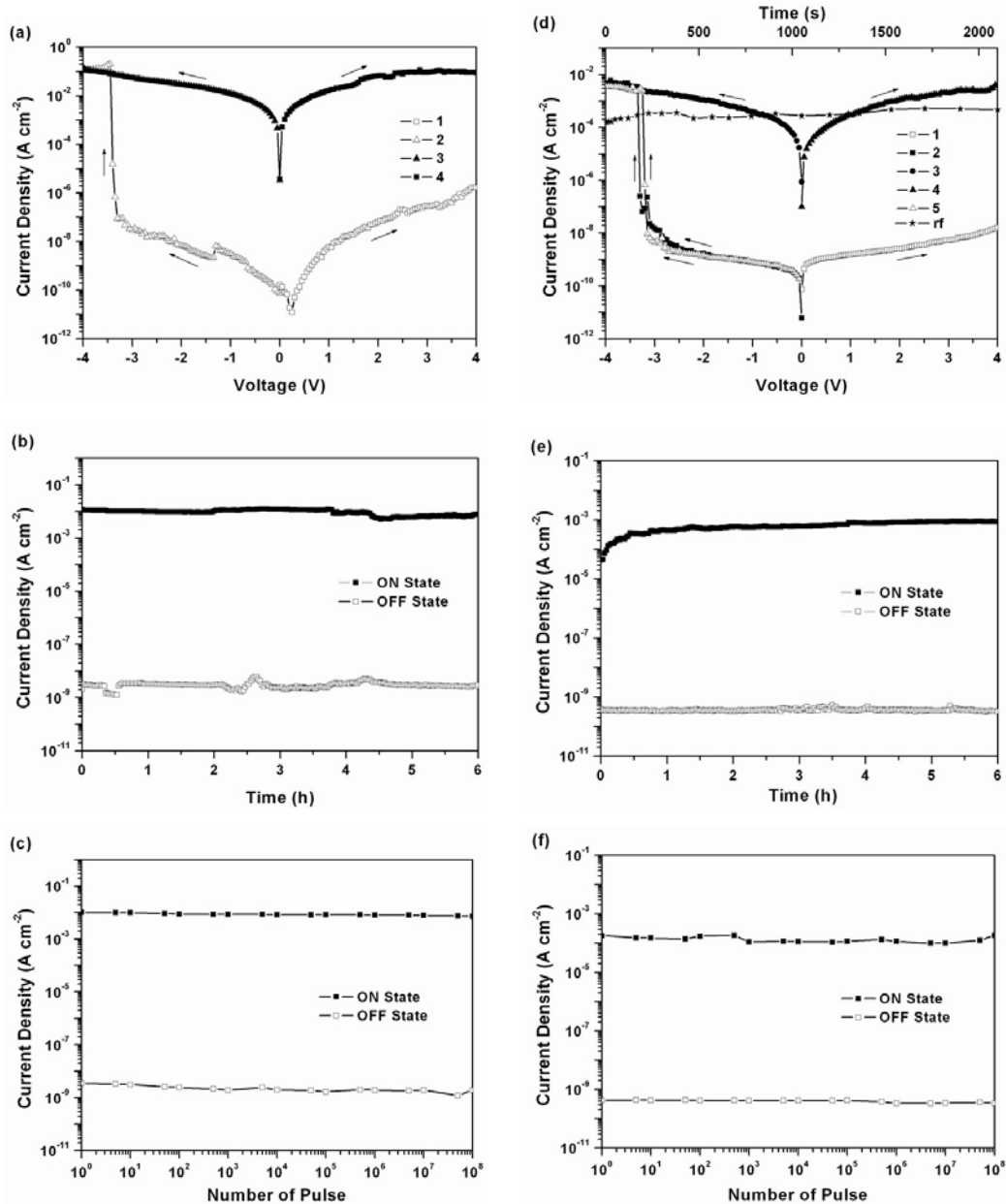
Figure 5.3 (a) *J-V* characteristics of a 0.4×0.4 mm^2 ITO/AzoNEtCN/Al device. The sequence and direction of each sweep are indicated by the respective number and arrow. (b and c) Stability of the ON and OFF states of the AzoNEtCN device under a constant stress of -1 V and read pulses of -1 V. (d) *J-V* characteristics of a 0.4×0.4 mm^2 ITO/AzoNEt/Al device. The sequence and direction of each sweep are indicated by the respective number and arrow. The 4th was conducted about 2 min after turning off the power. The ON state was sustained by a refreshing pulse of -1 V (1 ms duration) in every 5 s, as shown by the 'rf' trace. (e and f) Stability of the ON and OFF states of the AzoNEt device under a constant stress of -1 V and read pulses of -1 V.

During the experiment, the *J-V* characteristics are found to have good repeatability. In addition, along with the decrease in device area ($0.4 \times 0.4 \rightarrow 0.2 \times 0.2 \rightarrow 0.15 \times 0.15$ mm^2), the current magnitudes in both states decrease linearly, indicating that the current density is independent on the device area. The structure-dependant electrical switching effects, good reproducibility and area-independent characteristics rule out the possibility of filament effect (Henisch and Smith, 1974), metal diffusion (Lim et al., 1998; Ma et al., 2000), and dielectric break down.

5.3.3 Switching Mechanism

It is reported that azobenzene compounds, such as Sudan I and Disperse Red I, are capable of undergoing charge trapping/detrapping upon light irradiation. The trapped charges can be stored for a long time and give rise to a high photoconductivity state, making these azobenzene dyes promising for electrooptical information storage. As the two azo polymers studied in this chapter contain similar azobenzene chromophore in the pendant moiety, the ability of the azobenzene chromophore to trap and store charges probably accounts for the observed electrical bistability. As shown in the *J-V* characteristics of the two memory devices, the ON state is non-volatile when the polymer has an electron-withdrawing terminal group at its pendant moiety, while is volatile when there is no terminal group. Thus, charge trapping, mediated by the terminal group of the pendant azobenzene chromophore, is probably responsible for the observed different electrical switching behaviors.

In order to study the electrical switching effects, molecular simulations of the two polymers were carried out with the Gaussian 03 program package. As the backbone moiety probably does not significantly affect the electronic properties, only the pendant azobenzene moiety was taken account in the molecular simulation. The energy levels of the highest occupied molecular orbital (HOMO) and lowest unoccupied molecular orbital (LUMO) of the two polymers are demonstrated in Figure 5.4, along with the work functions of ITO and Al electrodes. During the negative sweep (with ITO as the anode and Al as the cathode), the lowest energy barriers in both devices are located between the work function of ITO and the HOMO of the polymer (0.67 eV for AzoNEtCN and 0.34 eV for AzoNEt), indicating that hole injection from ITO into the HOMO is a favored process. Electron injection from Al into the LUMO is, however, much more difficult, due to the large energy barriers (1.91 eV for AzoNEtCN and 2.51 eV for AzoNEt). Thus, during the negative electrical sweep, the injected holes dominate the conduction process. As indicated by the ESP surfaces (Figure 5.4), both polymers show the presence of some minor negative ESP regions associated with the diazene group. These negative ESP regions can act as the "traps" to block the mobility of the injected holes. Thus, during the initial electrical sweep, the injected holes are blocked by the traps while hopping along the pendant azobenzene chromophores (Oh-e et al., 2002), resulting in the low current density. At the switch-on threshold voltage, the majority of the traps are filled by holes and a "trap-free" channel is formed for the injected hole to migrate through. As a result, the current density increases rapidly and the device switches to the

high-conductivity (ON) state.

Properties		AzoNEtCN	AzoNEt
Energy Level			
Dipole Moment	Excited State	13.37 Debye	5.72 Debye
	Ground State	10.47 Debye	4.12 Debye
Molecular Orbitals	LUMO		
	HOMO		
ESP surfaces	Excited State		
	Ground State		
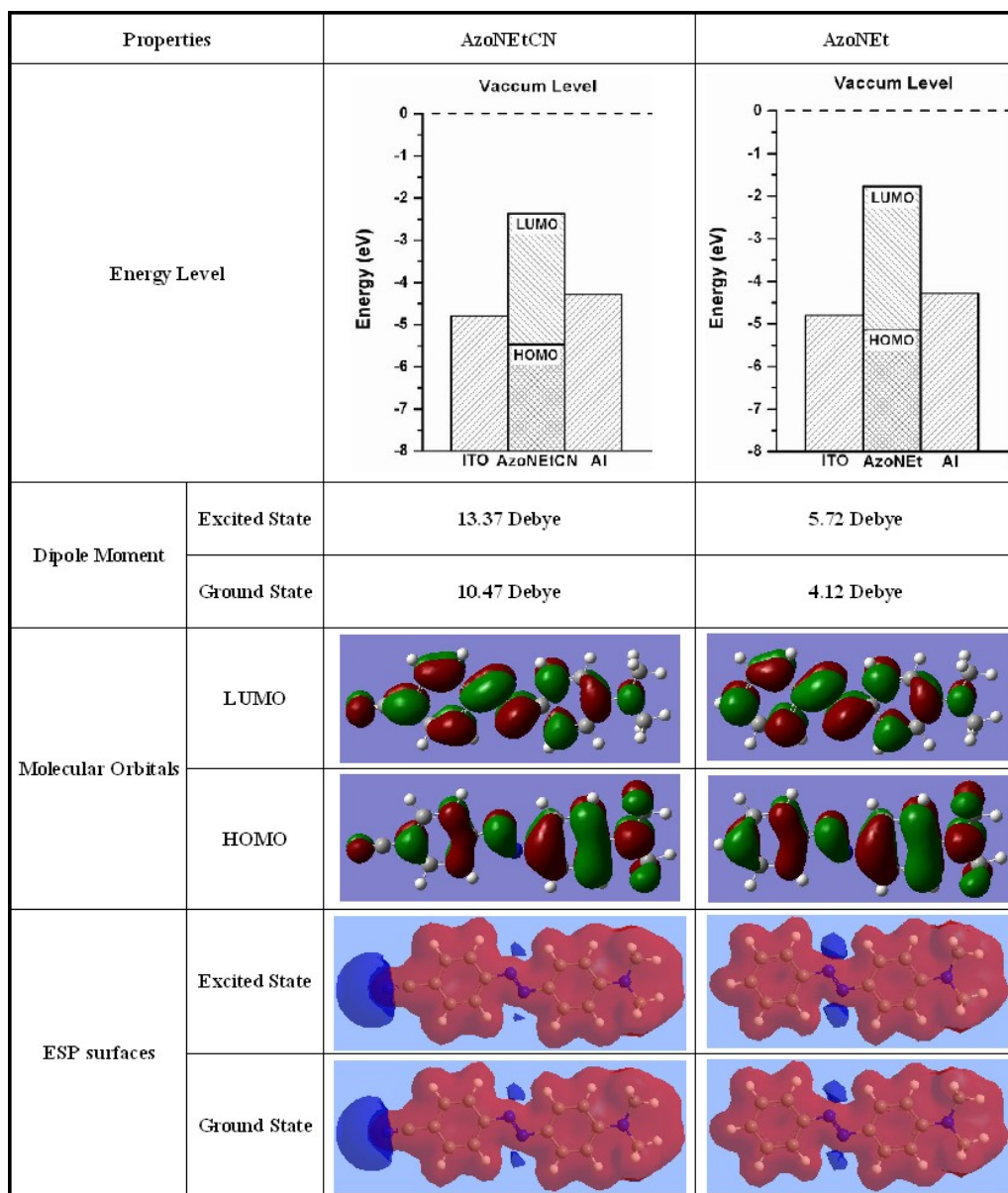
Figure 5.4 Summary of the HOMO and LUMO energy levels and surfaces, dipole moments, and ESP surfaces of AzoNEtCN and AzoNEt, determined by the molecular simulation.

However, when the device is swept positively (with ITO as the cathode and Al as the

anode), the energy barriers between the work function of Al and the HOMO of the

polymers (0.86 eV for AzoNEt and 1.19 eV for AzoNEtCN) is comparatively large, so the hole injection process is inhibited and the devices exhibit no electrical switching effect. This uni-directional switching behavior confirms that the electrical switching arises from the charge injection and trapping processes described above, rather than charge transfer process, which is normally associated with symmetric bi-directional electrical switching (Liu et al., 2009).

Despite the similar electrical switching behaviors described above, the two polymers exhibit different volatility in their ON states, i.e., AzoNEtCN exhibits non-volatile ON state, while AzoNEt exhibits volatile ON state which can retain for about only 2 min. As the two polymers differ only in the terminal groups of their pendant moieties, the different ON state volatilities are believed to arise from the different terminal groups. The effects of the terminal groups on the resultant memory behaviors will be elucidated with the molecular simulation results in the following parts.

As shown in Figure 5.4, the HOMO and LUMO surfaces of AzoNEtCN are comparatively asymmetric, with the former localized more on the amine side and the latter localized more on the cyano side. Such localization of electron density in the HOMO surface indicates a large ground state dipole moment. Upon HOMO $\rightarrow$ LUMO excitation, a larger dipole moment is generated for the excited state, due to the intramolecular CT between the amino and cyano groups. The HOMO and LUMO surfaces of AzoNEt are, however, more symmetric, due to the absence of any

electron-withdrawing terminal group. The more symmetric HOMO surface suggests a relatively small ground state dipole moment for AzoNEt. The molecular simulation results show that the ground state dipole moments of AzoNEtCN and AzoNEt are 10.47 Debye and 4.12 Debye, respectively. Upon excitation, their dipole moments increase to 13.37 Debye and 5.72 Debye, respectively. The different excited state dipole moments are believed to play an important role for the different volatilities of the ON states. The large excited state dipole moment of AzoNEtCN can generate a strong internal electric field, which favors holding of the trapped charges as well as the conducting channel for charge carriers. A non-volatile ON state is thus observed in the AzoNEtCN device. As regards to AzoNEt, the small excited state dipole moment is not strong enough to hold the trapped charges and the conducting channel effectively. After removal of the applied electric field, the trapped charges are believed to be detrapped, and the conducting channel is blocked. As a result, a volatile ON state is observed in the AzoNEt device.

Besides the dipole moment, intramolecular CT in the pendant azobenzene moiety is also affected by the terminal group. The intramolecular CT can be demonstrated by the different ESP surfaces of the azobenzene chromophore in ground and excited states. As ESP is the potential energy of a proton at a particular location of a molecule, it can reflect the local electron density. Accordingly, the negative ESP regions around the electron-withdrawing groups (diazene and cyano groups) suggest concentrated local electron density. For AzoNEtCN in the excited state, it exhibits a smaller

negative ESP region around the diazene group and a larger negative ESP region around the cyano group, in comparison to its ground state counterpart. This change in ESP surface indicates that upon excitation, intramolecular CT occurs from the amino donor group to the cyano acceptor group, through the mid-region conjugated azobenzene system. In the presence of the strong cyano acceptor group, the above intramolecular CT is stable, and can withstand the reverse bias and removal of the applied electric field. As a result, the trapped charges are stabilized, resulting in an irreversible and non-volatile ON state for the AzoNEtCN device. In comparison to AzoNEtCN, AzoNEt only exhibits a negative ESP region around the diazene group. Upon excitation, the negative ESP region is enlarged, indicating that in absence of the cyano group, the diazene group acts as the electron acceptor to pull electrons from the amino donor group. The acceptor effect of the diazole group is consistent with its moderate electron-withdrawing ability (Stoyanov et al., 1996). However, as the diazene group is only a weak acceptor, the intramolecular CT is unstable and cannot hold the trapped charges for a long time. After removal of the applied electric field, the conducting channel is easily blocked by the back transfer of charges, and the AzoNEt device relaxes to its initial OFF state.
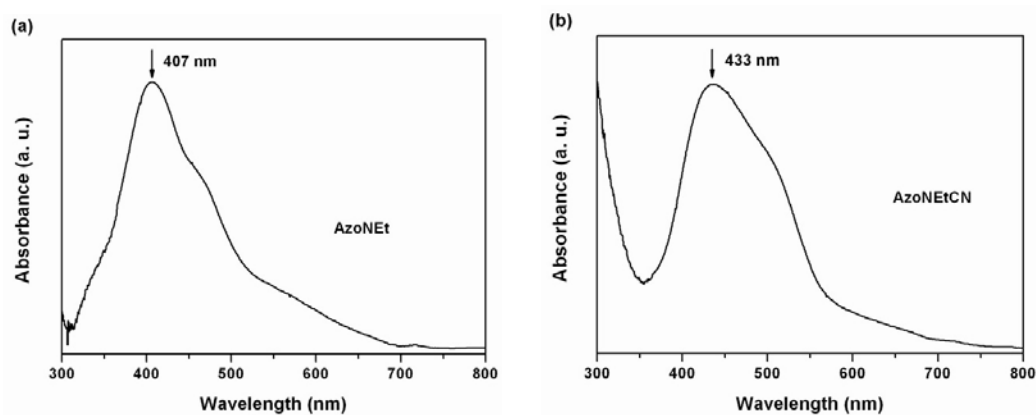
Figure 5.5 UV-visible absorption spectra of (a) AzoNEt and (b) AzoNEtCN films spin-coated on ITO substrate.

In addition to the above intramolecular CT, intermolecular CT is also likely to occur between the pendant azobenzene moieties. As indicated in Figure 5.5, the absorption maxima of the two azo polymers in solid state exhibit significant hypsochromic shift in comparison to those of their solutions. This shift in absorption band is associated with the formation of an antiparallel alignment between the neighboring pendant azobenzene moieties in the polymer films (Brown et al., 1995; Labarthet et al., 2000). In this alignment, the pendant azobenzene moieties in different molecule chains tend to antiparallelly interdigitate with each other, and the distance between the neighboring pendant moieties is decreased, as illustrated by schematic arrangement of the AzoNEtCN molecules (Figure 5.6). In the antiparallelly arranged AzoNEtCN molecules, the amino donor group of one pendant moiety faces the cyano acceptor group of a neighboring pendant moiety. This arrangement as well as the decreased inter-side chain distance facilitates the intermolecular CT between the cyano acceptor and amino donor groups, which is reported more stable than the intramolecular CT (Wu et al., 2003; Jiang et al., 2003). The trapped charges are thus further stabilized in

146

the excited AzoNEtCN molecules. The AzoNEt molecules also possess the antiparallel arrangement, with the diazene group of one pendant moiety facing the terminal phenyl ring of another pendant moiety. However, intermolecular CT is less likely to occur in AzoNEt, due to the weak interaction between the diazene and phenyl groups in neighboring pendant moieties. Thus, only the intramolecular CT occurs in AzoNEt, which is not strong enough to hold the trapped charges for a long time.
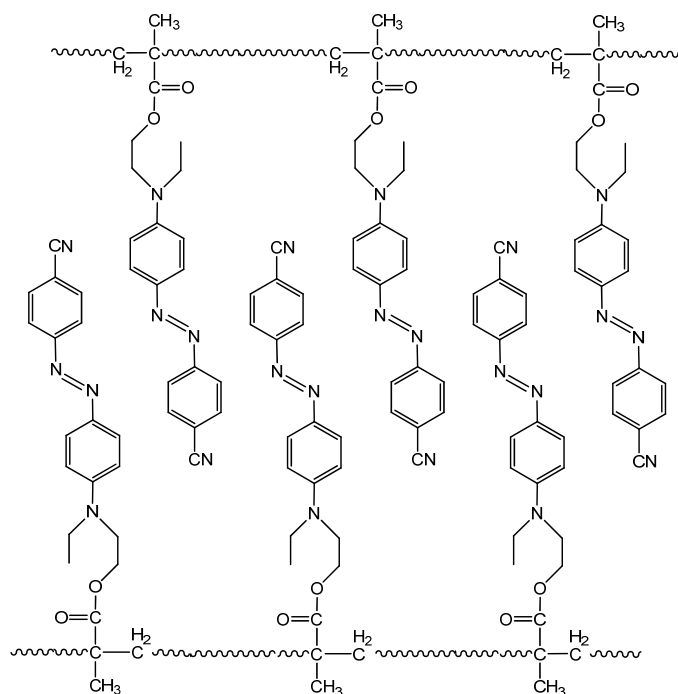
Figure 5.6 Schematic representation of the antiparallel and interdigited arrangement of AzoNEtCN.

5.4 Conclusion

Two azo polymers, AzoNEt and AzoNEtCN, with azobenzene chromophores in the pendant moieties, were studied for their electrical switching effects. Both polymers were found to exhibit uni-directional electrical switching from the OFF state to the ON state during the negative electrical sweep. The volatility of the ON state was found to be dependant on the electron-withdrawing ability of terminal group in the pendant azobenzene moiety. Non-volatile ON state was observed when the azobenzene moiety is attached by an electron-acceptor terminal group (cyano group in AzoNEtCN), while volatile ON state was observed when the azobenzene moiety has no terminal group (AzoNEt). The cyano group in AzoNEtCN gives rise to a large dipole moment and strong intramolecular CT, which help to stabilize the conducting channel for charge carriers and thus the high-conductivity (ON) state. On the other hand, without any terminal group, AzoNEt cannot hold the conducting channel, resulting in a volatile ON state.

CHAPTER 6

ELECTRICAL SWITCHING AND MEMORY EFFECTS IN GRAPHENE OXIDES FUNCTIONALIZED WITH DIFFERENT CONJUGATED POLYMER SEGMENTS

6.1 Introduction

Graphene is a one-atom-thick planar sheet of sp^2 hybridized carbon atoms that are densely packed in a honeycomb crystal lattice. Its two dimensional (2D) network is the fundamental building block of other carbon-based materials, such as 0D fullerenes, 1D carbon nanotubes and 3D graphite (Guldi and Sgobba, 2011; Ke et al., 2003; Saito et al., 1992). Due to this unique structure, graphene derivatives exhibit remarkable electronic (Eda et al., 2008; Geim and Novoselov, 2007; Novoselov et al., 2007), optical (Mak et al., 2008; Wang et al., 2008), magnetic (Nomura and MacDonald, 2006; Wang et al., 2009), and mechanical (Dikin et al., 2007; Lee et al., 2008) properties, making them useful in a wide range of applications, such as field-effect transistor (Gilje et al., 2007), ultracapacitor (Stoller et al., 2008), ultrasensitive sensor (Schedin et al. 2007) and organic photovoltaic device (Liu et al., 2008). However, unlike fullerenes and carbon nanotubes, graphene tends to aggregate or restack irreversibly to form graphite, giving rise to technical difficulty in the fabrication of graphene-based electronic devices. To break this bottleneck, chemical functionalization of graphene has been developed to improve its solubility and processability yet preserving its superior properties.

Incorporation of oxygen-containing groups, including hydroxyls, epoxides, carbonyls and carboxyls, into graphene can alter the interlayer van der Waals interaction and impart the desired water solubility. In addition, these groups can also provide sites for

chemical modification with specific functional groups that can improve the solubility of graphene in organic solvents. Along this line, two graphene oxide (GO)-polymer complexes, GO-PFTPA and GO-PFCzTPA, were designed in this chapter. In these two GO-polymer complexes, the GO moiety is attached by different polymer segments, which contains fluorene (GO-PFTPA) or fluorene and carbazole (GO-PFCzTPA) in the backbone and triphenylamine in the side chain, as shown in Figure 6.1.
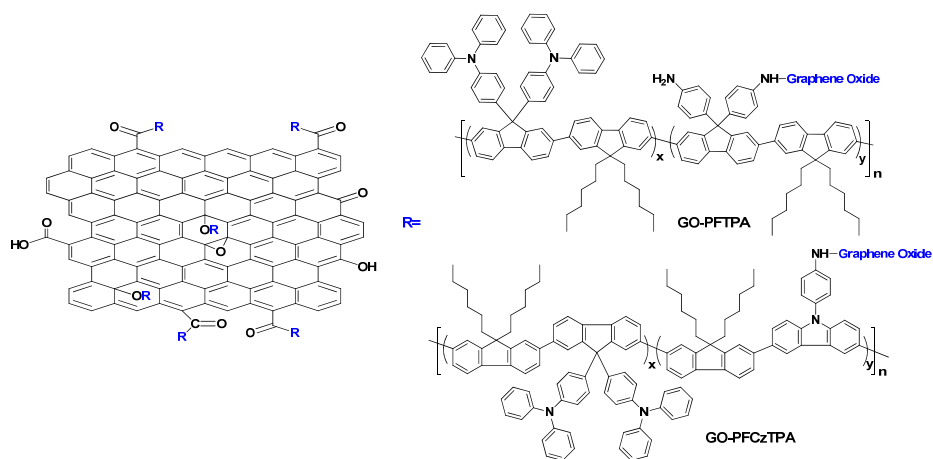
Figure 6.1 Molecular structures of the GO-polymer complexes

Applications of these two GO-polymer complexes in electronic memories have been investigated. Under the applied electric field, charge transfer (CT) occurs between the polymer donor and GO acceptor moieties, giving rise to a stable conductive CT state. As a result, memory devices based on the GO-polymer complexes are switched from the initial low-conductivity (OFF) state to the high-conductivity (ON) state. Due to the large π conjugation in the GO nanosheet, the electron delocalization is stabilized and a non-volatile ON state is observed. However, a reverse bias can extract electrons

from the GO moiety and reset the device back to the initial OFF state. Molecular simulations and *in-situ* photoluminescence (PL) spectra of the GO-PFCzTPA solid film were carried out to demonstrate the mechanism underlying the reversible electrical switching phenomenon.

6.2 Experimental Section

6.2.1 Materials

Purified natural graphite was purchased from Shanghai Yifan Graphite Co. All the rest chemicals were purchased from Sigma-Aldrich Chemical Co. and used without further purification. All the organic solvents were purified, dried and distilled under dry nitrogen. Graphite oxide was prepared from graphite by the Hummers method (Hummers and Offeman, 1958; Xu et al., 2009), and dried for 10 days over P_2O_5 in a vacuum oven before use.

6.2.2 Instrumentation

FT-IR spectra were recorded on a Nicolet Magna-IR 550 spectrophotometer using KBr pellets. NMR spectra were measured on a Bruker 400 spectrometer operating at 400 MHz in deuterated chloroform solution with a tetramethylsilane (TMS) as the reference for chemical shifts. Mass spectra (MS) were obtained on a Micromass GCTTM mass spectrometer. UV-visible absorption spectra were measured on a Shimadzu UV-2450 spectrophotometer. Photoluminescence (PL) spectra were measured on a HORIBA Jobin Yvon FluoroMax-4 spectrofluorometer, and the absolute photoluminescence quantum yields were measured by integrating sphere method (Porrès et al., 2006) on the same instrument. The samples for PL measurement were dissolved in dry THF, filtered and transferred to a long quartz cell, and then

capped and bubbled with high purity argon for at least 15 minutes before measurement. Other instruments used in this chapter are the same as in Chapter 3.

6.2.3 Synthesis of the GO-Polymer Complexes

The two GO-polymer complexes were prepared and characterized by Prof. Chen Yu, Mr. Zhuang Xiao-Dong and Mr. Zhang Bin from East China University of Science and Technology.

6.2.3.1 Synthesis of GO-PFTPA

The synthesis route of GO-PFTPA is illustrated in Figure 6.2. Details on the preparation and characterizations are given below.

Synthesis of 9,9-bis(4-diphenylaminophenyl)-2,7-dibromofluorene (2): A mixture of 2,7-dibromofluorenone (1.72g, 5.10 mmol) and triphenylamine (17.5g, 0.07 mol) in methylsulfonic acid (0.49g, 5.10 mmol) was reacted at 140°C with constant stirring under argon atmosphere for 6 h. After cooling to the room temperature, the mixture was extracted with dichloromethane, and the extract was washed with aqueous solution of Na_2CO_3 until the aqueous layer reached neutral. The extract was dried and concentrated, followed by purification with column chromatography on silica with hexane-dichloromethane as the eluent. The crude product was recrystallized from

acetone to give the triphenylamine-substituted 2,7-dibromofluorene (2.95g, 70%). MS: m/z=811[M+]. ^{1}H-NMR (CDCl$_3$, 400 MHz), δ(ppm): 6.99 (m, 20H, aryl H), 7.22 (m, 8H, aryl H), 7.46 (d, 2H), 7.51 (d, 2H),7.56 (d, 2H).

Synthesis of the PFTPA copolymer: Monomer **1** was synthesized from 2,7-dibromofluorenone according to the method reported previously (Chou et al., 2005). Pd(PPh$_3$)$_4$ (4 mg) was added to the mixture of monomer **1** (172 mg, 0.34 mmol), monomer **2** (274 mg, 0.34 mmol), 9,9-dihexylfluorene-2,7-bis(boronic acid pinacol ester) (**4**) (400 mg, 0.68 mmol), K$_2$CO$_3$ (400 mg, 3 mmol) and tetrabutylammonium bromide (TBAB, 60 mg, 0.2 mmol) in a glove box. Degassed toluene (10 mL) and deionized water (4 mL) were added into the above mixture by syringe. After heating the mixture at 80°C under nitrogen atmosphere for 42 h, excess phenylboronic acid and bromobenzene were added as the end-capping reagents sequentially in a 12 h interval. The mixture was then extracted with chloroform for three times, and the combined organic extract was washed with water and brine, and dried over anhydrous Na$_2$SO$_4$. The salt was filtered and concentrated into a small volume. The solution was added dropwise into stirred methanol. After filtration, the collected solid was purified by reprecipitating from methanol and then Soxhlet extraction with acetone. The precipitate was dried under vacuum to give the pale yellow PFTPA solid (296 mg, 52.8%). FT-IR (KBr, cm^{-1}): 1591, 1493, 1456, 1414, 1354, 1323, 1275, 1180, 1144, 1105, 1080, 1020, 964, 812, 752, 696, 633, 507. ^{1}H NMR (CDCl$_3$, 400 MHz), δ(ppm): 8.00-8.10 (m, 1H), 7.80-7.90 (m, 2H), 7.60-7.80 (m, 5H), 7.45-7.60 (m, 5H),

7.15-7.25 (m, 8H), 7.05-7.15 (m, 4H), 6.90-7.05 (br, 4H), 6.60 (br, 2H), 3.60 (br, 2H), 1.80-2.20 (br, 4H), 0.98-1.08 (m, 12H), 0.50-0.80 (m, 10H).

Synthesis of GO-PFTPA: The COOH-containing graphene oxide (15 mg) was reacted with a large excess of $SOCl_2$ containing a catalytic amount of *N,N*-dimethylformamide (DMF) under reflux for 24 h under argon atmosphere. After removal of the residual $SOCl_2$ under vacuum, the obtained graphene oxide with surface-bonded acryl chloride moieties was directly used to react with 150 mg of PFTPA, which contains side NH_2 groups in each polymer chain, in DMF (50 ml) at 130°C for 3 days under argon atmosphere in the presence of triethylamine (Et_3N, 30 mL). After cooling to room temperature, a large amount of water was added to the above reaction mixture to remove the triethylammonium salts formed during the reaction. The crude product was collected by filtration, re-dissolved in a small amount of DMF, and then precipitated from methanol for at least 3 times. The obtained GO-PFTPA (149 mg) was dried in vacuum at 65°C for 2 days.

6.2.3.2 Synthesis of GO-PFCzTPA

The synthesis route of GO-PFCzTPA is also illustrated in Figure 6.2. Details on the preparation and characterizations are given below.

Synthesis of 3,6-dibromo-N-(4-nitrophenyl)carbazole (3): N-(4-nitrophenyl) carbazole was synthesized according to the method reported previously (Chen et al., 2006). A

mixture of *N*-(4-nitrophenyl) carbazole (2.89 g, 10 mmol) and *N*-Bromosuccinimide (NBS) (3.91 g, 22 mmol) was stirred in 70 mL anhydrous DMF at room temperature for 48 h. Ice deionized water was then added to the mixture, and yellow precipitate appeared. The yellow solid was purified by washing with anhydrous methanol and then dried under vacuum overnight, to give the product (3.34 g, 75%). ^{1}H NMR (CDCl$_3$, 400 MHz), δ(ppm): 8.51 (d, 1H, aryl H), 8.49 (d, 1H, aryl H), 8.21 (m, 1H, aryl H), 8.21 (m, 1H, aryl H), 7.75(d, 1H, aryl H), 7.73 (d, 1H, aryl H), 7.57-7.54 (m, 2H, aryl H), 7.34 (m, 1H, aryl H), 7.32 (m, 1H, aryl H).

Synthesis of the copolymer P1: The copolymer P1 was synthesized by the similar procedure as the PFTPA copolymer, with monomer **2, 3** and **4** as the reactants. ^{1}H NMR (CDCl$_3$, 400 MHz), δ(ppm): 8.0-8.3 (m, 4H), 7.3-7.9 (m, 20H), 6.7-7.2 (m, 34H), 1.91-2.10 (m, 8H), 0.92-1.10 (m, 24H), 0.51-0.77 (m, 20H).

Synthesis of the PFCzTPA copolymer: A mixture of **P1** (200 mg) and SnCl$_2$·2H$_2$O (250 mg) in THF (40 mL) was refluxed for 6 h. The mixture was concentrated under reduced pressure and treated with 40 mL deionized water, followed by pH adjustment to 9 with 10% NaOH aqueous solution. The mixture was extracted with chloroform, and the extract was washed with saturated brine and deionized water. The extract was then dried and concentrated to afford the yellow PFCzTPA solid (178mg). ^{1}H NMR (CDCl$_3$, 400 MHz), δ(ppm): 8.0-8.3 (m, 2H), 7.3-7.9 (m, 22H), 6.7-7.2 (m, 34H), 3.79-3.85 (s, 2H), 1.91-2.10 (m, 8H), 0.92-1.10 (m, 24H), 0.51-0.77 (m, 20H).

Synthesis of GO-PFCzTPA: GO-PFCzTPA was prepared by reaction between the PFCzTPA polymer and the graphene oxide containing surface-bonded acryl chloride moieties, similar to the synthesis procedure of GO-PFTPA.
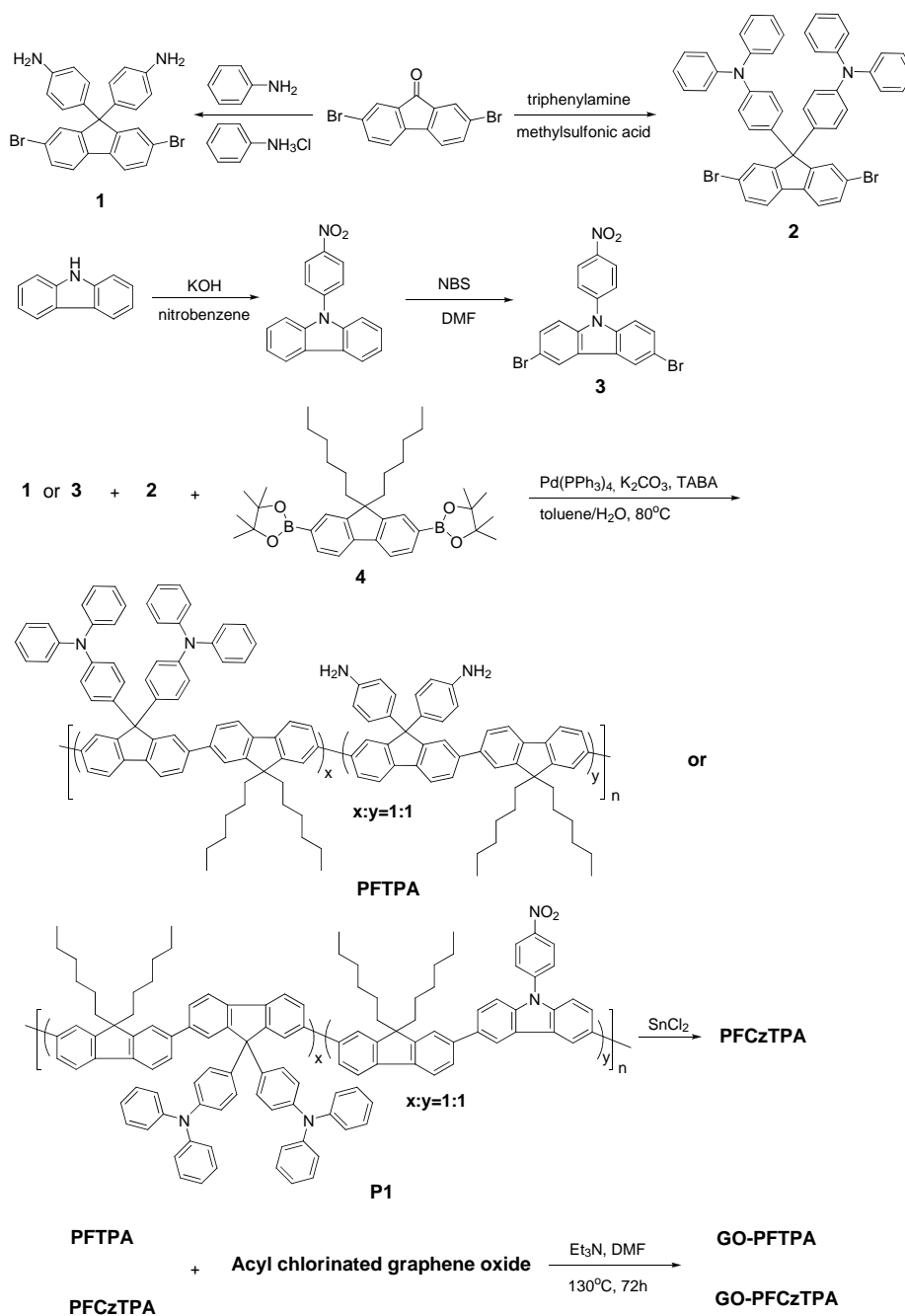
Figure 6.2 Synthesis routes for the monomers and the GO-polymer complexes

6.2.4 Fabrication and Characterization of the Memory Devices

The ITO coated glass substrate was pre-cleaned sequentially with deionized water, acetone and isopropanol in an ultrasonic bath for 15 min. A 100 μL *N,N*-dimethylacetamide (DMAc) solution of the functional graphene derivative (10 mg·mL^{-1}) was spin-coated onto the ITO substrate at a spinning rate of 1000 rpm, followed by solvent removal in a vacuum oven at 10^{-5} Torr and 50°C for 10 h. The thickness of the polymer layer was about 50 nm, as determined by the AFM edge profiling. Finally, an Al top electrode of about 400 nm in thickness was thermally deposited onto the material surface through a shadow mask at a pressure of about 10^{-7} Torr. Electrical property measurements were carried out on devices of 0.4×0.4 mm^2, 0.2×0.2 mm^2, and 0.15×0.15 mm^2 in size, under ambient conditions, using an Agilent 4155C semiconductor parameter analyzer equipped with an Agilent 41501B pulse generator. The current density-voltage (*J-V*) data reported were based on device units of 0.4×0.4 mm^2 in size, unless stated otherwise. ITO was maintained as the ground electrode during the electrical measurements.

6.2.5 Molecular Simulation

Molecular simulations of the two functional graphene derivatives were carried out with the Gaussian 03 (Revision E. 01) program package on a Hewlett-Packard Xeon Two Sockets Quad-Core workstation with 8 CPUs and 16 GByte memory. Molecular orbitals and their energy levels were calculated with density function theory (DFT) in

B3LYP/6-31G(d) level (Frisch et al., 2004). Vibrational frequencies were calculated analytically to ensure that the optimized geometries really correspond to the total energy minima.

6.3 Results and Discussion

6.3.1 Characterizations of the GO-Polymer Complexes

The solubilities of the GO-polymer complexes in common organic solvents are summarized in Table 6.1. Due to the presence of long alkyl substitutes in the polymer segments, the two functionalized GOs exhibit good solubilities in common solvents, such as DMAc, THF, chloroform and dichloromethane, at room temperature. Thus, they can be easily fabricated into electronic deivces via solution process.

Table 6.1 Solubilities of the GO-polymer complexes in common solvents

Polymer	Solubility[a]				
	DMAc	NMP	THF	CHCl$_3$	CH$_2$Cl$_2$
GO-PFTPA	++	+-	++	++	++
GO-PFCzTPA	++	+-	++	++	++

[a]Solubility measured in concentration of 1 mg·mL^{-1}
++: Soluble at room temperature
+-: Partially soluble at room temperature

Figure 6.3 shows the UV-visible absorption spectra of GO-PFTPA and GO-PFCzTPA in THF at a concentration of ~ 1×10^{-2} mg·L^{-1}. The absorption spectrum of GO-PFCzTPA was normalized to the maximum absorption of GO-PFTPA for ease of comparison. As shown in Figure 6.3, both spectra exhibit a sharp absorption at 239 nm and a maximum absorption at 303 nm, which arise, respectively, from the electronic transition of benzene ring within the fluorene group (Kim et al., 2005) and absorption of the triphenylamine group (Bolognesi et al., 2009). In addition,

GO-PFTPA also shows a strong absorption shoulder at 366 nm, originating from the π→π* transition of the conjugated fluorene backbones (Promarak et al., 2007). The absorption shoulder of GO-PFCzTPA, however, is significantly reduced, due probably to the fact that incorporation of the carbazole group reduces the effective conjugation of the fluorene backbone (Li et al., 2004; Lu et al., 2004).

The PL spectra of the two graphene derivatives in THF are shown in Figure 6.4. The concentration of GO-PFTPA and GO-PFCzTPA are both at ~ 1×10^{-2} mg·L^{-1}. All the emission spectra were obtained with the excitation wavelength of 370 nm. As shown in Figure 6.4, GO-PFTPA shows a series of well-resolved vibronic emissions at 416 nm, 437 nm and 470 nm, which are assigned, respectively, to the $S_1 \rightarrow S_0$ 0-0, 0-1 and 0-2 intrachain singlet transitions of the fluorene backbone (Li et al., 2004). In comparison to GO-PFTPA, the PL spectrum of GO-PFCzTPA becomes less resolved and exhibits blue-shifts in its vibronic emissions, attributed probably to the fact that incorporation of the carbazole group interrupts the effective conjugation and intrachain ordering of the fluorene backbone (Miguel et al., 2009). In addition, the PL quantum yields (Φ_{PL}) of the two graphene derivatives, and their respective polymer donor moieties were measured by integrating sphere method. The PL quantum yields of GO-PFTPA and GO-PFCzTPA are 0.31 and 0.24, respectively, smaller than those of their corresponding polymer segments, i.e., PFTPA (0.54) and PFCzTPA (0.31). The partial fluorescence quenching in the graphene-donor complexes originates probably from the CT between the GO moiety and the attached polymer donor segment (Shibano et al., 2006; Lukas et al., 2002).
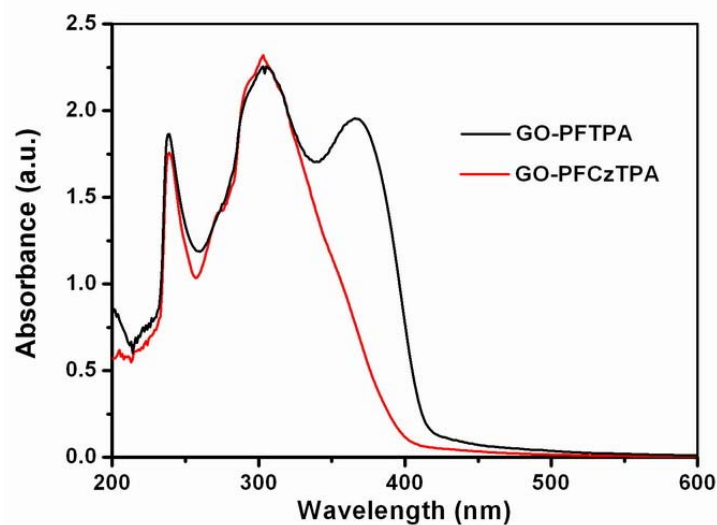
Figure 6.3 UV-visible absorption spectra of the two GO-polymer complexes in THF, at a concentration of ~ 1×10^{-2} mg·L^{-1}. The absorption spectrum of GO-PFCzTPA was normalized to the maximum of GO-PFTPA at 303 nm for ease of comparison.
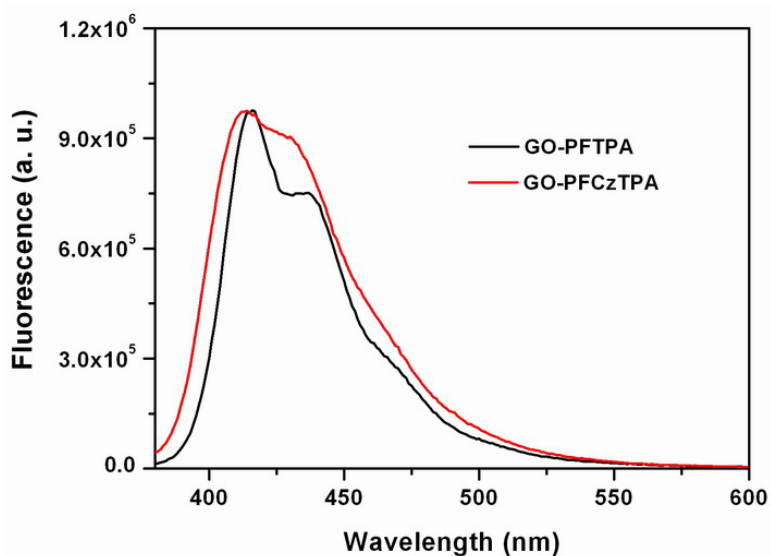
Figure 6.4 PL spectra of the two GO-polymer complexes in THF, at a concentration of ~ 1×10^{-2} mg·L^{-1}. All the emission spectra were obtained with the excitation wavelength of 370 nm. The emission spectrum of GO-PFCzTPA was normalized to the maximum emission of GO-PFTPA at 416 nm for ease of comparison.

Figure 6.5 shows the AFM images of GO-PFTPA and GO-PFCzTPA films, prepared

by spin-coating the corresponding DMAc solution (5 mg·mL^{-1}) onto ITO-coated glass and drying under vacuum. Both materials exhibit flat and uniform surfaces, indicating their superior processabilities and good morphologies. The sporadic pits on the film surface probably arise from unremoved particles on the ITO surface. The flat and uniform morphology is desirable for fabricating electronic devices with reproducible and durable performance.
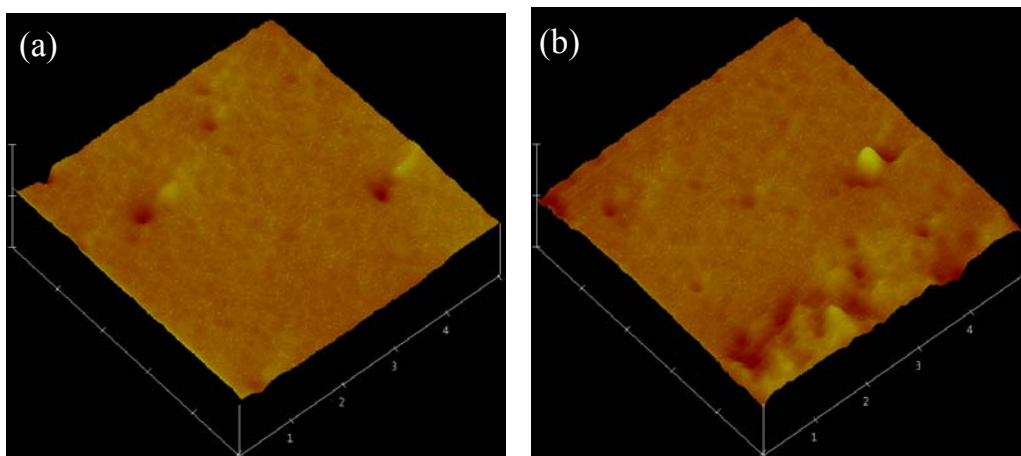
Figure 6.5 AFM images of (a) GO-PFTPA (0 - 5 μm) and (b) GO-PFCzTPA (0 - 5 μm) films spin-coated on ITO-coated glass from DMAc solution (5 mg·mL^{-1})

6.3.2 Electrical Switching and Memory effects of the GO-Polymer Complexes

The switching effect of GO-PFTPA is demonstrated by the *J-V* characteristics of an electronic device with the GO-PFTPA film sandwiched between the ITO and Al electrodes, as shown in Figure 6.6(a). The device was initially in the low-conductivity (OFF) state. During the 1st negative sweep (with Al as the cathode and ITO as the anode) from 0 to -4 V, the device exhibited an abrupt increase in current density at -1.2 V, indicating the electrical switching from the initial OFF state to the high-conductivity (ON) state. This electrical switching is equivalent to the "writing"

process in a digital memory cell. The ON/OFF current ratio is about 500 at -1 V. The ON state can be retained after turning off the power supply (the 2nd sweep), indicating the non-volatile nature of the ON state. When a positive sweep from 0 to 4 V was applied (the 3th sweep), the ON state can be reset to the initial OFF state at +2.8 V. This switch-off process is equivalent to the "erasing" process of a digital memory cell. The device is thus reversible and allows for application in a rewritable data storage system. The subsequent 4th sweep was applied after removing the power supply. The device was observed to retain in the low-conductivity state, indicating its good stability in the OFF state. The ability to write, read and erase the electrical states, as well as the non-volatile nature of the ON and OFF states, fulfill the functionality of a flash type memory. As indicated by the subsequent 5th to 12th sweeps, the above write-read-erase-read switching cycles can be repeated with good accuracy, except for the slight variations in switching threshold voltages, associated probably with conformational relaxation of the polymer chain. In addition, devices with different active areas of 0.4×0.4 mm^2, 0.2×0.2 mm^2 and 0.15×0.15 mm^2 show almost the same *J-V* characteristics, indicating that the current density is independent on the device areas. The rewritable electrical states, good reproducibility, and area-independent current density, rule out the possibility of filament conduction (Henisch and Smith, 1974), metal diffusion (Lim et al., 1998; Ma et al., 2000), and dielectric breakdown in the present device.
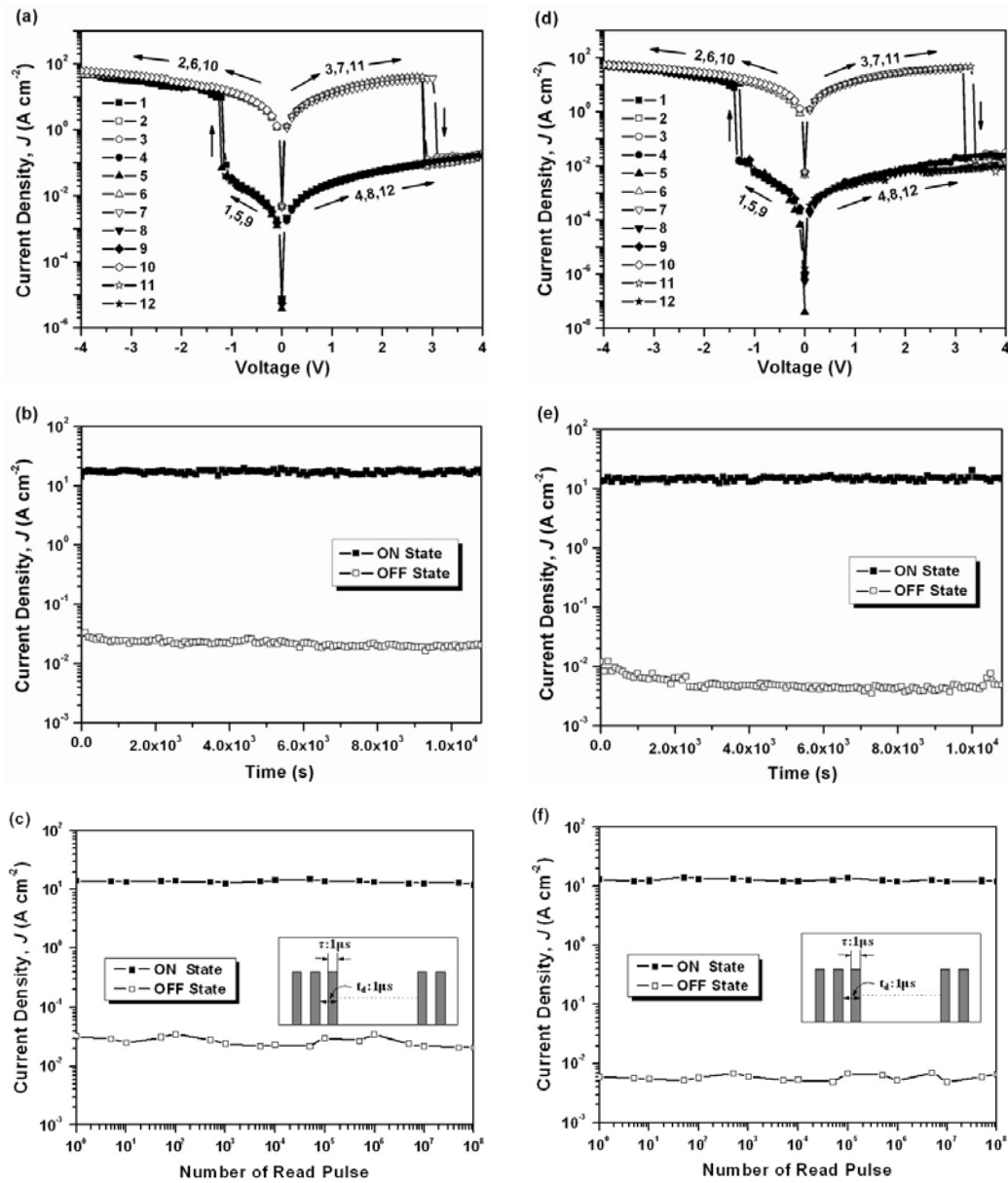
Figure 6.6 (a) *J-V* characteristics of a 0.4×0.4 mm^2 ITO/GO-PFTPA/Al device. The sequence and direction of each sweep are indicated by the respective number and arrow. (b and c) Stability of the ON and OFF states of the GO-PFTPA device under a constant stress of -1 V and read pulses of -1 V. (d) *J-V* characteristics of a 0.4×0.4 mm^2 ITO/GO-PFCzTPA/Al device. (e and f) Stability of the ON and OFF states of the GO-PFCzTPA device under a constant stress of -1 V and read pulses of -1 V. The insets of (c) and (f) show the pulse used for measurement.

Figure 6.6(b) shows the effect of operation time on the stability of the GO-PFTPA device. Under a constant stress of -1 V, no obvious degradation in current density was

observed for both the ON and OFF states over a 3 h period. In addition, the two electrical states were also stable up to 10^8 read pulses of -1 V, as shown in Figure 6.6(c).

The GO-PFCzTPA device exhibits similar rewritable electrical switching effects as the above GO-PFTPA device, except for a slightly higher ON/OFF current ratio and a larger switch-off threshold voltage, as shown in Figure 6.6(d). The difference in memory effects arises probably from incorporation of the carbazole group in the attached polymer segment. The detailed mechanism will be elucidated in the following section. Figures 6.5(e) and 6.5(f) show, respectively, the effect of operation time and read pulses on the stability of the GO-PFCzTPA device. Under a constant stress of -1 V or read pulses of -1 V, no obvious degradation in current density was observed for both the ON and OFF states.

6.3.3 Switching Mechanism

To better understand the switching behaviors of the GO-polymer complexes, computational studies have been performed on the two GO-polymer complexes using DFT method at the B3LYP/6-31G(d) level (Frisch et al., 2004). To save the computing resources, simplified GO-polymer modals were employed for the calculation. In the modals, the GO moiety contains 4×4 aromatic rings together with four kinds of oxygen functionalities, i.e., epoxide, hydroxyl, carbonyl and carboxyl, and the polymer segment contains one repeat unit, including all the functional moieties. The first three highest occupied molecular orbitals (HOMO, HOMO2, and HOMO3) and the lowest unoccupied molecular orbitals (LUMO) of the modal, as well as the plausible electronic transitions under excitation, are demonstrated in Figure 6.7. As the two graphene derivatives have similar molecular structures and thus electronic properties, only the molecular simulation results of GO-PFTPA were elaborated in detail. As shown in Figure 6.7(a), the LUMO of GO-PFTPA is located on the GO moiety, indicating that the GO moiety acts as the electron acceptor. The first three highest occupied molecular orbitals (HOMO, HOMO2, and HOMO3) are located on the triphenylamine, GO and fluorene moieties, respectively, indicating that all the functional moieties are able to donate electrons.

In the as-cast GO-PFTPA film, the oxygen functionalities introduce a number of defect sites composed of sp^3 hybridized C atoms, which limit the in-plane charge

transportation in the GO nanosheets and lead to a low electrical conductivity of the functionalized GO (Kong et al., 2009; Stankovich et al., 2007). In addition, the attached polymer segment tends to intercalate between the neighboring GO nanosheets and acts as a tunneling barrier for the transverse charge transportation (Connolly et al., 2009). As a result, the as-fabricated GO-PFTPA device remained in the low conductivity (OFF) state during the initial electrical sweep. At the switching threshold voltage, electrons transit readily from HOMO2 to LUMO within the GO moiety, forming a locally excited state. Electron transition from HOMO and HOMO3 to LUMO, however, is inhibited, due to the absence of overlapping between LUMO and the two HOMOs. Alternatively, electrons in HOMO3 can overcome the energy barrier between HOMO3 and HOMO2 (0.66 eV) and fill the generated holes in HOMO2, followed by the spontaneous electron transition from HOMO to HOMO3. As a result, the excited electrons in LUMO can reside in the GO nanosheet and delocalize among the giant π-conjugation system. Due to the strong reducibility, these electrons can probably reduce the GO to graphene. Based on the *J-V* curve and film thickness, the electrical conductivity of GO-PFTPA in ON state is calculated to be 6.7×10^{-3} S m^{-1}, comparable to that (6.7×10^{-3} S m^{-1}) (Kong et al., 2009) of GO treated by hydrazine solution for 1 h according to the method reported previously (Li et al., 2008). In the partially reduced GO nanosheets, the defect sites associated with oxygen functionalities are significantly eliminated, allowing a better electron delocalization and transportation in both in-plane and transverse directions. As a result, the device is switched from the OFF state to the ON state. The above electrical field-induced CT in

the GO-polymer donor complexes is consistent with the previously reported

photoinduced CT between graphene and functionalized polyfluorene (Qi et al., 2010)

or CdSe nanoparticles (Lin et al., 2010; Geng et al., 2010)
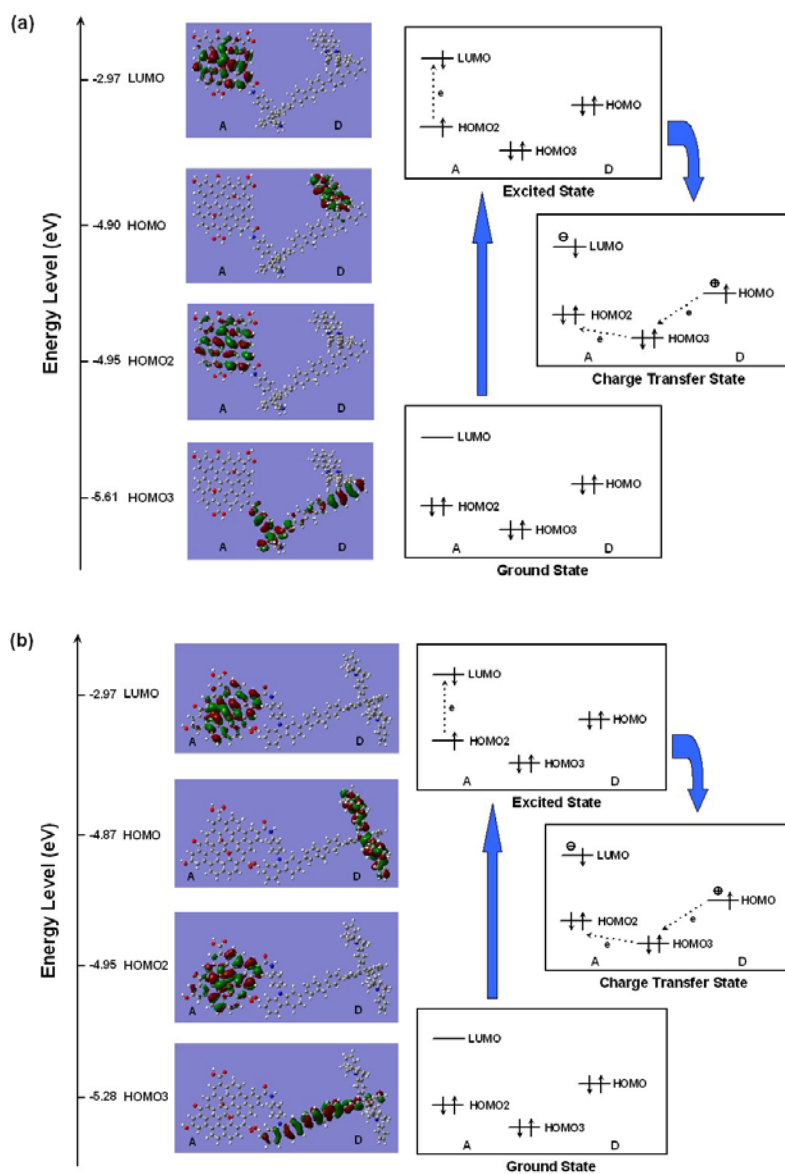
Figure 6.7 Calculated molecular orbitals and plausible electronic transitions under the electric field of (a) GO-PFTPA and (b) GO-PFCzTPA modals

Due to the giant π-conjugation plane, the electrons can delocalize intensively in the

GO nanosheets, making the conductive CT state stable even after removing the

applied bias. The flexible amide linker between GO and polymer segment can also inhibit the backwards CT. A non-volatile ON state is thus observed. However, a reverse positive bias with sufficient energy can extract electrons from the graphene nanosheet and dissociate the CT state, returning the device back to the initial OFF state.

When the carbazole group is incorporated into the fluorene backbone of the polymer segment (GO-PFCzTPA), the molecular orbitals associated with the polymer segment (HOMO1 and HOMO3) exhibit increases in energies, as shown in Figure 6.7(b). This is attributed to the fact that the carbazole group possesses better electron-donating ability than the fluorene group (Yang et al., 2005). As a result, the CT complexes in GO-PFCzTPA are more stable and require a higher energy to dissociate. A larger switch-off threshold voltage (3.3 V) is thus observed in the GO-PFCzTPA device in comparison to that of the GO-PFTPA device (2.8 V). The HOMO2 and LUMO located in the GO moiety, however, do not show any change in energy. As the electronic excitation is dominated by the HOMO2 → LUMO transition, the two devices exhibit comparable switch-on threshold voltages (-1.2 V for GO-PFTPA *vs* -1.3 V for GO-PFCzTPA). In addition, as indicated by the UV-visible absorption and PL spectra, incorporation of the carbazole group interrupts the effective conjugation and intrachain ordering of the fluorene backbone (Li et al., 2004; Lu et al., 2004). Thus, the charge migration along the polymer backbone is limited in the pre-excited GO-PFCzTPA molecule, resulting in a lower OFF state current. Due to the

comparable ON state currents of the two devices, a higher ON/OFF current ratio (~

2000 at -1 V) is observed in the GO-PFCzTPA device in comparison to that of the

GO-PFTPA device (~ 500 at -1 V).
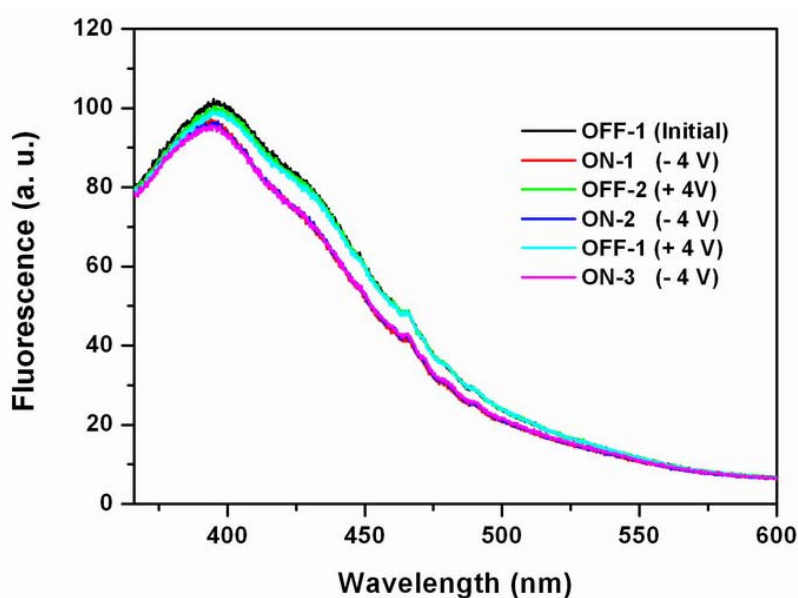
Figure 6.8 *In-situ* PL spectra of the GO-PFCzTPA film in an ITO/polymer/Al
sandwich device under electrical biases. OFF-1 denotes the emission spectrum before
applying any electric bias, while ON-1 to OFF-3 denote, respectively, the emission
spectra after applying the respective electrical bias indicated in the bracket (with Al as
the working electrode and ITO as the ground electrode).

To elucidate the above electric field-induced CT process, *in-situ* PL spectra of the

GO-PFCzTPA film in an ITO/polymer/Al sandwich device under electrical biases

were studied (Figure 6.8). The electrical biases were applied on the Al electrode, with

ITO as the ground electrode. All the emission spectra were obtained at the excitation

wavelength of 320 nm. In Figure 6.8, OFF-1 denotes the PL spectrum of the

GO-PFCzTPA film prior to application of the electrical bias, corresponding to the

initial OFF state in the *J-V* characteristics of the GO-PFCzTPA device (Figure 6.6(d)).

The PL spectrum exhibits a maximum fluorescence at 396 nm and a fluorescence

shoulder at around 430 nm, arising probably from the conjugated backbone of the

polymer segments (Ying et al., 2009). In addition to the above two intense emission

features, the GO-PFCzTPA film also exhibits a less obvious, structureless emission in

the green region (between 450 nm ~ 550 nm), which is believed to arise from the

inter-chain/inter-segmental interactions between the oxidation-induced fluorenone

defects (Sims et al., 2004).

When a negative bias (-4 V) larger than the switch-on threshold voltage (-1.3 V) is

applied on the GO-PFCzTPA device, electrical switching of the film from the OFF

state to the ON state is triggered. The corresponding PL spectrum (denoted by ON-1)

exhibits a decrease in intensity of all the three emission components. This partial

fluorescence quenching indicates decay of the excited singlet state of the polymer

backbone, which is believed to arise from CT from the polymer segment to the

graphene moiety, as described above (Shibano et al., 2004). As a result, the

conductive CT states are formed, and the current density increases abruptly to switch

the device to the ON state. When a positive electrical sweep is applied on the

GO-PFCzTPA device, for example, the 3th sweep in Figure 6.6(e), electrons in the

graphene nanosheets are extracted and the CT states dissociate. The device is thus

switched back to the initial OFF state. The erasing of the ON state is supported by the

recovery of the initial PL spectrum corresponding to the OFF state after applying a

positive bias of +4 V (OFF-2 spectrum in Figure 6.8). However, a slight decrease in intensity of the main emission bands is observed in the OFF-2 spectrum in comparison to the initial OFF-1 spectrum, indicating that the conformational relaxation of the polymer chain lags behind the corresponding change in the applied electric field (Ling et al., 2007; Liu et al., 2009). The "ON-OFF" changes in the PL spectra matches the write-erase processes in the J-V characteristics of the GO-PFCzTPA device, and can be repeated with good accuracy, as indicated by the subsequent ON-2, OFF-3 and ON-3 spectra in Figure 6.8.

6.4 Conclusion

Two solution-processable GO-polymer complexes, GO-PFTPA and GO-PFCzTPA, containing the GO moiety and conjugated polymer segments, were characterized with respect to their electrical switching and memory effects. Devices based on the two materials with the ITO/polymer/Al sandwich structure can be switched "ON" and "OFF" during the negative and positive electrical sweeps, respectively. The switch-on threshold voltages of the two devices are comparable, while the switch-off threshold voltage and ON/OFF current ratio of the GO-PFCzTPA device are slightly larger than those of the GO-PFTPA device. This difference in electrical switching effects arises from incorporation of the carbazole group in GO-PFCzTPA, which can interrupt the backbone conjugation and further stabilize the CT state. The molecular simulation results indicate that the polymer segment acts as the electron donor, while the GO moiety acts as the electron acceptor. Electric field-induced CT between the donor and acceptor moieties gives rise to a conductive CT state, accounting for the electrical switching from the OFF state to the ON state. The large π conjugation surface of the GO nanosheets facilitates the electron delocalization and stabilizes the CT state, dictating the non-volatile nature of the ON state. A reverse bias can extract electrons from the GO moiety and reset the device back to the initial OFF state. The electric field-induced CT process was further elucidated from the fluorescence quenching and recovery in the PL spectra, obtained *in-situ*, of the GO-PFCzTPA film under electrical biases.

CHAPTER 7

CONCLUSION AND RECOMMENDATIONS FOR

FUTURE WORK

The present research work has attempted to develop a series of solution-processable copolymers, which can provide the required electronic properties within a single macromolecule and yet still possess good chemical, mechanical and morphological characteristics. Memory devices based on the copolymers have been fabricated with a polymer thin film sandwiched between the ITO and Al electrodes. Current density-voltage characteristics of the memory devices indicate that the switching effects, including current magnitudes, ON state volatility and reversibility, and switching threshold voltages, are dependant to a large extent on the molecular structures of the copolymers. The effect of different functional groups (electron-donor or -acceptor moieties) on the resultant memory effects have been studied with the aid of molecular simulation and experimental characterizations.

First of all, a series of functional polyimides, containing the same electron-acceptor moiety (phthalimide) but different electron-donor moieties (e.g., oxadiazole, triphenylamine-substituted oxadiazole, triphenylamine-substituted triazole, etc), were designed and studied for their electrical switching and memory effects. Electric field-induced charge transfer (CT) between the electron-donor and -acceptor moieties is responsible for the electrical switching effects. In TP6F-PI containing the simple triphenylamine donor moiety, an unstable CT occurs between the donor and acceptor moieties and results in the volatile and rewritable ON state. When oxadiazole or triazole group is incorporated between the phthalimide and triphenylamine moieties (such as in OXTA-PI, AZTA-PI and AZTA-PEI), the free volume in polymer matrix is

increased and the electric field-induced conformational change is facilitated, which can introduce an energy barrier for dissociation of the conductive CT complexes. Non-volatile and non-rewritable ON states were thus observed in memory devices fabricated from these materials. In P(BPPO)-PI, the strong triphenylamine donor moiety is removed, while an additional phenoxyl group is incorporated between the phthalimide and oxadiazole moieties. The flexible phenoxyl group facilitates conformational change under the electrical field, giving rise to an energy barrier for dissociation of the CT complexes. As a result, the high-conductivity (ON) state cannot be erased by a reverse bias, and exhibited "remanence" for a period of 4 min after turning off the power. Due to the limited charge delocalization in the weak oxadiazole donor moiety, the ON state is volatile in nature and is eventually lost when the memory is not powered.

Next, two polyfluorene copolymers, TPATz-F8 and TPATz-F8BT, containing fluorene, triphenylamine and triazole moieties, with TPATz-F8BT containing also the benzothiadiazole moieties, were characterized for their memory effects. Memory devices based on the two polymers exhibited similar non-volatile and rewritable electrical switching effects. Molecular simulation results indicate that the fluorene and triphenylamine groups act as the electron donors, while the triazole and/or benzothiadiazole groups act as the electron acceptors. Electric field-induced CT between the donor and acceptor moieties gives rise to a conductive CT state, accounting for the electrical bistability. Incorporation of the electron-deficient

benzothiadiazole group in TPATz-F8BT blocks charge migration along the conjugated backbone and thus lowers the ON state current by about one order of magnitude, indicating the possibility of tuning the ON/OFF current ratio by tailoring the molecular structure.

Subsequently, two azo polymers, with the pendant azobenzene moieties attached by cyano terminal group (AzoNEtCN) or no terminal group (AzoNEt), were developed for memory applications. Both polymers exhibited uni-directional electrical switching during the negative sweep. Charge injection and trapping process is responsible for the observed electrical bistability. The volatility of the ON state was found to be dependant on the terminal group in the pendant azobenzene moiety. The ON state is non-volatile when the azobenzene moiety is attached by an electron-acceptor terminal group (AzoNEtCN), while it is volatile when the azobenzene moiety has no terminal group (AzoNEt). The strong cyano acceptor group in the pendant azobenzene miety of AzoNEtCN can induce a large dipole moment and a strong intramolecular CT, which help to hold the conducting channel for charge carriers. However, in the absence of any terminal group in the pendant azobenzene moiety (AzoNEt), the dipole moment is not strong enough to hold the conducting channel effectively.

Lastly, two functionalized graphene oxides (GOs), GO-PFTPA and GO-PFCzTPA, were designed and studied for their memory effects. In these two functionalized GOs, the GO moiety is attached by different polymer segments, which contain fluorene

(GO-PFTPA) or fluorene and carbazole (GO-PFCzTPA) in the backbone and triphenylamine in the side chain. Both graphene derivatives exhibited similar non-volatile and rewritable electrical bistability under the electrical sweeps. Electrical field-induced CT between the polymer donor and graphene acceptor moieties accounts for the electrical switching effects. The intensive π conjugation in the GO nanosheets facilitates the electron delocalization and stabilizes the conductive CT state (ON state). However, a reverse bias can extract electrons from the GO moiety and reset the device back to the OFF state. Incorporation of the carbazole group in GO-PFCzTPA further stabilizes the CT state and interrupts the effective backbone conjugation, resulting in a larger switch-off threshold voltage and a higher ON/OFF current ratio in the GO-PFCzTPA device.

The present research work has focused on investigating a series of electroactive polymers with different functional groups for electrical switching and memory application. The effects of molecular structures on the resultant switching and memory behavior have been studied to elucidate the underlying mechanisms. Despite these efforts, it is still a long way to go to realize the practical application of polymers in memory devices. In the future work, novel copolymers with different electron-donor or -acceptor moieties should be investigated for their memory behaviors, to systemically study the relationship between the functional groups and the resultant switching effects. More experimental works, including electrical and optical characterizations, should also be carried out to validate the mechanisms

underlying the switching effects and memory behavior. In addition, to minimize the environmental impact and improve the device stability and lifetime, encapsulation techniques should be introduced into the polymer memory devices. Polymer memory can be further integrated into cross-point memory array and 3D stacked multilayer devices for high-density data storage.

REFERENCES

Adler, D., M.S. Shur, M. Silver and S.R. Ovshinsky. Threshold Switching in Chalcogenide-Glass Thin Films, J. Appl. Phys., *51*, pp.3289-3309. 1980.

Ahonen, P., D.J. Schiffrin, J. Paprotny and K. Kontturi. Optical Switching of Coupled Plasmons of Ag-Nanoparticles by Photoisomerization of an Azobenzene Ligand, Phys. Chem. Chem. Phys., *9*, pp.651-658. 2007.

Aleksandrova, E.K., L.P. Kazakova and A.V. Chernyshev. Polyimide Structures with High Charge-Carrier Mobility for Electroluminescent Devices and Liquid-Crystal Light Modulators, J. Opt. Technol., *68*, pp.805-808. 2001.

Alemani, M., M.V. Peters, S. Hecht, K.H. Rieder, F. Moresco and L. Grill. Electric Field-Induced Isomerization of Azobenzene by STM, J. Am. Chem. Soc., *128*, pp.14446-14447. 2006.

Anders, J., H.J. Byrne, J. Poplawski, S. Roth, T. Bjoerholm, M. Jöergensen, P. Sommer-Larsen and K. Schaumburg. Excited State Transient Spectroscopy of Anthracene Based Photochromic Systems, Synth. Met., *57*, pp.4820-4826. 1993.

Arias, A.C., I.A. Huemmelgen, A. Meneguzzi and C.A. Ferreira. Conjugated Polymer-Based Voltage-Regulator Device, Adv. Mater., *9*, pp.972-974. 1997.

Ariu, M., M. Sims, M.D. Rahn, J. Hill, A.M. Fox, D.G. Lidzey, M. Oda, J. Cabanillas-Gonzalez and D.D.C. Bradley. Exciton Migration in β-Phase Poly(9,9-Dioctylfluorene), Phys. Rev. B, *67*, pp.195333(1-11). 2003.

Attianese, D., M. Petrosino, P. Vacca, S. Concilio, P. Iannelli, A. Rubino and S. Bellone. Switching Device Based on a Thin Film of an Azo-Containing Polymer for Application in Memory Cells, IEEE Electron Device Lett., *29*, pp.44-46. 2008.

Azuma, H., K. Asada, T. Kobayashi and H. Naito. Fabrication of α- and β-Phase Poly(9,9-Dioctylfluorene) Thin Films, Thin Solid Films, *509*, pp.182-184. 2006.

Babel, A. and S.A. Jenekhe. Charge Carrier Mobility in Blends of Poly(9,9-Dioctylfluorene) and Poly(3-Hexylthiophene), Macromolecules, *36*, pp.7759-7764. 2003.

Bandyopadhyay, A. and A.J. Pal. Multilevel Conductivity and Conductance Switching in Supramolecular Structures of an Organic Molecule, Appl. Phys. Lett., *84*, pp.999-1001. 2004.

Bandyopadhyay, A. and A.J. Pal. Tuning of Organic Reversible Switching via Self-Assembled Supramolecular Structures, Adv. Mater., *15*, pp.1949-1952. 2003.

Becker, S., C. Ego, A.C. Grimsdale, E.J.W. List, D. Marsitzky, A. Pogantsch, S. Setayesh, G. Leising and K. Müllen. Optimisation of Polyfluorenes for Light Emitting Applications, Synth. Met., *125*, pp.73-80. 2002.

Benson-Smith, J. J., L. Goris, K. Vandewal, K. Haenen, J.V. Manca, D. Vanderzande, D.D.C. Bradley and J. Nelson. Formation of a Ground-State Charge-Transfer Complex in Polyfluorene/[6,6]-Phenyl-C_{61} Butyric Acid Methyl Ester (PCBM) Blend Films and Its Role in the Function of Polymer/PCBM Solar Cells, Adv. Funct. Mater., *17*, pp.451-457. 2007.

Bing, Y. J., L.M. Leung and G. Menglian. Synthesis of Efficient Blue and Red Light Emitting Phenanthroline Derivatives Containing Both Hole and Electron Transporting Properties, Tetrahedron. Lett., *45*, pp.6361-6363. 2004.

Boeck, J.D., W.V. Roy, J. Das, V. Motsnyi, Z. Liu, L. Lagae, H. Boeve, K. Dessein and G. Borghs. Technology and Materials Issues in Semiconductor-Based Magnetoelectronics, Semicond. Sci. Technol., *17*, pp.342-354. 2002.

Bolognesi, A., P. Betti, C. Botta, S. Destri, U. Giovanella, J. Moreau, M. Pasini and W. Porzio. From Block Copolymers to End-Capped Polymers: A Suitable Method to Control the Electro-Optical Properties of Polymeric Materials, Macromolecules, *42*, PP.1107-1113. 2009.

Bozano, L.D., B.W. Kean, M. Beinhoff, K.R. Carter, P.M. Rice and J.C. Scott. Organic Materials and Thin-Film Structures for Cross-Point Memory Cells Based on Trapping in Metallic Nanoparticles, Adv. Funct. Mater., *15*, pp.1933-1939. 2005.

Bozano, L.D., B.W. Kean, V.R. Deline, J.R. Salem and J.C. Scott. Mechanism for Bistability in Organic Memory Elements, Appl. Phys. Lett., *84*, pp.607-609. 2004.

Brar, A.S. and M. Markanday. Comprehensive Analysis of Stereoregularity and Sequence Distribution in 2-*N*-Carbazolylethyl Acrylate and Methyl Methacrylate Copolymers by 2D NMR Spectroscopy and Their Thermal Studies, Polymer, *46*, pp.11527-11539. 2005.

Brown, D., A. Natansohn and P. Rochon. Azo Polymers for Reversible Optical Storage. 5. Orientation and Dipolar Interactions of Azobenzene Side Groups in Copolymers and Blends Containing Methyl Methacrylate Structural Units, Macromolecules, *28*, pp.6116-6123. 1995.

Cacelli, I., A. Feretti, M. Girlanda and M. Macucci. *I/V* Characteristics of a Molecular Switch, Chem. Phys., *333*, pp.26-36. 2007.

Cacelli, I., A. Feretti, M. Girlanda and M. Macucci. Theoretical Study of Building Blocks for Molecular Switches Based on Electrically Induced Conformational Changes, Chem. Phys., *320*, pp.84-94. 2006.

Cai, L., M. Feng, H.M. Guo, W. Ji, S.X. Du, L.F. Chi, H. Fuchs and H.J. Gao. Reversible and Reproducible Conductance Transition in a Polyimide Thin Film, J. Phys. Chem. C., *112*, pp.17038-17041. 2008.

Casalbore-Miceli, G., N. Camaioni, A. Geri, G. Ridolfi, A. Zanelli, M.C. Gallazzi, M. Maggini and T. Benincori. "Solid state charge trapping": Examples of Polymer Systems Showing Memory Effect, J. Electroanal. Chem., *603*, pp.227-234. 2007.

Chang, H.W., K.H. Lin, C.C. Chueh, G.S. Liou and W.C. Chen. New P-Type of Poly(4-Methoxy-Triphenylamine)s Derived by Coupling Reactions: Synthesis, Electrochromic Behaviors, and Hole Mobility, J. Polym. Sci., Part A: Polym. Chem., *47*, pp.4037-4050. 2009.

Chen, S.H. and Y. Chen. Optical and Electrochemical Properties of Copoly(acryl ether)s Consisting of Alternate 2,5-Distyrylbenzene and Electron-Transporting Oxadiazole or Triazole Derivatives, J. Polym. Sci., Part A: Polym. Chem., *43*, pp.5083-5096. 2005.

Chen, X.W., C.Y. Liu, T.H. Jen, S.A. Chen and S. Holdcroft. Synthesis and Characterization of a Fullerene Bearing a Triazole Group, Chem. Mater., *19*, pp.5194-5199. 2007.

Chen, Y.C., G.S. Huang, C.C. Hsiao and S.A. Chen. High Triplet Energy Polymer as Host for Electrophosphorescence with High Efficiency, J. Am. Chem. Soc., *128*, pp.8549–8558. 2006.

Choi, B.Y., S.J. Kahng, S. Kim, H. Kim, H.W. Kim, Y.J. Song, J. Ihm and Y. Kuk1. Conformational Molecular Switch of the Azobenzene Molecule: A Scanning Tunneling Microscopy Study, Phys. Rev. Lett., *96*, pp.156106(1-4). 2006.

Chong, Y.K., J. Krstina, T.P.T. Le, G. Moad, E. Rizzardo and S.H. Thang. Thiocarbonylthio Compounds [S=C(Ph)S-R] in Free Radical Polymerization with Reversible Addition-Fragmentation Chain Transfer (RAFT Polymerization). Role of the Free-Radical Leaving Group (R), Macromolecules, *36*, pp.2256-2272. 2003.

Chou, C.H., S.L. Hsu, K. Dinakaran, M.Y. Chiu and K.H. Wei. Synthesis and Characterization of Luminescent Polyfluorenes Incorporating Side-Chain-Tethered

Polyhedral Oligomeric Silsesquioxane Units, Macromolecules, *38*, pp.745-751. 2005.

Chu, C. W., J. Ouyang, J.H. Tseng and Y. Yang. Organic Donor-Acceptor Sytem Exhibiting Electrical Bistability for Use in Memory Devices, Adv. Mater., *17*, pp.1440-1443. 2005.

Compano, R. Trends in Nanoelectronics, Nanotechnology, *12*, pp.85-88. 2001.

Connolly, T., R.C. Smith, Y. Hernandez, Y. Gun'ko, J.N. Coleman and J.D. Carey. Carbon-Nanotube-Polymer Nanocomposites for Field-Emission Cathodes, Small, *5*, pp.826-831. 2009.

de Abajo, J. and J.G. de la Campa. Processable Aromatic Polyimides, Adv. Polym. Sci., *140*, pp.23-59. 1999.

Dearnaley, G., D.V. Morgan and A.M. Stoneham. A Model for Filament Growth and Switching in Amorphous Oxide Films, J. Non-Cryst. Solids, *4*, pp.593-612. 1970.

Dei, A., D. Gatteschi, C. Sangregorio and L. Sorace. Quinonoid Metal Complexes: Toward Molecular Switches, Acc. Chem. Res., *37*, pp.827-835. [2004].

Diau, E.W.G. A New Trans-to-Cis Photoisomerization Mechanism of Azobenzene on the $S_1(n,\pi^*)$ Surface, J. Phys. Chem. A, *108*, pp.950-956. 2004.

Dikin, D.A., S. Stankovich, E.J. Zimney, R.D. Piner, G.H.B. Dommett, G. Evmenenko, S.T. Nguyen and R.S. Ruoff. Preparation and Characterization of Graphene Oxide Paper, Nature, *448*, pp.457-460. 2007.

Donhauser, Z.J., B.A. Mantooth, K.F. Kelly, L.A. Bumm, J.D. Monnell, J.J. Stapleton, D.W. Price Jr, A.M. Rawlett, D.L. Allara, J.M. Tour and P.S. Weiss. Conductance Switching in Single Molecules Through Conformational Changes, Science, *292*, pp.2303-2307. 2001.

Gong, J. P. and Y. Osada. Preparation of Polymeric Metal-Tetracyanoquinodimethane Film and Its Bistable Switching, Appl. Phys. Lett. *61*, pp.2787-2789. 1992.

Gordon, D. G., Montemerlo, M. S., Love, J. C., Opiteck, G. J. and Ellenbogen, J. C. Overview of Nanoelectronic Devices. Proc. of the IEEE, *85*, pp.521- 540.1997.

Eda, G., G. Fanchini and M. Chhowalla. Large-Area Ultrathin Films of Reduced Graphene Oxide as a Transparent and Flexible Electronic Material, Nat. Nanotechnol., *3*, pp.270-274. 2008.

Elias, D.C., R.R. Nair, T.M.G. Mohiuddin, S.V. Morozov, P. Blake, M.P. Halsall, A.C.

Ferrari, D.W. Boukhvalov, M.I. Katsnelson, A.K. Geim and K.S. Novoselov. Control of Graphene's Properties by Reversible Hydrogenation: Evidence for Graphene, Science, *323*, pp.610-613. 2009.

Foresman, J. B., M. Head-Gordon, J.A. Pople and M.J. Frisch. Towards a Systematic Molecular Orbital Theory for Excited States, J. Phys. Chem., *96*, pp.135-149. 1992.

Franco, O., I. Orgzall, W. Regenstein and B. Schulz. Structural and Spectroscopical Study of a 2,5-Diphenyl-1,3,4-Oxadiazole Polymorph under Compression, J. Phys.: Condens. Matter., *18*, pp.1459-1472. 2006.

Freilich, S.C. Photoconductivity of Donor-Loaded Polyimides, Macromolecules, *20*, pp.973-978. 1987.

Frisch, M.J., G.W. Trucks, H.B. Schlegel, G.E. Scuseria, M.A. Robb, J.R. Cheeseman, J.A. Montgomery, Jr., T. Vreven, K.N. Kudin, J.C. Burant, J.M. Millam, S.S. Iyengar, J. Tomasi, V. Barone, B. Mennucci, M. Cossi, G. Scalmani, N. Rega, G.A. Petersson, H. Nakatsuji, M. Hada, M. Ehara, K. Toyota, R. Fukuda, J. Hasegawa, M. Ishida, T. Nakajima, Y. Honda, O. Kitao, H. Nakai, M. Klene, X. Li, J.E. Knox, H.P. Hratchian, J.B. Cross, V. Bakken, C. Adamo, J. Jaramillo, R. Gomperts, R.E. Stratmann, O. Yazyev, A.J. Austin, R. Cammi, C. Pomelli, J.W. Ochterski, P.Y. Ayala, K. Morokuma, G.A. Voth, P. Salvador, J.J. Dannenberg, V.G. Zakrzewski, S. Dapprich, A.D. Daniels, M.C. Strain, O. Farkas, D.K. Malick, A.D. Rabuck, K. Raghavachari, J.B. Foresman, J.V. Ortiz, Q. Cui, A. G. Baboul, S. Clifford, J. Cioslowski, B. B. Stefanov, G. Liu, A. Liashenko, P. Piskorz, I. Komaromi, R.L. Martin, D.J. Fox, T. Keith, M.A. Al-Laham, C.Y. Peng, A. Nanayakkara, M. Challacombe, P.M.W. Gill, B. Johnson, W. Chen, M.W. Wong, C. Gonzalez and J.A. Pople. Gaussian 03, (Revision E.01), Gaussian, Inc., Wallingford CT. 2004.

Geim, A.K. and K.S. Novoselov. The Rise of Graphene, Nat. Mater., *6*, pp.183-191. 2007.

Geng, X.M., L. Niu, Z.Y. Xing, R.S. Song, G.T. Liu, M.T. Sun, G.S. Cheng, H.J. Zhong, Z.H. Liu, Z.J. Zhang, L.F. Sun, H.X. Xu, L. Lu and L.W. Liu. Aqueous-Processable Noncovalent Chemically Converted Graphene-Quantum Dot Composites for Flexible and Transparent Optoelectronic Films, Adv. Mater., *22*, pp.638-642. 2010.

Ghosh, M.K. and K.L. Mittal. Polyimides: Fundamentals and Applications, New York: Marcel Dekker, Inc. 1996.

Gilje, S., S. Han, M. Wang, K.L. Wang and R.B. Kaner. A Chemical Route to Graphene for Device Applications, Nano. Lett., *7*, pp.3394-3398. 2007.

Grazulevicius, J.V., P. Strohriegl, J. Pielichowski and K. Pielichowski. Carbazole-Containing Polymers: Synthesis, Properties and Applications, Prog. Polym. Sci., *28*, pp.1297-1353. 2003.

Gómez, R., J.L. Segura and N. Martín. Highly Efficient Light-Harvesting Organofullerenes, Org. Lett., *7*, pp.717-720. 2005.

Gong, Z.J. and J.B. Lagowski. Electronic Structure Properties of Fluorene-Phenylene Monomer and Its Derivatives: TD-DFT Study, J. Mol. Struct. (Theochem), *729*, pp.211-222. 2005.

Gong, Z.J. and J.B. Lagowski. Singlet Excitation Energies of Thiophene Derivatives of Fluorene: TD-DFT Study, Int. J. Quantum. Chem., *107*, pp.159-171. 2007.

Gore, P.H. and D.W. Wheeler. Absorption Spectra of Aromatic Azo and Related Compounds. III. Substituted Azobenzene, *26*, pp.3295-3298. 1961.

Grell, M., D.D.C. Bradley, M. Inbasekaran and E.P. Woo. A Glass-Forming Conjugated Main-Chain Liquid Crystal Polymer for Polarized Electroluminescence Applications, Adv. Mater., *9*, pp.798-802. 1997.

Grice, A.W., D.D.C Bradley, M.T. Bernius, M. Inbasekaran, W.W. Wu and E.P. Woo. High Brightness and Efficiency Blue Light-Emitting Polymer Diodes, Appl. Phys. Lett., *73*, pp.629-631. 1998.

Guldi, D.M. and V. Sgobba. Carbon Nanostructures for Solar Energy Conversion Schemes, Chem. Commun., *47*, pp.606-610. 2011.

Hahm, S.G., S. Choi, S.H. Hong, T.J. Lee, S. Park, D.M. Kim, W.S. Kwon, K. Kim, O. Kim and M. Ree. Novel Rewirtable, Non-Volatile Memory Devices Based on Thermally and Dimensionally Stable Polyimide Thin Films, Adv. Funct. Mater., *18*, pp.3276-3282. 2008.

Hamciuc, C., E. Hamciuc and M. Bruma. Poly(1,3,4-Oxadiazole-Amide)s Containing Pendent Phenoxy Groups, High. Perform. Polym., *8*, pp.507-514. 1996.

Hamciuc, E., C. Hamciuc and M. Cazacu. Poly(1,3,4-Oxadiazole-Ether-Imide)s and Their Polydimethylsiloxane-Containing Copolymers, Eur. Polym. J., *43*, pp.4739–4749. 2007.

Hasegawa, M. and K. Horie. Photophysics, Photochemistry, and Optical Properties of Polyimides, Prog. Polym. Sci., *26*, pp.259-335. 2001.

Heeger, A.J., S. Kivelson, J.R. Schrieffer and W.P. Su. Solitons in Conducting

Polymers, Rev. Mod. Phys., *60*, pp.781-850. 1988.

Heliotis, G., D.D.C. Bradley, G.A. Turnbull and I.D.W. Samuel. Light Amplification and Gain in Polyfluorene Waveguides, Appl. Phys. Lett., *81*, pp.415-417. 2002.

Heliotis, G., R. Xia, D.D.C. Bradley, G.A. Turnbull, I.D.W. Samuel, P. Andrew and W.L. Barnes. Blue, Surface-Emitting, Distributed Feedback Polyfluorene Lasers, Appl. Phys. Lett., *83*, pp.2118-2120. 2003.

Henisch, H.K. and W.R. Smith. Switching in Organic Polymer Films, Appl. Phys. Lett. *24*, pp.589-591. 1974.

Hsu, S. C., W.T. Whang and C.S. Chao. Electroluminescence and Electron Transport Characteristics of Aromatic Polyimides Containing 1,3,4-Oxadiazole Moiety, Thin Solid Films, *515*, pp.6943-6948. 2007.

Hu, J.P., Y.F. Li, Z.Y. Ji, G.Y. Jiang, L.M. Yang, W.P. Hu, H.J. Gao, L. Jiang, Y.Q. Wen, Y.L. Song and D.B. Zhu. A Non-Planar Organic Molecule with Non-Volatile Electrical Bistability for Nano-Scale Data Storage, J. Mater. Chem., *17*, pp.3530-3535. 2007.

Huang, W., X. Zhang, L.H. Ma, C.J. Wang and Y.B. Jiang. Intramolecular Charge Transfer Dual Fluorescence of Substituted-Phenyl *p*-Dimethylaminobenzoates with Comparable Electron Acceptors, Chem. Phys. Lett., *352*, pp.401-407. 2002.

Hudgens, S. and B. Johnson. Overview of Phase-Change Chalcogenide Nonvolatile Memory Technology, MRS Bull., *29*, pp.829-832. 2004.

Hummers, W. S. and R. E. Offeman. Preparation of Graphitic Oxide, J. Am. Chem. Soc., *80*, pp.1339-1339. 1958.

Hwang, S.W. and Y. Chen. Synthesis and Characterization of New Poly(acryl ether)s Containing Alternate Emitting and Electron Transporting Chromophores, Polymer, *41*, pp.6581-6587. 2000.

Ichimura, K. Photoalignment of Liquid-Crystal Systems, Chem. Rev., *100*, pp.1847-1874. 2000.

Ikeda, T. and O. Tsutsumi. Optical Switching and Image Storage by Means of Azobenzene Liquid-Crystal Films, Science, *268*, pp.1873-1875. 1995.

Imai, Y. Synthesis of Novel Organic-Soluble High-Temperature Aromatic Polymers, High. Perform. Polym., *7*, pp.337-345. 1995.

Jakobsson, F.L.E., X. Crispin, M. Cölle, M. Büchel, D.M. de Leeuw and M. Berggren. On the Switching Mechanism in Rose Bengal-Based Memory Devices, Org. Electron., *8*, pp.559-565. 2007.

Jansson, E., P.C. Jha and H. Ågren. Density Functional Study of Triazole and Thiadiazole Systems as Electron Transporting Materials, Chem. Phys., *330*, pp.166-171. 2006.

Jenekhe, S.A. and J.A. Osaheni. Excimers and Exciplexes of Conjugated Polymers, Science, *265*, pp.765-768. 1994.

Jiang, G.Y., T. Michinobu, W.F. Yuan, M. Feng, Y.Q. Wen, S.X. Du, H.J. Gao, L. Jiang, Y.L. Song, F. Diederich and D.B. Zhu. Crystalline Thin Film of a Donor-Substituted Cyanoethylnylethene for Nanoscale Data Recording Through Intermolecular Charge-Transfer Interactions, Adv. Mater., *17*, pp.2170-2173. 2005.

Jiang, G.Y., Y.L. Song, X.F. Guo, D.Q. Zhang and D.B. Zhu. Organic Functional Molecules Towards Information Processing and High-Density Information Storage, Adv. Mater., *20*, pp.2888-2898. 2008.

Jiang, Y.M., X.G. Wan, F. Guo, H.B. Xie, P. Liu and J. Li. A New Polymer Thin Film with Electrical Bistable States, Phys. Status Solidi. A, *202*, pp.1804-1807. 2005.

Jiang, Z.Q., W.J. Zhang, H.Q. Yao, C.L. Yang, Y. Cao, J.G. Qin, G. Yu and Y.Q. Liu. Copolyfluorenes Containing Bridged Triphenylamine or Triphenylamine: Synthesis, Characterization, and Optoelectronic Properties, J. Polym. Sci., Part A: Polym. Chem., *47*, pp.3651-3661. 2009.

Jin, S.H., M.Y. Kim, J.Y. Kim, K. Lee and Y.S. Gal. High-Efficiency Poly(*p*-phenylenevinylene)-Based Copolymers Containing an Oxadiazole Pendant Group for Light-Emitting Diodes, J. Am. Chem. Soc., *126*, pp.2474-2480. 2004.

Joo, W.J., T.L. Choi, J. Lee, S.K. Lee, M.S. Jung, N. Kim and J.M. Kim. Metal Filament Growth in Electrically Conductive Polymers for Nonvolatile Memory Application, J. Phys. Chem. B., 110, pp.23812-23816. 2006.

Jung, M.S., T.W. Lee, J.H. Lee, B.H. Sohn and I.S. Jung. Synthesis and Characterizations of a Polyimide Containing a Triphenylamine Derivative as an Interlayer in Polymer Light-Emitting Diode, Polymer, *47*, pp.2670-2676. 2006.

Kawata, S. and Y. Kawata. Three-Dimensional Optical Data Storage Using Photochromic Mateirals, Chem. Rev., *100*, pp.1777-1788. 2000.

Ke, S.H., H.U. Baranger and W.T. Yang. Addition Energies of Fullerenes and Carbon

Nanotubes as Quantum Dots: The Role os Symmetry. Phys. Rev. Lett., *91*, pp.116803(1-4). 2003.

Khan, R.U.A., D. Poplavskyy, T. Kreouzis and D.D.C. Bradley. Hole Mobility within Arylamine-Ccontaining Polyfluorene Copolymers: A Time-of-Flight Transient-Photocurrent Study, Phys. Rev. B, *75*, pp.035215(1-14). 2007.

Kido, J., C. Ohtaki, K. Hongawa, K. Okuyama and K. Nagai. 1,2,4-Triazole Derivative as an Electron Transport Layer in Organic Electroluminescent Devices, Jpn. J. Appl. Phys., *32*, pp.L917-L920. 1993.

Kido, J., H. Hayase, K. Hongawa, K. Nagai and K. Okuyama. Bright Red Light-Emitting Organic Electroluminescent Devices Having a Europium Complex as an Emitter, Appl. Phys. Lett., 65, pp.2124-2126. 1994.

Kim, J.S., L. Lu, P. Sreearunothai, A. Seeley, K.H. Yim, A. Petrozza, C.E. Murphy, D. Beljonne, J. Cornil and R.H. Friend. Optoelectronic and Charge Transport Properties at Organic-Organic Semiconductor Interfaces: Comparison between Polyfluorene-Based Polymer Blend and Copolymer, J. Am. Chem. Soc., *130*, pp.13120-13131. 2008.

Kim, T.W., S.H. Oh, H. Choi, G. Wang, H. Hwang, D.Y. Kim and T. Lee. Reversible Switching Characteristics of Polyfluorene-Derivative Single Layer Film for Nonvolatile Memory Devices, Appl. Phys. Lett., *92*, pp.253308(1-3). 2008.

Kim, W.S., J. Kim, J.K. Park, S. Mukamel, S.K. Rhee, Y.K. Choi and J.Y. Lee. Stacking Effect of Polyfluorene on the Chemical Shift and Electron Transport, J. Phys. Chem. B, *109*, pp.2686-2692. 2005.

Kirby, A.J. Polyimides: Materials, Processing and Applications, Rapra Technology Ltd. 1996.

Kishore, V.C., R. Dhanya, K. Sreekumar, R. Joseph and C.S. Kartha. On the Dipole Moments and First-Order Hyperpolarizability of *N,N*-Bis(4-Bromobutyl)-4-Nitrobenzenamine, Spectrochim. Acta, Part A, *70*, pp.1227-1230. 2008.

Kong, B.S., H.W. Yoo and H.T. Jung. Electrical Conductivity of Graphene Films with a Poly(allylamine hydrochloride) Supporting Layer, Langmuir, *25*, pp.11008-11013. 2009.

Kurihara, S., M. Moritsugu, S. Kubo, S.N. Kim, T. Ogata, T. Nonaka and O. Sato. Photoswitching Properties of Photonic Band Gap Material Containing Azo-Polymer Liquid Crystal, Eur. Polym. J., *43*, pp.4951-4960. 2007.

Labarthet, F.L., S. Freiberg, C. Pellerin, M. Pézolet, A. Natansohn and P. Rochon. Spectroscopic and Optical Characterization of a Series of Azobenzene-Containing Side-Chain Liquid Crystalline Polymers, Macromolecules, *33*, pp.6815-6823. 2000.

LaFemina, J. P. Photoconduction in Polyimide, Chem. Phys. Lett., *159*, pp.307-309. 1989.

Lai, Y.S., C.H. Tu, D.L. Kwong and J.S. Chen. Bistable Resistance Switching of Poly(*N*-vinylcarbazole) Films for Nonvolatile Memory Applications, Appl. Phys. Lett., *87*, pp.122101(1-3). 2005.

Lai, Y.S., C.H. Tu, D.L. Kwong and J.S. Chen. Charge-Transport Characteristics in Bistable Resistive Poly(*N*-vinylcarbazole) Films, IEEE Electron Device Lett., *27*, pp.451-453. 2006.

Lecler, M. Polyfluorenes: Twenty Years of Progress, J. Polym. Sci., Part A: Polym. Chem., *39*, pp.2867-2873. 2001.

Lei, B., W.L. Kwan, Y. Shao and Y. Yang. Statistical Characterization of the Memory Effect in Polyfluorene Based Non-Volatile Resistive Memory Devices, Org. Electron., *10*, pp.1048-1053. 2009.

Lee, C., X.D. Wei, J.W. Kysar and J. Hone. Measurement of the Elastic Properties and Intrinsic Strength of Monolayer Graphene, Science, *321*, pp.385-388. 2008.

Lee, J., B.J. Jung, S.K. Lee, J.I. Lee, H.J. Cho and H.K. Shim. Fluorene-Based Alternating Polymers Containing Electron-Withdrawing Bithiazole Units: Preparation and Device Applications, J. Polym. Sci., Part A: Polym. Chem., *43*, pp.1845-1857. 2005.

Lee, R.H., H.F. Hsu, L.H. Chan and C.T. Chen. Synthesis and Electroluminescence Properties of a Novel Tetraphenylsilane-Diphenyl(*para*-tolyl)amine Polymer, Polymer, *47*, pp.7001-7012. 2006.

Lee, S.A., T. Yamashita and K. Horie. Photoconductivity of a Polyimide with an Alicyclic Diamine: Charge Carrier Photogeneration in the Mixed Layer Packing Arrangement, J. Polym. Sci., Part B: Polym. Phys., *36*, pp.1433-1442. 1998.

Lee, Y.Z., X.W. Chen, S.A. Chen, P.K. Wei and W.S. Fann. Soluble Electroluminescent Poly(phenylene vinylene)s with Balanced Electron- and Hole-Injections, J. Am. Chem. Soc., *123*, pp.2296-2307. 2001.

Lemmer, U., S. Heun, R.F. Mahrt, U. Scherf, M. Hopmeier, U. Siegner, E.O. Göbel, K. Müllen and H. Bässler. Aggregate Fluorescence in Conjugated Polymers, Chem.

Phys. Lett., *240*, pp.373-378.

Li, C., W. Fan, B. Lei, D.H. Zhang, S. Han, T. Tang, X.L. Liu, Z.Q. Liu, S. Asano, M. Meyyappan, J. Han and C.W. Zhou. Multilevel Memory Based on Molecular devices, Appl. Phys. Lett., *84*, pp.1949-1951. 2004.

Li, D., M.B. Müller, S. Gilje, R.B. Kaner and G.G. Wallace. Processable Aqueous Dispersions of Graphene Nanosheets, Nat. Nanotechnol., *3*, pp.101-105. 2008.

Li, F.S., D.I. Son, H.M. Cha, S.M. Seo, B.J. Kim, H.J. Kim, J.H. Jung and T.W. Kim. Memory Effect of CdSe/ZnS Nanoparticles Embedded in a Conducting Poly[2-methoxy-5-(2-ethylhexyloxy)-1,4-phenylene-vinylene] Polymer Layer, Appl. Phys. Lett., *90*, pp.222109(1-3). 2007.

Li, L., Q.D. Ling, S.L. Lim, Y.P. Tan, C.X. Zhu, D.S.H. Chan, E.T. Kang and K.G. Neoh. A Flexible Polymer Memory Device., Org. Electron., *8*, pp.401-406. 2007.

Li, Y.N., J.F. Ding, M. Day, Y. Tao, J.P. Lu and M. D'iorio. Synthesis and Properties of Random and Alternating Fluorene/Carbazole Copolymers for Use in Blue Light-Emitting Devices, Chem. Mater., *16*, pp.2165-2173. 2004.

Li, Y.Z., S.S. Liu, M.D. Chen and F.C. Ma. Photoinduced Intermolecular and Intramolecular Charge Transfer in the Mixed Coaggregates of Pyrazoline and Dicyanonaphthalene, J. Photoch. Photobio., A: Chemistry, *25*, pp.139-144. 2009.

Liang, W.Z., Y. Zhao, J. Sun, J. Song, S.L. Hu and J.L. Yang. Electronic Excitation of Polyfluorenes: A Theoretical Study, J. Phys. Chem. B, *110*, pp.9908-9915. 2006.

Liaw, D.J., F.C. Chang, M.K. Leung, M.Y. Chou and K. Muellen. High Thermal Stability and Rigid Rod of Novel Organosoluble Polyimides and Polyamides Based on Bulky and Noncoplanar Naphthalene-Biphenyldiamine, Macromolecules, *38*, pp.4024-4029. 2005.

Liaw, D.J., K.L. Wang and F.C. Chang. Novel Organosoluble Poly(pyridine-imide) with Pendent Pyrene Group: Synthesis, Thermal, Optical, Electrochemical, Electrochromic, and Protonation Characterzation, Macromolecules, 40, pp.3568-3574. 2007.

Lim, E., B.J. Jung and H.K. Shim. Improved EL Efficiency of Fluorene-Thieno[3,2-*b*] Thiophene-Based Conjugated Copolymers with Hole-Transporting or Electron-Transporting Units in the Main Chain, J. Polym. Sci., Part A: Polym. Chem., *44*, pp.243-253. 2006.

Lim, S.L., K.L. Tan and E.T. Kang. In Situ XPS Study of the Interactions of

Evaporated Copper Atoms with Neutral and Protonated Polyaniline Films, Langmuir, *14*, pp.5305-5313. 1998.

Lim, S.L., Q.D. Ling, E.Y.H. Teo, C.X. Zhu, D.S.H. Chan, E.T. Kang and K.G. Neoh. Conformation-Induced Electrical Bistability in Non-Conjugated Polymers with Pendant Carbazole Moieties, Chem. Mater., *19*, pp.5148-5157. 2007.

Lin, H.T., Z. Pei and Y.J. Chan. Carrier Transport Mechanism in a Nanoparticle-Incorporated Organic Bistable Memory Device, IEEE Electron Device Lett., *28*, pp.569-571. 2007.

Lin, J., M. Zheng, J.S. Chen, X. Gao and D.G. Ma. Negative Differential Resistance and Memory Effect in Diodes Based on 1,4-Dibenzyl C60 and Zinc Phthalocyanine Doped Polystyrene Hybrid Material, Inorg. Chem., *46*, pp.341-344. 2007.

Lin, Y., K. Zhang, W.F. Chen, Y.D. Liu, Z.G. Geng, J. Zeng, N. Pan, L.F. Yan, X.P. Wang and J.G. Hou. Dramatically Enhanced Photoresponse of Reduced Graphene Oxide with Linker-Free Anchored CdSe Nanoparticles, ACS Nano, *4*, pp.3033-3038. 2010.

Ling, Q.D., D.J. Liaw, E.Y.H. Teo, C.X. Zhu, D.S.H. Chan, E.T. Kang and K.G. Neoh. Polymer Memories: Bistable Electrical Switching and Device Performance, Polymer, *48*, pp.5182-5201. 2007.

Ling, Q.D., F.C. Chang, Y. Song, C.X. Zhu, D.J. Liaw, D.S.H. Chan, E.T. Kang and K.G. Neoh. Synthesis and Dynamic Random Access Memory Behavior of a Functional Polyimide, J. Am. Chem. Soc., *128*, pp.8732-8733. 2006.

Ling, Q.D., S.L. Lim, Y. Song, C.X. Zhu, D.S.H. Chan, E.T. Kang and K.G. Neoh. Nonvolatile Polymer Memory Device Based on Bistable Electrical Switching in a Thin Film of Poly(N-Vinylcarbazole) with Covalently Bonded C_{60}, Langmuir, *23*, pp.312-319. 2007.

Ling, Q.D., Y. Song, E.Y.H. Teo, S.L. Lim, C.X. Zhu, D.S.H. Chan, D.L. Kwong, E.T. Kang and K.G. Neoh. WORM-Type Memory Device Based on a Conjugated Copolymer Containing Europium Complex in the Main Chain, Electrochem. Solid-State Lett., *9*, pp.G268-G271. 2006.

Ling, Q.D., Y. Song, S.L. Lim, E.Y.H. Teo, Y.P. Tan, C.X. Zhu, D.S.H. Chan, D.L. Kwong, E.T. Kang and K.G. Neoh. A Dynamic Random Access Memory Based on a Conjugated Copolymer Containing Electron-Donor and -Acceptor Moieties, Angew. Chem. Int. Ed., *45*, pp.2947-2951. 2006.

Ling, Q.D., Y. Song, S.J. Ding, C.X. Zhu, D.S.H. Chan, D.L. Kwong, E.T. Kang and

K.G. Neoh. Non-Volatile Polymer Memory Device Based on a Novel Copolymer of *N*-Vinylcarbazole and Eu-Complexed Vinylbenzoate, Adv. Mater., *17*, pp.455-459. 2005.

Liu, C.Y. and A.J. Bard. Optoelectric Charge Trapping/Detrapping in Thin Solid Films of Organic Azo Dyes: Application of Scanning Tunneling Miscroscopic Tip Contact to Photoconductive Films for Data Storage, Chem. Mater., *10*, pp.840-846. 1998.

Liu, G., D.J. Liaw, W.Y. Lee, Q.D. Ling, C.X. Zhu, D.S.H. Chan, E.T. Kang and K.G. Neoh. Tristable Electrical Conductivity Switching in a Polyfluorene-Diphenylpyridine Copolymer with Pendant Carbazole Groups, Phil. Trans. R. Soc. A, *367*, pp.4203-4214. 2009.

Liu, G., Q.D. Ling, E.T. Kang, K.G. Neoh, D.J. Liaw, F.C. Chang, C.X. Zhu and D.S.H. Chan. Bistable Electrical Switching and Write-Once Read-Many-Times Memory Effect in a Donor-Acceptor Containing Polyfluorene Derivative and Its Carbon Nanotube Composites, J. Appl. Phys., *102*, pp.024502(1-8). 2007.

Liu, J., L.J. Bu, J.P. Dong, Q.G. Zhou, Y.H. Geng, D.G. Ma, L.X. Wang, X.B. Jing, F.S. Wang. Green Light-Emitting Polyfluorenes with Improved Color Purity Incorporated with 4,7-Diphenyl-2,1,3-Benzothiadiazole Moieties, J. Mater. Chem., *17*, pp.2832-2838. 2007.

Liu, Y.L., K.L. Wang, G.Y. Huang, C.X. Zhu, E.S. Tok, K.G. Neoh and E.T. Kang, Volatile Electrical Switching and Static Random Access Memory Effect in a Functional Polyimide Containing Oxadiazole Moieties, Chem. Mater., *21*, pp.3391-3399. 2009.

Liu, Y.L., Q.D. Ling, E.T. Kang, K.G. Neoh, D.J. Liaw, K.L. Wang, W.T. Liou, C.X. Zhu and D.S.H. Chan. Volatile Electrical Switching in a Functional Polyimide Containing Electron-Donor and -Acceptor Moieties, J. Appl. Phys., *105*, pp.044501(1-9). 2009

Liu, Z.C., F.L. Xue, Y. Su and K. Varahramyan. Memory Effect in the Current-Voltage Characteristics of Diodes Based on PEDOT:PSS, Mater. Res. Soc. Symp. Proc., *871*, pp.381-386. 2005.

Liu, Z.F., Q. Liu, Y. Huang, Y.F. Ma, S.G. Yin, X.Y. Zhang, W. Sun and Y.S. Chen. Organic Photovoltaic Devices Based on a Novel Acceptor Material: Graphene, Adv. Mater., *20*, pp.3924-3930. 2008.

Lozano, A.E., J. de Abajo, J.G. de la Campa, C. Guillén, J. Herrero and M.T. Gutiérrez. Thin-Film Polyimide/Indium Tin Oxide Composites for Photovoltaic

Applications, J. Appl. Polym. Sci., *103*, pp.3491-3497. 2007.

Lu, J.P., Y. Tao, M. D'iorio, Y.N. Li, J.F. Ding and M. Day. Pure Deep Blue Light-Emitting Diodes from Alternating Fluorene/Carbazole Copolymers by Using Suitable Hole-Blocking Materials, Macromolecules, *37*, pp.2442-2449. 2004.

Lukas, A.S., Y.Y. Zhao, S.E. Miller and M.R. Wasielewski. Biomimetic Electron Transfer Using Low Energy Excited States: A Green Perylene-Based Analogue of Chlorophyll, J. Phys. Chem. B., *106*, pp.1299-1306. 2002.

Ma, D.G., M. Aguiar, J.A. Freire and I.A. Hummelgen. Organic Reversible Switching Devices for Memory Applications, Adv. Mater., *12*, pp.1063-1066. 2000.

Ma, Z.H., S.L. Lim, K.L. Tan, S. Li and E.T. Kang. In Situ X-Ray Photoelectron Spectroscopy Studies of Interactions of Evaporated Metals with Electroactive Polyaniline Films, J. Mater. Sci. -Mater. Electron., *11*, pp.311-317. 2000.

Majee, S.K., H.S. Majumdar, A. Bolognesi and A.J. Pal. Electrical Bistability and Memory Applications of Poly(*p*-phenylene vinylene) Films, Synth. Met., *156*, pp.828-832. 2006.

Mak, K.F., M.Y. Sfeir, Y. Wu, C.H. Lui, J.A. Misewich and T.F. Heinz. Measurement of the Optical Conductivity of Graphene, Phys. Rev. Lett. *101*, pp.196405(1-4). 2008.

Mello, R.M., E.C. Azevedo, A. Meneguzzi, M. Aguiar, L. Akcelrud and I.A. Hummelgen. Naphthalene Containing Poly(urethane-urea) for Volatile Memory Device Applications, Macromol. Mater. Eng., *287*, pp.466-469. 2002.

Miguel, M., B. Ferrer, L. Teruel, H. García, Y.N. Jin, Y.N. Li and J.F. Ding. Photophysics of Fluorene Copolymers: Control of Fluorescence and Charge Separation by the Presence of Carbazole, Oxadiazole, or Biphenyl Units, J. Phys. Chem. C., *113*, pp.8471-8477. 2009.

Möller, S., C. Perlov, W. Jackson, C. Taussig and S.R. Forrest. A Polymer/Semiconductor Write-Once-Read-Many-Times Memory, Nature, *426*, pp.166-169. 2003.

Mort, J. Transient Photoinjection of Holes From Amorphous Se Into Poly(*N*-Vinylcarbazole), Phys. Rev. B, *5*. pp.3329-3336. 1972.

Mukherjee, B. and A.J. Pal. On the Origin of Multilevel Conductance and Memory in Ultrathin Organic Films, Synth. Met., *155*, pp.336-339. 2005.

Murase, T., S. Sato and M. Fujita. Switching the Interior Hydrophobicity of a

Self-Assembled Spherical Complex Through the Photoisomerization of Confined Azobenzene Chromophores, Angew. Chem. Int. Ed., *46*, pp.5133-5136. 2007.

Natansohn, A. and P. Rochon. Photoinduced Motions in Azo-Containing Polymers, Chem. Rev., *102*, pp.4139-4176. 2002.

Nomura, K. and A.H. MacDonald. Quantum Hall Ferromagnetism in Graphene, Phys. Rev. Lett., 96, pp.256601(1-4). 2006.

Novoselov, K.S., Z. Jiang, Y. Zhang, S.V. Morozov, H.L. Stormer, U. Zeitler, J.C. Maan, G.S. Boebinger, P. Kim and A.K. Geim. Room-Temperature Quantum Hall Effect in Graphene, Science, *315*, pp.1379-1379. 2007.

Oh-e, M., T. Asahi and H. Masuhara. Ultrafast Charge Separation and Recombination Dynamics in a Nanometer Thin Film of Polyimide Observed by Femtosecond Transient Absorption Spectroscopy, J. Phys. Chem. B, *106*, pp.5840-5844. 2002.

Ohmoro, Y., M. Uchida, K. Muro and K. Yoshino. Blue Electroluminescent Diodes Utilizing Poly(alkylfluorene), Jpn. J. Appl. Phys., *30*, pp.L1941-1943. 1991.

Ouyang, J., C.W. Chu, C.R. Szmanda, L.P. Ma and Y. Yang. Programmable Polymer Thin Film and Non-Volatile Memory Device, Nat. Mater., *3*, pp.918-922. 2004.

Ouyang, J., C.W. Chu, D. Sieves and Y. Yang. Electric Field-Induced Charge Transfer between Gold Nanoparticle and Capping 2-Naphthalenethiol and Organic Memory Cells, Appl. Phys. Lett., *86*, pp.123507(1-3). 2005.

Ouyang, J., C.W. Chu, R.J. Tseng, A. Prakash and Y. Yang. Organic Memory Device Fabricated Through Solution Processing, Proc. IEEE., *93*, pp.1287-1296. 2005.

Paul, S. Realization of Nonvolatile Memory Devices Using Small Organic Molecules and Polymer, IEEE Transactions on Nanotechnology, *6*, pp.191-195. 2007.

Paul, S., A. Kanwal and M. Chhowalla. Memory Effect in Thin Films of Insulating Polymer and C60 Nanocomposites, Nanotechnology, *17*, pp.145-151. 2006.

Paul, P.K., S.A. Hussain and D. Bhattacharjee. Photophysical Characterizations of 2-(4-Biphenylyl)-5-Phenyl-1,3,4-Oxadiazole in Restricted Geometry, J. Lumin., *128*, pp.41-50. 2008.

Pei, Q.B., G. Zuccarello, M. Ahlskog and O. Inganäs. Electrochromic and Highly Stable Poly(3,4-Ethylenedioxythiophene) Switches between Opaque Blue-Black and Transparent Sky Blue, Polymer, *35*, 1347-1351. 1994.

Pender, L.F. and R.J. Fleming. Memory Switching in Glow Discharge Polymerized Thin Films, J. Appl. Phys., *46*, pp.3426-3431. 1975.

Porrès, L., A. Holland, L.O. Palsson, A.P. Monkman, C. Kemp and A. Beeby. Absolute Measurements of Photoluminescence Quantum Yields of Solutions Using an Integrating Sphere, J. Fluoresc., *16*, pp.267-272. 2006.

Potember, R.S., T.O. Poehler and D.O. Cowan. Electrical Switching and Memory Phenomena in Cu-TCNQ Tthin Films, Appl. Phys. Lett., *34*, pp.405-407. 1979.

Prakash, A., J. Ouyang, J.L. Lin and Y. Yang. Polymer Memory Device Based on Conjugated Polymer and Gold Nanoparticles, J. Appl. Phys., *100*, pp.054309(1-5). 2006.

Pradhan, B., S.K. Batabyal and A.J. Pal. Electrical Bistability and Memory Phenomenon in Carbon Nanotube-Conjugated Polymer Matrixes, J. Phys. Chem. B., *110*, pp.8274-8277. 2006.

Promarak, V., M. Ichikawa, T. Sudyoadsuk, S. Saengsuwan and T. Keawin. Synthesis and Properties of Hole-Transporting Fluorene Linked Bistriphenylamine, Opt. Mater., *30*, pp.364-369. 2007.

Qi, X.Y., K.Y. Pu, X.Z. Zhou, H. Li, B. Liu, F. Boey, W. Huang and H. Zhang. Conjugated-Polyelectrolyte-Functionalized Reduced Graphene Oxide with Excellent Solubility and Stability in Polar Solvents, Small, *6*, pp.663-669. 2010.

Raymo, F.M. Digital Processing and Communication with Molecular Switches, Adv. Mater., *14*, pp.401-414. 2002.

Redecker, M., D.D.C. Bradley, M. Inbasekaran, W.W. Wu and E.P. Woo. High Mobility Hole Transport Fluorene-Triarylamine Copolymers, Adv. Mater., *11*, pp.241-246. 1999.

Robinson, J.T., F.K. Perkins, E.S. Snow, Z. Wei and P.E. Sheehan. Reduced Graphene Oxide Molecular Sensors, Nano Lett., *8*, pp.3137-3140. 2008.

Rumyantsev, B. M., V.I. Berendyaev, A.Y. Tsegel'skaya, T.S. Zhuravleva and I.V. Klimenko. Photoconducting Polymer Nanocomposites with Efficient Photogeneration and Bipolar Transport for Optoelectronic Applications. Synth. Met., *152*, pp.85-88. 2005.

Sadaoka, Y. and Y. Sakai. Switching in Poly(*N*-Vinylcarbazole) Thin Films, J. Chem. Soc. Faraday Trans. II, *72*, pp.1911-1915. 1976.

Saito, R., M. Fujita, G. Dresselhaus and M.S. Dresselhaus. Electronic Structure of Graphene Tabules Based on C_{60}, Phys. Rev. B, *46*, pp.1804-1811. 1992.

Sakai, Y., Y. Sadaoka and G. Okada. Switching in Poly(*N*-Vinylcarbazole) Thin Films Effect of Molecular Weight and Impurities, Polym. J., *15*, pp.195-199. 1983.

Sancho-García, J.C., C.L. Foden, I. Grizzi, G. Greczynski, M.P. de Jong, W.R. Salaneck, J.L. Brédas and J. Cornil. Joint Theoretical and Experimental Characterization of the Structural and Electronic Properties of Poly(dioctylfluorene-*alt*-butylphenyl diphenylamine), J. Phys. Chem. B, *108*, pp.5594-5599. 2004.

Schedin, F., A.K. Geim, S.V. Morozov, E.W. Hill, P. Blake, M.I. Katsnelson and K.S. Novoselov. Detection of Individual Gas Molecules Adsorbed on Graphene, Nat. Mater., *6*, pp.652-655. 2007.

Scherf, U. and E.J.W List. Semiconducting Polyfluorene – Towards Reliable Structure-Property Relationships, Adv. Mater., *14*, pp.477-487. 2002.

Segui, Y., Bui Ai and H. Carchano. Switching in Polystyrene Films: Transition from On to Off State, J. Appl. Phys., *47*, pp.140-143. 1976.

Service, R.F. Electronics: Organic Device Bids to Make Memory Cheaper, Science, *293*, pp.1746-1746. 2001.

Service, R.F. Next-Generation Technology Hits an Early Midlife Crisis, Science, *302*, pp.556-557. 2003.

Setter, N., D. Damjanovic, L. Eng, G. Fox, S. Gevorgian, S. Hong, A. Kingon, H. Kohlstedt, N.Y. Park, G.B. Stephenson, I. Stolitchnov, A.K. Taganstev, D.V. Taylor, T. Yamada and S. Streiffer. Ferroelectric Thin Films: Review of Materials, Properties, and Applications. J. Appl. Phys., *100*, pp.051606(1-46). 2006.

Shang, T., F. Yang, W. Zheng and C. Wang. Fabrication of Electrically Bistable Nanofibers, Small, *2*, pp.1007-1009. 2006.

Shang, Y.L., Y.Q. Wen, S.L. Li, S.L. Du, S.X. Du, X.B. He, L. Cai, Y.F. Li, L.M. Yang, H.J. Gao and Y.L. Song. A Triphenylamine-Containing Donor-Acceptor Molecule for Stable, Reversible, Ultrahigh Density Data Storage, J. Am. Chem. Soc., *129*, pp.11674-11675. 2007.

Shi, W., L. Wang, H.Y. Zhen, D.X. Zhu, T. Awut, H.Y. Mi and I. Nurulla. Novel Luminescent Polymers Containing Backbone Triphenylamine Groups and Pendant Quinoxaline Groups, Dyes. Pigments., *83*, pp.102-110. 2009.

Shibano, Y., T. Umeyama, Y. Matano, N.V. Tkachenko, H. Lemmetyinen and H. Imahori. Synthesis and Photophysical Properties of Electron-Rich Perylenediimide-Fullerene Dyad, Org. Lett., *8*, pp.4425-4428. 2006.

Shin, J. H., J.W. Park, W.K. Lee, N.J. Jo, W.J. Cho and C.S. Ha. Organic Electroluminescent Devices Using Fluorine-Containing Polyimides as a Hole Transporting Layer, Synth. Met., *137*, pp.1017-1018. 2003.

Simmons, J.G. and R.R. Verderber. New Conduction and Reversible Memory Phenomena in Thin Insulating Films, Proc. R. Soc. Lond. A, *301*, pp.77-102. 1967.

Simon, D.T., M.S. Griffo, R.A. DiPietro, S.A. Swanson and S.A. Carter. Admittance Spectroscopy of Polymer-Nanoparticle Nonvolatile Memory Devices, Appl. Phys. Lett., *89*, pp.133510(1-3). 2006.

Sims, M., D.D.C. Bradley, M. Ariu, M. Koeberg, A. Asimakis, M. Grell and D.G. Lidzey. Understanding the Origin of the 535 nm Emission Band in Oxidized Poly(9,9-Dioctylfluorene): The Essential Role of Inter-Chain/Inter-Segment Interactions, Adv. Funct. Mater., *14*, pp.765-781. 2004.

Sivaramakrishnan, S., P.J. Chia, Y.C. Yeo, L.L. Chua and P.K. Ho. Controlled Insulator-to-Metal Transformation in Printable Polymer Composites with Nanometal Clusters, Nat. Mater., *6*, pp.149-155. 2007.

Sliva, P.O., G. Dir and C. Griffiths. Bistable Switching and Memory Devices, J. Non-Cryst. Solids, *2*, pp.316-333. 1970.

Smith, S. and S.R. Forrest. A Low Switching Voltage Organic-on-Inorganic Heterojunction Memory Element Utilizing a Conductive Polymer Fuse on a Doped Silicon Substrate, Appl. Phys. Lett., *84*, pp.5019-5021. 2004.

Stankovich, S., D.A. Dikin, R.D. Piner, K.A. Kohlhaas, A. Kleinhammes, Y.Y. Jia, Y. Wu, S.T. Nguyen and R.S. Ruoff. Synthesis of Graphene-Based Nanosheets via Chemical Reduction of Exfoliated Graphite Oxide, Carbon, *45*, pp.1558-1565. 2007.

Stikeman, A. Polymer Memory: The Plastic Path to Better Data Storage, Technol. Rev., *105*, pp.31-31. 2002.

Stoller, M.D., S.J. Park, Y.W. Zhu, J.H. An and R.S. Ruoff. Graphene-Based Ultra Capacitors, Nano. Lett., *8*, pp.3498-3502. 2008.

Stoyanov, S., L. Antonov, T. Stoyanova and V. Petrova. Ammonium-Azonium Tautomerism in Some *N,N*-Dialkylaminoazodyes-II. Compounds Containing More

Than Two Protonation Sites, Dyes. Pigments., *32*, pp.171-185. 1996.

Strukelj, M., F. Papadimitrakopoulos, T.M. Miller, L.J. Rothberg and E.A. Chandross. Design and Application of Electron-Transporting Organic Materials, Science, *267*, pp.1969-1972. 1995.

Song, Y., Q.D. Ling, S.L. Lim, E.Y.H. Teo, Y.P. Tan, L. Li, E.T. Kang, D.S.H. Chan and C.X. Zhu. Electrically Bistable Thin-Film Device Based on PVK and GNPs Polymer Material, IEEE Electron Device Lett., *28*, pp.107-110. 2007.

Song, Y., Y.P. Tan, E.Y.H. Teo, C.X. Zhu, D.S.H. Chan, Q.D. Ling, K.G. Neoh and E.T. Kang. Synthesis and Memory Properties of a Conjugated Copolymer of Fluorene and Benzoate with Chelated Europium Complex, J. Appl. Phys., *100*, pp.084508(1-6). 2006.

Sun, S.Q., P.J. Wu and D.B. Zhu. The Preparation, Characterization of Amorphous Cu-TCNQ Film with a Low Degree of Charge-Transfer (DCT) and Its Electric Switching Properties, Thin Solid Films, *301*, pp.192-196. 1997.

Svensson, M., F.L. Zhang, S.C. Veenstra, W.J.H. Verhees, J.C. Hummelen, J.M. Kroon, O. Inganäs and M.R. Anderson. High-Performance Polymer Solar Cells of an Alternating Polyfluorene Copolymer and a Fullerene Derivative, Adv. Mater., *15*, pp.988-991. 2003.

Szymanski, A., D.C. Larson and M.M. Labes. A Temperature-Independent Conducting State in Tetracene Thin Film, Appl. Phys. Lett., *14*, pp.88-90. 1969.

Takimoto, K., H. Kawade, E. Kishi, K. Yano, K. Sakai, K. Hatanaka, K. Eguchi and T. Nakagiri. Switching and Memory Phenomena in Langmuir-Blodgett Films with Scanning Tunneling Microscope, Appl. Phys. Lett., *61*, pp.3032-3034. 1992.

Tamoto, N., C. Adachi and K. Nagai. Electroluminescence of 1,3,4-Oxadiazole and Triphenylamine-Containing Molecules as an Emitter in Organic Multilayer Light Emitting Diodes, Chem. Mater., *9*, pp.1077-1085. 1997.

Tao, Y.T., Q. Wang, Y. Shang, C.L. Yang, L. Ao, J.H. Qin, D.G. Ma and Z.G. Shuai. Multifunctional Bipolar Triphenylamine/Oxadiazole Derivatives: Highly Efficient Blue Fluorescence, Red Phosphorescence Host and Two-Color Based White OLEDs, Chem. Commun., pp.77-79. 2009.

Teo, E.Y.H., Q.D. Ling, Y. Song, Y.P. Tan, W. Wang, E.T. Kang, D.S.H. Chan and C.X. Zhu. Nonvolatile WORM Memory Device Based on an Acrylate Polymer with Electron Donating Carbazole Pendant Groups, Org. Electron., *7*, pp.173-180. 2006.

Thompspon, B.C. and J.M.J. Fréchet. Polymer-Fullerene Composite Solar Cells, Angew. Chem. Int. Ed., *47*, pp.58-77. 2008.

Torrance, J.B. The Difference between Metallic and Insulating Salts of Tetracyanoquinodimethane (TCNQ): How to Design an Organic Metal, Acc. Chem. Res., *12*, pp.79-86. 1979.

Tseng, R.J., J.X. Huang, J. Ouyang, R.B. Kaner and Y. Yang. Polyaniline Nanofiber/Gold Nanoparticle Nonvolatile Memory, Nano. Lett., *5*, pp.1077-1080. 2005.

Tyczkowski, J. Bistable Switching in Plasma-Polymerized Acrylonitrile Films, Thin Solid Films, *199*, pp.335-342. 1991.

Wang, F., Y.B. Zhang, C.S. Tian, C. Girit, A. Zettl, M. Crommie and Y.R. Shen. Gate-Variable Optical Transitions in Graphene, Science, *320*, pp.206-209. 2008.

Wang, K.L., T.Y. Tseng, H.L. Tsai and S.C. Wu. Resistive Switching Polymer Materials Based on Poly(acryl ether)s Containing Triphenylamine and 1,2,4-Triazole Moieties, J. Polym. Sci., Part A: Polym. Chem., *46*, pp.6861-6871. 2008.

Wang, K.L., W.T. Liou, D.J. Liaw and S.T. Huang. High Glass Transition and Thermal Stability of New Pyridine-Containing Polyimides: Effect of Protonation on Fluorescence, Polymer, *49*, pp.1538-1546. 2008.

Wang, Y.F., T.M. Chen, K. Okada, M. Uekawa and T. Nakaya. Electroluminescent Devices Based on Polymers Forming Hole Transporting Layers. I, Macromol. Chem. Phys., *199*, pp.1263-1270. 1998.

Wang, Y.F., T.M. Chen, K. Okada, M. Uekawa, T. Nakaya, M. Kitamura and H. Inoue. Electroluminescent Devices Based on Polymers Forming Hole-Transporting Layers. II. Polyimides Containing β-Naphthyldiphenylamine Units, J. Polym. Sci., Part A: Polym. Chem., *38*, pp.2032-2040. 2000.

Wang, Y., Y. Huang, Y. Song, X.Y. Zhang, Y.F. Ma, J.J. Liang and Y.S. Chen. Room-Temperature Ferromagnetism of Graphene, Nano. Lett., *9*, pp.220-224. 2009.

Wang, Z.Y., Y. Qi, J.P. Cao, G.C. Sacripante, P.R. Sundararajan and J.D. Duff. Synthesis, Characterization, and Xerographic Electrical Characgteristics of Perylene-Containing Polyimides, Macromolecules, *31*, pp.2075-2079. 1998.

Wen, Y.Q., J.X. Wang, J.P. Hu, L. Jiang, H.J. Gao, Y.L. Song and D.B. Zhu. Reversible Nanometer-Scale Data Storage on a Self-Assembled, Organic, Crystalline Thin Film, Adv. Mater., *18*, pp.1983-1987. 2006.

Wolarz, E., E. Chrzumnicka, T. Fischer and J. Stumpe. Orientational Properties of 1,3,4-Oxadiazoles in Liquid-Crystalline Materials Determined by Electronic Absorption and Fluorescence Measurements, Dyes. Pigments., *75*, pp.753-760. 2007.

Wu, C.S. and Y. Chen. Copolyfluorenes Containing Bipolar Groups: Synthesis and Application to Enhance Electroluminescence of MEH-PPV, Macromolecules, *42*, pp.3729-3737. 2009.

Wu, F.I., P.I. Shih, C.F. Shu, Y.L. Tung and Y. Chi. Highly Efficient Light-Emitting Diodes Based on Fluorene Copolymer Consisting of Triarylamine Units in the Main Chain and Oxadiazole Pendent Groups, Macromolecules, *38*, pp.9028-9036. 2005.

Wu, F.I., P.I. Shih, Y.H. Tseng, C.F. Shu, Y.L. Tung and Y. Chi. Highly Efficient White-Electrophosphorescent Devices Based on Polyfluorene Copolymers Containing Charge-Transporting Pendent Units, J. Mater. Chem., *17*, pp.167-173. 2007.

Wu, H.M., Y.L. Song, S.X. Du, H.W. Liu, H.J. Gao, L. Jiang and D.B. Zhu. Nanoscale Data Recording on an Organic Monolayer Film, Adv. Mater., *15*, pp.1925-1929. 2003.

Wu, W.C., C.L. Liu and W.C. Chen. Synthesis and Characterization of New Fluorene-Acceptor Alternating and Random Copolymers for Light-Emitting Applications, Polymer, *47*, pp.527-538. 2006.

Xia, R., G. Heliotis, Y. Hou and D.D.C. Bradley. Fluorene-Based Conjugated Polymer Optical Gain Media, Org. Electron., *4*, pp.165-177. 2003.

Xu, Y.F., Z.B. Liu, X.L. Zhang, Y. Wang, J. G. Tian, Y. Huang, Y.F. Ma, X.Y. Zhang and Y.S. Chen. A Graphene Hybrid Material Covalently Functionalized with Porphyrin: Synthesis and Optical Limiting Property, Adv. Mater., *21*, pp.1275-1279. 2009.

Yager, K.G. and C.J. Barrett. Novel Photo-Switching Using Azobenzene Functional Materials, J. Photoch. Photobio., A: Chemistry, *182*, pp.250-261. 2006.

Yang, L., J.K. Feng and A.M. Ren. Theoretical Studied on the Electronic and Optical Properties of Two New Alternating Fluorene/Carbazole Copolymers, J. Comput. Chem., *26*, pp.969-979. 2005.

Yang, Y., J. Ouyang, L.P. Ma, R.J. Tseng and C.W. Chu. Electrical Switching and Bistability in Organic/Polymeric Thin Films and Memory devices, Adv. Funct. Mater., *16*, pp.1001-1014. 2006.

Yasuda, T., T. Imase, Y. Nakamura and T. Yamamoto. New Alternative Donor-Acceptor Arranged Poly(acryleneethynylene)s and Their Related Compounds Composed of Five-Membered Electron-Accepting 1,3,4- Thiadiazole, 1,2,4-Triazole, or 3,4-Dinitrothiophene Units: Synthesis, Packing Structure, and Optical Properties, Macromolecules, *38*, pp.4687-4697. 2005.

Yesodha, S.K., C.K.S. Pillai and N. Tsutsumi. Stable Polymeric Materials for Nonlinear Optics: A review Based on Azobenzene Systems, Prog. Polym. Sci., *29*, pp.45-74. 2004.

Ying, L., J.H. Zou, W. Yang, H.B. Wu, A.Q. Zhang, Z.L. Wu and Y. Cao. Novel Red Light-Emitting Fluorene-*alt*-Carbazole Copolymetalated Ir Complexes, Macromol. Chem. Phys., *210*, pp.457-466. 2009.

Yu, L.S. and S.A. Chen. Full-Range Tunability of Electron and Hole Carrier Mobilities and Density Ratios via Incorporation of Hihgly Electron-Deficient Moieties in Poly(phenylene vinylene) Sich Chains, Adv. Mater., *16*, pp.744-748. 2004.

Zaumseil, J., C.L. Donley, J.S. Kim, R.H. Friend and H. Sirringhaus. Efficient Top-Gate, Ambipolar, Light-Emitting Field-Effect Transistors Based on a Green-Light-Emitting Polyfluorene, Adv. Mater., *18*, pp.2708-2712. 2006.

Zhang, W., S.P. Bian, S.I. Kim and M.G. Kuzyk. Highly-Efficiently Holographic Volume Index Gratings in DR1-Dye-Doped Poly(methyl methacrylate), Opt. Lett., *27*, pp.1105-1107. 2002.

Zhang, Z.G., K.L. Zhang, G. Liu, C.X. Zhu, K.G. Neoh an E.T. Kang. Triphenylamine-Fluorene Alternating Conjuaged Copolymers with Pendant Acceptor Groups: Synthesis, Structure-Property Relationship, and Photovoltaic Application. Macromolecules, *42*, pp.3104-3111. 2009.

Zhong, G.L., K.K. Kim and J.I. Jin. Intermolecular Energy Transfer in Photo- and Electroluminescence Properties of a Europium (III) Complex Dispersed in Poly(vinlcarbazole), Synth. Met., *129*, pp.193-198. 2002.

Zimmerman, G., L.Y. Chow and U.J. Paik. The Photochemical Isomerization of Azobenzene, J. Am. Chem. Soc., *80*, pp3528-3531. 1958.

PUBLICATIONS

(1) Liu, Y.L., K.L. Wang, G.Y. Huang, C.X. Zhu, E.S. Tok, K.G. Neoh and E.T. Kang, Volatile Electrical Switching and Static Random Access Memory Effect in a Functional Polyimide Containing Oxadiazole Moieties, **Chem. Mater.**, *21*, pp.3391-3399. 2009.

(2) Liu, Y.L., Q.D. Ling, E.T. Kang, K.G. Neoh, D.J. Liaw, K.L. Wang, W.T. Liou, C.X. Zhu and D.S.H. Chan. Volatile Electrical Switching in a Functional Polyimide Containing Electron-Donor and -Acceptor Moieties, **J. Appl. Phys.**, *105*, pp.044501(1-9). 2009.

(3) Wang, K.L., Y.L. Liu, J.W. Lee, K.G. Neoh and E.T. Kang, Nonvolatile Electrical Switching and Write-Once Read-Many-Times Memory Effects in Functional Polyimides Containing Triphenylamine and 1,3,4-Oxadiazole Moieties, **Macromolecules**, *43*, pp.7159-7164. 2010.

(4) Wang, K.L., Y.L. Liu, I. H. Shi, K.G. Neoh and E.T. Kang. Synthesis of Polyimides Containing Triphenylamine-Substituted Triazole Moieties for Polymer Memory Applications, **J. Polym. Sci., Part A: Polym. Chem**., *48*, pp.5790-5800. 2010.

(5) Zhang, Z.G., Y.L. Liu, Y. Yang, K.Y. Hou, B. Peng, G.J., Zhao, M.J. Zhang, X. Guo, E.T. Kang, Y.F. Li. Alternating Copolymers of Carbazole and Triphenylamine with Conjugated Side Chain Attaching Acceptor Groups Synthesis and Photovoltaic Application, **Macromolecules**, *43*, pp.9376-9383. 2010.

(6) Xu, L.Q., Y.L. Liu, K.G. Neoh, E.T. Kang, G.D. Fu. Reduction of Graphene Oxide by Aniline with Its Concomitant Oxidative Polymerization, **Macromol Rapid Comm**, *32*, pp.684-688. 2011.

(7) Zhang, B., Y.L. Liu, Y. Chen, K.G. Neoh, Y.X. Lia, C.X. Zhuang, E.S. Tok, E.T. Kang. Nonvolatile Rewritable Memory Effects in Graphene Oxide Functionalized by Conjugated Polymer Containing Fluorene and Carbazole units, *submitted* to **Chem. Mater.**